Calculation of Fluorine and Nitrogen NMR Properties

Tristan Kemp

B.Sc. CS

A thesis submitted in partial fulfilment of the requirement for the degree of

Master of Science

Department of Chemistry and Physics

La Trobe Institute for Molecular Science

La Trobe University

College of Science, Health, and Engineering

Victoria, Australia

February 2021

Table of Contents

Standard Statement of Authorship and Ethics

Except where reference is made in the text of the thesis, this thesis contains no material published elsewhere or extracted in whole or in part from a thesis, this thesis contains no material published elsewhere or extracted in whole or in part from a thesis accepted for the award or any other degree or diploma. No other person's work has been used without due acknowledgement in the main text of the thesis. This thesis has not been submitted for the award of any degree or diploma in any other tertiary institution. None of the research undertaken in connection with this thesis required approval by a University Ethics Committee.

Name: Tristan Kemp

Date: 25/02/2021

Acknowledgements

I would like to take a moment to thank and acknowledge those who help me during my time of writing this thesis.

Firstly, I want to thank my supervisor, Assoc. Prof. David Wilson. Without his guidance, assistance, and knowledge over the length of my Honours and Masters years, the quality of my work would not be where it is now. Your care for the research and for your students is something that I look up to, and I would not have been able to make it through the development of this thesis and research without you.

Next, I would like to thank my close family, especially my parents, who have supported me throughout the years. My family have been by my side every step of the way, and their presence and belief in my abilities is something that helped me constantly throughout the years. I wish to extend this acknowledge out to my close friends, who were always there to support me in any way I needed.

Lastly, I would like to thank our group's collaborator Dr Marcelo Tavares De Oliveira, who has provided much of the DFT benchmarking results discussed in parts of this thesis.

This work was supported by an Australian Government Research Training Program Scholarship.

Abbreviations

AO	Atomic Orbital
CBS	Complete Basis Set
CC	Coupled-Cluster
CCSD[T][Q][P][H]	Coupled-Cluster Single, Doubles, [Triples], [Quadruples], [Pentuples], [Hextuples] Excitations
CFC	Chlorofluorocarbon
DFT	Density Functional Theory
FCI	Full Configuration-Interaction
GGA	Generalised Gradient Approximation
GIAO	Gauge-Including-Atomic-Orbital
GTO	Gaussian-Type Orbital
HF-SCF	Hartree-Fock Self-Consistent Field
LSDA	Local Spin-Density Approximation
MAD	Mean Absolute Deviation
MAX	Maximum Absolute Deviation
MO	Molecular Orbital
MP	Møller-Plesset
NMR	Nuclear Magnetic Resonance
PES	Potential Energy Surface
STO	Slater-Type Orbital
TMS	Tetramethylsilane

Abstract

^{19}F NMR properties such as absolute shielding and spin-rotation constants within a series of molecules have been investigated via quantum mechanical calculations. The use of coupled-cluster methods up to CCSDTQP and large basis sets up to aug-cc-pCV7Z has allowed the accurate determination and benchmarking of ^{19}F NMR properties. These have been calculated at geometries optimised with the CCSD(T)/aug-cc-pCVQZ level of theory to provide equilibrium absolute shieldings and spin-rotation constants. In an attempt to benchmark these NMR properties with experiment, important effects on the absolute shielding were calculated, such as vibrational averaging and temperature effects at the CCSD(T)/aug-cc-pCVXZ level of theory and relativistic effects at the PBE0/dyall-aug-cvqz level of theory have been further calculated. The calculation of absolute shielding and spin-rotation constants was first conducted and investigated for the ^{1}H nucleus in H_2, HF, and H_2O then implemented for ^{19}F within HF, F_2, FCl, HOF, F_2O, CH_3F, and FCN. Comparison between theory and experiment has been carried out using currently available chemical shifts and spin-rotation data, which agree well with the NMR properties calculated within this investigation. Experimental spin-rotation data along with calculated diamagnetic shieldings are used to develop a series of semi-experimental shielding constants that are further compared to experiment and theory. A revised absolute ^{19}F shielding in HF is also proposed based on the present calculated results and recent experiments, which will serve to anchor the relative ^{19}F shielding scale. Investigation into the usefulness of DFT GGA functionals KT1, KT2, KT3, as well as the meta-GGA functional RevTPSS was then performed on a large series of ^{15}N containing molecules to obtain a wide range of absolute shieldings. These shieldings are compared with available experimental data resulting in the determination of average and maximum deviations from experiment. These statistics as well as the individual calculated shieldings are compared between functionals and the usefulness of the compared series is discussed.

Chapter 1:
Introduction

1.1 NMR Absolute Shielding, Chemical Shifts and Spin-Rotation Constants

Nuclear Magnetic Resonance (NMR) is one of the most useful tools for the determination of molecular structure, interaction, and reactivity. Some of the most important quantities derived from the interaction of molecules and magnetic fields include chemical shifts and spin-spin coupling constants, while related spin-rotation constants and electric-field gradients are closely related. Chemical shifts (δ) are one of the most common and important properties produced by NMR experiments, which provide an understanding of the electronic environment in which a nucleus resides. Nuclei produce consistent chemical shifts between experiments, and hence NMR is capable of precise reproduction of results. Chemical shifts represent the degree of shielding of a nucleus from an external magnetic field due to the presence of electrons.

The magnetic shielding tensor, σ, is the fundamental property that underpins the chemical shift. Magnetic shielding is a second-order property (second-rank tensor), which is represented as a 3 x 3 matrix. The isotropic average (average of the diagonal xx, yy, and zz components) of the shielding tensor is the shielding constant, σ_{iso}, which represents the shielding or deshielding with respect to the bare nucleus. In this thesis, only the isotropic shielding constant is considered.

The magnetic shielding constant cannot be measured directly in an experiment; however, the difference in shielding constants between two nuclei can be determined, which is defined as the chemical shift (δ). Chemical shifts from NMR experiments are measured relative to some reference compound (that includes the same nucleus) which yields a relative scale for each nuclei. Therefore, is interest in determining non-relative shielding constants of nuclei, known as the absolute magnetic shielding (σ), to complement the chemical shifts routinely used in NMR studies. The relationship between the absolute magnetic shielding constant and chemical shift of a nucleus is given by:[1]

$$\delta_n = \sigma_{\mathrm{ref}} - \sigma_n \tag{1.1}$$

where δ_n and σ_n are the chemical shift and absolute magnetic shielding constant of nucleus n, respectively, and σ_{ref} is the absolute magnetic shielding constant of the reference compound. Examples of reference compounds include tetramethylsilane (TMS) for ^{1}H and ^{13}C nuclei, CH_3NO_2 for ^{15}N, and $CFCl_3$ for ^{19}F nuclei. Evidently, if the absolute shielding constant of a reference compound is accurately known, then the absolute shielding of other nuclei can be deduced from reported experimental chemical shifts via eq. 1.1. Unfortunately, there is a lack of accurate absolute magnetic shielding values due to the difficulty in their experimental determination. As such, there is a need to obtain highly accurate magnetic shielding constants for possible NMR reference compounds via computational methods.[2]

The magnetic shielding tensor is a second-order property, which may be defined as an energy derivative,[1]

$$\sigma_n = \frac{\partial^2 E}{\partial \boldsymbol{\mu} \partial \mathbf{B}} \tag{1.2}$$

where E is the total energy of the system, $\mathbf{B}$ is the external magnetic field, and $\boldsymbol{\mu}$ is the nuclear magnetic moment. Due to the dependence on the nuclear magnetic moment, only "NMR active" nuclei can be investigated. That is, a nucleus must have a non-zero nuclear spin ($\boldsymbol{I}_n$) such as ^{1}H, ^{13}C, ^{15}N, ^{17}O, ^{19}F, ^{33}S, and ^{119}Sn.

Nuclear spin-rotation constants are a related magnetic property, which describes the interaction between nuclear magnetic moments and the magnetic field generated via the rotational motion of a molecule.[3,4] The nuclear spin-rotation constant, $\boldsymbol{C}$, is used in microwave and molecular beam spectroscopy. Similar to the absolute shielding, the spin-rotation constant is a second-order property and is the isotropic average of a 3 x 3 tensor ($\boldsymbol{C}_{\text{iso}}$). The nuclear spin-rotation constant of nucleus n is dependent on the nuclear spin ($\boldsymbol{I}_n$) and the rotational angular momentum ($\boldsymbol{J}$):[3,5]

$$\boldsymbol{C}_n = \frac{\partial^2 E}{\partial \boldsymbol{I}_n \partial \boldsymbol{J}} \tag{1.3}$$

The spin-rotation tensor and the subsequent spin-rotation constant is comprised of electronic ($\boldsymbol{C}^{\text{el}}$) and nuclear ($\boldsymbol{C}^{\text{nuc}}$) parts, which are tensors themselves:[6]

$$\boldsymbol{C}_n = \boldsymbol{C}^{\text{el}} + \boldsymbol{C}^{\text{nuc}} \tag{1.4}$$

There is an important relationship between spin-rotation constants and shielding constants, which is detailed below, from which absolute magnetic shielding constants may be derived in

a semi-experimental manner from experimental spin-rotation constants. As such, there is significant interest in the calculation of nuclear magnetic shielding constants (and chemical shifts) and nuclear spin-rotation constants, which has the potential of providing quantitative values.

The importance of theoretical absolute shieldings, chemical shifts, and spin-rotation constants establishes a need to benchmark theoretical methods. The level of theory required to calculate shielding constants and spin-rotation constants with sufficient accuracy, as well as which experimental factors will make a significant impact on results, must be considered in order to advance investigations of both nuclear shielding and spin-rotation constants. In this thesis, the theoretical methods and approach to calculating shielding constants and spin-rotation constants has been explored in detail for several nuclei. The results will allow theoreticians to extend nuclear shielding scales for these nuclei and provide a better understanding of the computational requirements to reach a high level of accuracy.

The present investigation is focused on gas-phase NMR properties unless otherwise specified. Chemical shifts from gas-phase and liquid-phase NMR experiments will inherently be slightly different due to the presence of intermolecular interactions in the liquid-phase. In gas-phase experiments, there are minimal intermolecular interactions, which is more consistent with the single-molecule computational results.

1.2 Experimental Derivation of ^{19}F Absolute Shielding Constants

The experimental determination of absolute nuclear shielding constants may be achieved by combining gas-phase chemical shifts extrapolated to the zero-density limit together with previously determined absolute nuclear shielding constants of reference compounds using eq. 1.1. For example, Makulski has extrapolated a zero-density gas-phase chemical shift of 170.170 ppm for SiF_4 relative to $CFCl_3$. Combining the chemical shift with an absolute ^{19}F nuclear shielding in $CFCl_3$ of 192.07 ppm leads to an experimental absolute ^{19}F shielding in SiF_4 of 362.87 ppm (170.170 ppm + 192.70 ppm).[7] In this procedure, σ_{ref} contains the greatest uncertainty as its accuracy is often difficult to determine and verify. As such, most experimentally determined absolute magnetic shielding constants are derived using the Ramsey-Flygare method.

Ramsey has shown that the absolute shielding can be separated into paramagnetic (σ^{p}) and diamagnetic (σ^{d}) components.[8]

$$\sigma_n = \sigma_n^{\mathrm{p}} + \sigma_n^{\mathrm{d}} \tag{1.5}$$

Additionally, Flygare showed that the paramagnetic contribution to the absolute shielding tensor is related to the nuclear spin-rotation constant ($\boldsymbol{C}$) by the equation:[9,10]

$$\sigma_n^{\mathrm{p}} = \frac{m_{\mathrm{p}}}{2m_{\mathrm{e}}g_n}\left(\frac{1}{3}\sum\frac{\boldsymbol{C}_{gg}^{\mathrm{el}}}{B_{gg}}\right) \tag{1.6}$$

where m_{p} and m_{e} are the mass of a proton and an electron, respectively, g_n is the nuclear g-factor of nucleus n, and $\boldsymbol{C}_{gg}^{\mathrm{el}}$ and B_{gg} are the electronic contribution to the spin-rotation tensor in kHz, and the molecular rotational constant in GHz of the matching axis (g), respectively. Here gg refers to the three principal molecular axes, which could be xx, yy, and zz (Cartesian coordinates), or 11, 22, and 33 in the more general case. It is noted that in attempting to use eq. 1.6 in the current project, an error was found in the representation of this expression published by Gauss where the multiplication of $\frac{1}{2}$ is not applied.[11]

Unlike the paramagnetic shielding constant contribution that is related to the experimental spin-rotation constant, the diamagnetic nuclear shielding contribution has no direct experimental measurement. However, a semi-experimental nuclear shielding constant may be derived by combining an experimental paramagnetic shielding constant (potentially derived from an experimental spin-rotation constant through the use of eq. 1.6), along with a theoretically calculated diamagnetic shielding via eq. 1.5.[11-15] The calculation of the diamagnetic contribution is not significantly affected by computational method or basis set (it is a nuclear contribution rather than an electronic contribution), and thus diamagnetic contribution calculations tend to be highly accurate.[1,9,16]

It has been shown by Malkin *et al*. that Flygare's relationship (eq. 1.6) is valid only within the non-relativistic limit.[16] This is largely because the effect of relativity on the spin-rotation constant is much smaller than the relativistic effect on the magnetic shielding constant.[17] It was originally suggested that the shielding constant scales of heavy nuclei such as ^{119}Sn would be highly impacted by the difference in relativistic effects, and while that is true, it has since been found that relativistic effects on lighter nuclei such as ^{33}S and ^{17}O are non-negligible.[13]

The process of determining semi-experimental absolute nuclear shielding constants is illustrated in Figure 1.1, whereby experimental spin-rotation and calculated shielding constants

are combined using eq. 1.5 and 1.6. Starting from the experimental spin-rotation constant, one must first remove the calculated effects of relativity and (ro)vibrational averaging to the experimental spin-rotation constant. This produces a non-relativistic equilibrium spin-rotation constant ($\boldsymbol{C}_e^{\mathrm{nonrel}}$), which is converted to a paramagnetic nuclear shielding constant (σ_e^{p}) using eq. 1.6. The addition of a theoretically calculated diamagnetic shielding constant (σ_e^{d}) with eq. 1.5, yields a semi-experimental non-relativistic equilibrium magnetic shielding constant ($\sigma_e^{\mathrm{nonrel}}$). Finally, calculated (ro)vibrational averaging and relativistic effects to the nuclear magnetic shielding constant may then be added to obtain a relativistic vibrationally-averaged absolute shielding constant (σ_0^{rel}).[11,12,14,16] Absolute nuclear shielding constants of different molecules can then be combined to obtain chemical shifts, which can be compared with directly measured experimental chemical shifts. Agreement of the semi-experimental chemical shifts with the directly measured values provides support for the absolute nuclear shielding constants.

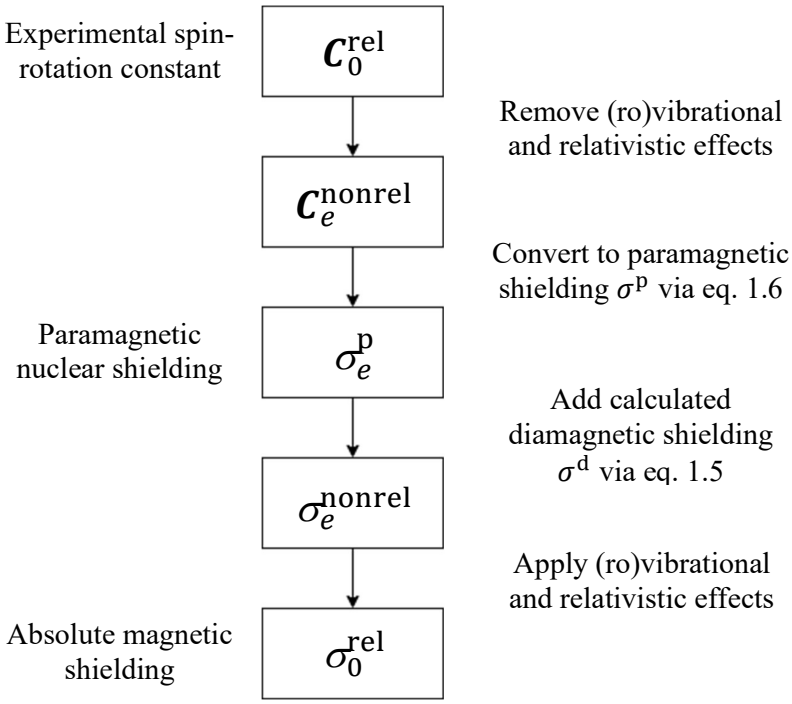

Figure 1.1: Procedure for deriving semi-experimental relativistic absolute shielding constants from experimental spin-rotation constants.

1.3 Calculation of Nuclear Shielding and Spin-Rotation Constants

An alternative and efficient approach for obtaining absolute nuclear shielding tensors is to calculate both the paramagnetic and diamagnetic contributions using quantum chemistry methods to provide a fully theoretical value.

Today, NMR parameters can be calculated with the hierarchy of computational chemistry methods. It has become routine to calculate NMR chemical shifts using density-functional theory (DFT) to aid the interpretation of experimental spectra. The highest accuracy is obtained with extensive coupled-cluster calculations; however, the significant computational demands ensure that these high-level methods can only be employed for smaller molecules. In this thesis, both approaches have been investigated, with high-level coupled-cluster calculations of fluorine-containing molecules with the aim to provide benchmark (quantitative) quality results, and a separate investigation of the performance of DFT in the calculation of nitrogen chemical shifts. In both cases, the accuracy of the computational methods and basis sets was investigated through a critical comparison of calculated and experimental values for an appropriate test set of molecules.

A purely computational approach was used less often in the past due to the difficulty in assessing the accuracy of the derived results that did not have an experimental foundation. However, in the last decade, it has been shown that theoretical nuclear shielding constants can be very close to experiment if proper treatment of method and basis set, vibrational effects, and relativity is employed.[12,18] Moreover, this approach is necessary in the case where experimental spin-rotation constants or absolute nuclear shielding constants are not available. In cases where experimental spin-rotation data is available, calculating the spin-rotation constants may be used to access the validity of such reported data. Additionally, the discrepancy between semi-experimental and calculated magnetic shielding constants arise from differences between experimental and theoretical spin-rotation constants. Therefore, experimental spin-rotation constants may also be verified by close agreement between semi-experimental and fully calculated absolute shielding constants.

There are a number of challenges and requirements for the accurate calculation of magnetic properties, including shielding constants and spin-rotation constants. Teale *et al*. have demonstrated that coupled-cluster methods such as coupled-cluster singles doubles with perturbative triple excitations (CCSD(T)) are required to produce accurate shielding constant

results.[18] The requirement of large coupled-cluster methods presents an issue to theoretical size, and therefore, only small molecules can be studied accurately.

One important factor in the calculation of nuclear shielding constants is that they are dependent on the applied magnetic field **B** via eq. 1.2, as the origin of the magnetic field vector (or gauge-origin) is not fixed. Therefore, calculated shielding constants will change with translation of the Cartesian coordinates of the molecule (and be dependent on the origin of the Cartesian coordinates of the molecular system). One elegant solution to this problem is to employ the gauge-including-atomic-orbitals (GIAOs) approach.[19] GIAOs define the gauge origin for each atomic orbital (at the nucleus of the atomic-orbital), generating reproducible results regardless of translation of said molecule's coordinates.[20] GIAO methods are now available for various methods, including Hartree-Fock, density functional theory, and coupled-cluster theory.[21] The GIAO approach has the additional benefit of improving the rate of basis set convergence.

The dependence of the absolute magnetic shielding constant on the nuclear magnetic moment $\boldsymbol{\mu}$ means both the valence and core electrons in the molecular system must be explicitly considered. Therefore, calculations must disable the often used frozen-core approximation, where core electrons are not explicitly treated in the electron-correlation component of the calculation. Rather, additional tight core basis functions must be included in the basis set.[22] The combination of all-electron and specific core basis functions reduces the size of molecules that can be studied, as replacing light atoms for heavier ones increases the number of electrons in a molecule, and as such, rapidly increases computational cost.

Relativity can be expected to affect nuclear shielding constants to a greater extent than valence-only properties, as the inner core electrons may travel at a much greater speed (closer to the speed of light) than the outer valence electrons. This is especially true for heavier nuclei, which requires that relativistic effects be considered in any accurate theoretical treatment of nuclear shielding constants.

Absolute shielding tensors that are derived completely from theory are typically calculated with an equilibrium geometry at 0 K. Therefore, it is important to apply calculated vibrational averaging, temperature, and relativistic effects to obtain a vibrationally averaged relativistic absolute shielding (σ_0^{rel}) that can then be accurately compared with experimental data that is measured at a finite temperature at a thermal equilibrium.

An important consideration when comparing experimental and theoretical for NMR parameters is the geometry and conformational flexibility of the molecule. Calculations are typically

carried out at a single static structure (an optimised geometry). For experiments carried out at ambient temperatures and likely also in solution, the effects of thermal motion (averaging of position/conformation) and solvation can be significant. Such effects can be incorporated into a calculation, for example, with molecular dynamics simulations and averaging of calculated NMR parameters over many distinct geometries. In the work presented in this thesis, sets of molecules were used that are both symmetry unique and not subject to conformational flexibility that avoids any need for conformational averaging. For example, the set of molecules included in the ^{15}N chemical shift study are fused rings without single-bond rotors, while for ^{19}F, only small molecules without rotational isomers were considered.

1.4 Fluorine (^{19}F) NMR

1.4.1 Experimental ^{19}F NMR

Fluorine magnetic shielding is an invaluable tool in synthetic chemistry, in large part due to the exquisite sensitivity to the electronic environment. Fluorine magnetic shielding is often a part of absolute nuclear shielding investigations; however, it is difficult to calculate accurately. The difficulty in obtaining accurate ^{19}F shielding constants arises from the large electronegativity and number of lone pairs that the fluorine atom possesses, which causes fluorine to be highly sensitive to its electronic environment.[23] The sensitivity to the electronic environment is reflected in the large ^{19}F chemical shift range (-500 to 500 ppm relative to $CFCl_3$). The high sensitivity to electronic structure makes the calculation of fluorine nuclear shielding constants an extreme test of computational chemistry methods.

Rosenau *et al.* have shown that there is difficulty in reproducing fluorine NMR chemical shift results, partly due to the lack of up-to-date information on the currently used reference compound $CFCl_3$.[24] The team concluded that an updated neat $CFCl_3$ reference could mitigate fluorine NMR errors from ±1 ppm to ±0.03 ppm. However, $CFCl_3$ is a banned chlorofluorocarbon (CFC) under the Montreal Protocol, which prevents new experimental work. Therefore, an accurate absolute nuclear shielding scale for ^{19}F would greatly benefit the accuracy of fluorine NMR experiments.

1.4.2 Absolute Shielding Constants for ^{19}F Nuclei

The ^{19}F shielding constant in HF has regularly been investigated due to HF previously being a reference compound for ^{19}F chemical shifts, which allows other absolute shielding constants to be determined via relative chemical shifts. Sundholm *et al.* reported a semi-experimental absolute ^{19}F shielding constant in HF of 409.6 ± 1.0 ppm.[12] This shielding value was derived by combining an experimental spin-rotation constant and a calculated diamagnetic nuclear shielding. The derived shielding constant agreed well with a previously determined semi-experimental value of 410 ± 6 ppm,[14] as well as a fully calculated value of 409.2 ppm at the CCSD(T) level of theory.[12]

$CFCl_3$ is currently the most widely used reference compound for ^{19}F chemical shifts. An often-referenced ^{19}F nuclear shielding constant in $CFCl_3$ is 188.7 ppm.[14] However, this was derived from a liquid-phase chemical shift rather than a gas-phase chemical shift. A gas-phase absolute nuclear shielding constant of $CFCl_3$ has been reported as 195.6 ppm.[14] These absolute shielding constants were derived using the experimental chemical shift relative to HF in combination with the older 410 ± 6 ppm ^{19}F shielding constant in HF. Our group has recently updated the absolute shielding of $CFCl_3$ to a completely calculated value of 197.07 ppm, which included high-level coupled-cluster calculations of the equilibrium value together with vibrational corrections and account of relativity.[25] The 197.07 ppm value is considered to be the most accurate value to date for the ^{19}F nuclear magnetic shielding in $CFCl_3$. The ^{19}F absolute shielding in other molecules can be calculated from the ^{19}F absolute shielding in $CFCl_3$ of 197.07 ppm together with their respective chemical shifts via eq. 1.1. There remains interest in reinvestigating the absolute ^{19}F nuclear shielding in HF and establishing a fluorine magnetic shielding scale from such a value.

It is possible to calculate NMR shielding constants and spin-rotation constants by systematically increasing the accuracy of wavefunction methods used in calculations. This allows one to obtain highly accurate theoretical contributions to the total ^{19}F absolute shielding constant and spin-rotation constant. The ^{19}F absolute shielding in HF of 409.6 ppm reported by Sundholm *et al.*[12] (together with associated spin-rotation constants) serves as an appropriate benchmark for electronic structure calculations.

In this project, the computational requirements of accurate nuclear shielding and spin-rotation constant calculations have been explored, with a particular focus on ^{19}F nuclei. The calculation of nuclear shielding in small fluorine-containing molecules enables the importance of basis set

convergence and expansion of the coupled-cluster wavefunction beyond CCSD(T) to be established. Additionally, the level of consideration of vibrational, temperature, and relativistic effects required for accurate ^{19}F shielding constants and spin-rotation constants has been investigated. The calculation of benchmark quality constants enables an analysis of the accuracy and validity of currently available experimental shielding and spin-rotation values. For all molecules considered in this project, spin-rotation constants have also been calculated for comparison with the derived semi-experimental shielding constants as outlined in Section 1.2.

1.5 DFT Calculation of ^{15}N NMR Chemical Shifts

At the other end of the spectrum, density functional theory (DFT) is useful for calculating the magnetic properties of medium to large molecules. Due to DFT being more useful for larger molecules than coupled-cluster methods, there is a general need to benchmark which functionals provide the most reliable shielding results. This is because, unlike coupled-cluster methods which systematically improve the wavefunction, different DFT functionals provide a different estimate of the electronic energy. This means that different DFT functionals will produce molecular property values unrelated to each other. The majority of published studies that address this issue have focussed on ^{1}H and ^{13}C nuclei.

The reliability of absolute nuclear shielding constants, chemical shifts, and spin-rotation constants from DFT calculations also need to be determined in different conditions. If a particular functional is reliable for obtaining gas-phase absolute shielding constants, there may be an alternative functional which provides more reliable results for liquid-phase nuclear shielding constants where solvent effects are important. This concept can be extended to which functionals are better suited for components of the calculated properties; a particular DFT functional may produce accurate vibrational and relativistic effects to shielding constants; however, the same functional may produce unreliable equilibrium shielding constants. This uncertainty leads to a need for benchmarking and evaluating DFT functionals for specific conditions so that the reliability of future studies in absolute shielding constants in lager systems can be validated.

There remains no consensus on the best functional for the calculation of NMR parameters, although there have been a significant number of studies that have investigated the accuracy of density functionals. Teale *et al.* have investigated absolute shielding and spin-rotation constant

results from a series of DFT functionals and compared them with CCSD and CCSD(T) results as well as reported experimental data.[18] They were able to report that the DFT functional KT2 performed much better than the other selected functionals in terms of mean absolute error and maximum absolute error. This study focused solely on gas-phase results, although their list of 28 molecules did consider multiple nuclei.

In the work presented in this thesis, the performance of DFT in the calculation of ^{15}N chemical shifts has been investigated by a critical comparison with experimentally reported chemical shifts. Krivdin has reviewed the current literature of ^{15}N magnetic shielding constants and made recommendations on how to best account for different effects and conditions, including solvent effects, vibrational corrections and relativistic effects.[26] Krividin carried out a benchmark study of 23 heterocyclic nitrogen-containing molecules, from which he recommended using the KT2 or KT3 functionals together with Jensen's pcS-2 and pcS-3 basis sets, with the KT3/pcS-3 level of theory yielding a mean absolute error of only 5 ppm from the experimental chemical shifts for the selected set of molecules.[27] Krividin's recommendation is similar to the conclusions of Teale *et al*., even though the studies consisted of contrasting approaches, one with a broad benchmark overview and the other with focused analysis on the effects of shielding.

While both studies considered a range of DFT functionals and basis sets in the calculation of NMR chemical shifts, there remains a number of factors that warrant further exploration. The set of molecules and set of functionals was limited. As such, there is a need to assess the performance of newer functionals and a broader collection of basis sets across a wider set of molecules. This would serve to assess the wider applicability of DFT methods in the calculation of ^{15}N chemical shifts, while progressing the search for the most reliable and accurate DFT functionals. Most benchmark studies overlook several important effects, including DFT integration grid, solvation (including solvent model), vibrational averaging, and relativistic effects. The omission of these factors is computationally appealing; however, any resultant comparison of experiment and theory is less rigorous and can lead to incorrect conclusions as to the best functionals (ranked by mean deviation from experimental data).

1.6 Summary

NMR properties are extremely important in all areas of chemistry. The chemical shift is widely used in synthetic and structural chemistry; however, they are reported as relative shifts rather than absolute shieldings. There is a clear interest in being able to determine absolute nuclear

magnetic shielding constants. A small number of absolute shielding constants have been reported from experiment; however, a drawback is a lack of reliability in the results due to the difficulties associated with determining absolute shielding constants.

Theoretical calculations provide an alternative and potentially more effective means to determine absolute shielding constants. Theoretical calculations of NMR chemical shifts are calculated in terms of non-relative absolute nuclear shielding constants. Calculated shielding constants will vary with the level of theory used but will also be affected by experimentally relevant factors such as vibrational and relativistic effects. As it is near impossible to use full configuration-interaction (FCI) wavefunction methods along with an infinitely large complete basis set, approximations must be employed. However, the use of *ab initio* methods such as coupled-cluster theory enables a systematic improvement of results towards the exact value.

Quantum chemistry investigations of nuclear chemical shifts and shielding constants are assisted greatly by experimentally reported spin-rotation constants due to Flygare's relationship (eq. 1.6), which enables semi-experimental shielding constants to be determined at a greater accuracy which can be measured directly. Spin-rotation constants can also be calculated using quantum chemistry methods, allowing for another series of data points to benchmark the reliability of calculated results.

Absolute shielding constants of ^{19}F nuclei are difficult to determine accurately due to their high electronegativity. Due to advancements in quantum chemistry and understanding of absolute shielding constants, re-investigation into the ^{19}F shielding scale is warranted through the use of high accuracy coupled-cluster methods.

Coupled-cluster methods are only viable for small molecules in the gas-phase, whereas DFT is the standard workhorse for larger molecules. As such, there is a general need to benchmark the calculation of chemical shifts from various DFT functionals to determine the most reliable strategy for calculating chemical shifts.

Chapter 2:
Computational Methods

2.1 Introduction

In this chapter, the methods used throughout the computational study of nuclear magnetic shielding, chemical shifts, and spin-rotation constants are outlined. A key aim of computational chemistry is to provide understanding and predict the interactions of real chemical systems. As the modern computer increases in power, so too does the capability of computational chemistry. The computational chemistry approach employed in this thesis is built upon electronic structure theory, which is underpinned by quantum chemistry and the Schrödinger equation.

2.2 The Schrödinger Equation

In order to predict the physical properties of a molecule from a theoretical basis, the electronic structure of the molecule in question must be understood. Computational chemistry achieves this within the non-relativistic framework using the time-independent Schrödinger equation:

$$\boldsymbol{H}\psi = E\psi \tag{2.1}$$

where $\boldsymbol{H}$ is the Hamiltonian operator, E is the energy of the system, and ψ represents the wave function. The Hamiltonian is used to describe the energy as a function of the kinetic and potential energy of the system by,

$$\boldsymbol{H} = T_n + T_e + V_{nn} + V_{ne} + V_{ee} \tag{2.2}$$

where T_n and T_e represent the kinetic energy of the nuclei and electrons, respectively, V_{nn} and V_{ee} are the nuclear-nuclear and electron-electron repulsive potential energies, respectively, and V_{ne} is the attractive potential energy between the nuclei and electrons. Due to the size of the nuclei compared to the electrons, it is possible to assume the nuclei are non-dynamic entities and approximate the Hamiltonian via the Born-Oppenheimer approximation, which enables the separation of nuclear and electronic motion and in the electronic Schrödinger equation sets the kinetic energy of the nuclei to zero. This gives an equation that describes the electronic structure of the molecule in the form of,

$$\boldsymbol{H}_e = T_e + V_{nn} + V_{ne} + V_{ee} \tag{2.3}$$

2.3 Molecular Orbital and Hartree-Fock Theory

Due to the complexity of the wave function, the Schrödinger equation can only be solved exactly for one-electron systems. Therefore, approximations are made in order to treat many-electron systems or molecules. The simplest approach is Hartree-Fock theory, which is the fundamental basis of molecular orbital (MO) theory. Throughout this thesis, Hartree-Fock is referred to as HF-SCF (self-consistent field) to avoid confusion with the HF molecule.

Hartree-Fock theory simplifies the wave function for many-electron systems through a product of one-electron wave functions (orbitals) known as a Slater determinant.

$$\psi(e_1, e_2, \dots, e_n) = \psi(e_1)\psi(e_2) \dots \psi(e_n) \tag{2.4}$$

The description of the system as a single electronic configuration is a significant assumption. One consequence of the single configuration in HF-SCF theory is that electrons only experience the effect of an implicit "electron cloud" (field) rather than their motion being correlated. Specifically, the motion of opposite spin electrons is not correlated (Coulombic correlation is omitted). The limitations of HF-SCF theory do not enable the calculation of accurate results for magnetic properties.[18]

2.4 Electron-Correlation Methods

The assumptions and approximations made by HF-SCF theory cause over-estimates of the total energy (due to the variational principle) and limit the accuracy of calculated molecular properties. An exact wave function generally requires multiple determinants rather than a single determinant. Electron-correlation methods such as coupled-cluster (CC) theories seek to account for electron correlation by including additional determinants, while methods such as Møller-Plesset (MP) provide correlated energies by perturbing the HF-SCF wave function (without including additional determinants). The correlation energy can be defined as the difference between the exact energy and the HF-SCF energy. Electron-correlation methods aim to recover the total energy of an electron correlated system. Coupled-cluster methods generate a many-bodied wave function by augmenting a reference state Φ (HF-SCF wavefunction) by the exponential correlation operator T:

$$\psi = e^{T}\Phi_0 \tag{2.5}$$

where T can be expressed as:

$$T = T_1 + T_2 + T_3 + \cdots + T_n \tag{2.6}$$

for an n electron problem, where T_1 represents the operator for single excitations, T_2 is the operator for double excitations and so forth. The total exponential correlation operator T can be truncated to a given order to reduce computational effort at the cost of accuracy. Successive truncation of T results in the series of coupled-cluster methods and allows for a systematic improvement of the wavefunction and calculated properties. Truncating T to $T_1 + T_2$ yields the coupled-cluster singles and doubles (CCSD) method, the addition of triple excitations ($T = T_1 + T_2 + T_3$) will produce the coupled-cluster singles, doubles, and tripes (CCSDT) method and so on. No truncation of the coupled-cluster wavefunction is equivalent to a full configuration interaction (FCI) calculation, which provides an exact wavefunction within the given basis set. Truncation of T provides a substantial decrease in computational cost as each successive coupled-cluster method scales largely with the size of the system, with CCSD scaling at $O(N^6)$, where N is a measure of the system size, CCSDT scaling at $O(N^8)$, and so on. It is therefore useful to account for additional excitations via perturbation theory. A method such as CCSD(T) has a full account for single and double excitations (i.e. $T = T_1 + T_2$) and perturbative treatment of triple excitations (T_3) and has a scaling cost of $O(N^7)$, whereas CCSDT(Q) correlates single, double, and triple excitations ($T = T_1 + T_2 + T_3$) and treats quadruple excitations (T_4) via perturbation theory. The CCSD(T) approach has become recognised as the gold-standard in computational chemistry. In the case of magnetic shielding and spin-rotation calculations, it is important to explore coupled-cluster wavefunction expansions beyond single and double excitations.[18]

2.5 Density Functional Theory Methods

Instead of basing a system's electronic energy on wavefunctions, density functional theory (DFT) calculates the electronic energy from the electron density. This arises from the Hohenberg-Kohn Theorem, which states that the ground-state energy is directly proportional to the electron density. This reduces the calculation of the electronic system from a 3*N*-dimensional problem, where *N* is the number of electrons (arising from the (*x*, *y*, *z*) coordinates of each electron), to a 3-dimensional problem (the Cartesian coordinates of electron density). This large decrease in problem size is advantageous for computational cost, making DFT calculations much more efficient than electron correlation calculations. However, unlike wavefunction methods, it is difficult to systematically improve DFT approaches.

The closest description to successive improvement between DFT functionals is represented by "Jacob's ladder". Jacob's ladder describes the theoretical improvement between series of DFT functionals from no exchange-correlation energy ("Hartree world") towards the "heaven of chemical accuracy".[28] The simplest approximation for DFT exchange-correlation is the local spin-density approximation (LSDA), which assumes the electron density (ρ) is uniform across the molecule. This approximation is exact for an infinite uniform electron gas; however, it is typically quite inaccurate for molecular properties due to the naturally inhomogeneous electron density distributions of molecular systems.[29] Overcoming the errors in LSDA that arise from inhomogeneous density distributions prompted the creation of the generalised gradient approximation (GGA) functionals. GGA functionals use the gradient of the density ($\nabla\rho$) in addition to the density itself to account for inhomogeneity within the electron density. Further improvement on GGAs can be achieved with the inclusion of the Laplacian of the density ($\nabla^2\rho$, second derivative) or the kinetic energy density to provide second derivative information. As these two terms are related, only one needs to be considered and are the basis of meta-GGAs. Usage of the kinetic energy density is more popular in meta-GGA functionals than $\nabla^2\rho$ as it allows more flexibility within the generated DFT functional.

The previously mentioned families of DFT functionals are often referred to as pure functionals and are unfortunately often not self-interaction error-free due to the exchange-correlation being an empirical function. Therefore, it is possible for pure functionals to incorrectly return a non-zero electron correlation energy for the hydrogen atom, which in turn produces inaccuracies within molecular property calculations. This is not the case within Hartree-Fock theory and is the basis of theory behind the family of hybrid functionals. By replacing part of the local exchange functional with the exact exchange functional from Hartree-Fock theory, whilst still treating correlation energy from pure functionals, a new hybrid functional can be produced. Hybrid functionals have been demonstrated to increase accuracy in bond distances, ionisation energies, and vibrational frequencies.[30] A further improvement upon hybrid functionals is to combine the correlation energy from pure functionals with PT2 method such as MP2. This allows for an exact exchange and exact correlation functional and is the basis for the double-hybrid functionals.

2.6 Basis Sets

Basis functions are used to describe atomic orbitals (AOs) in mathematical terms. At the heart of HF-SCF theory is the generation of a molecular orbital (MO) as a linear combination of AOs, or more specifically atomic basis functions. As such, the accuracy of the calculated energy is dependent on the size of the basis set used.

The first form of basis sets were the Slater-type orbital functions (STOs), which have the form:

$$\mathrm{R(r)} = NY_l^m(\theta, \phi)r^{n-1}e^{-\zeta r} \tag{2.7}$$

where N is a normalisation constant, Y_l^m is the spherical harmonic function, n, m, and l are the principal, magnetic, and angular momentum quantum numbers, respectively, r is the distance from the nucleus, and ζ is the exponent. Although the behaviour of STOs is theoretically correct, they are only applicable for hydrogen-like atoms due to their lack of radical nodes. Additionally, evaluating integrals with STOs is difficult, and as such Gaussian-type orbitals (GTOs) were created with the form:

$$\mathrm{R(r)} = NY_l^m(\theta, \phi)r^{2n-2-l}e^{-\zeta r^2} \tag{2.8}$$

The main difference between an STO and a GTO is the exponential dependence on r and r^2, respectively. This makes GTOs easier to integrate at the cost of accuracy. However, a series of GTOs can be combined to approximate an STO.

A minimal basis set is the smallest set of required basis functions to describe an AO. This is achieved by using only a single GTO basis function for each AO. The accuracy of the basis set can be expanded by increasing the number of GTOs used per AO. Basis sets with two functions per AO are labelled double-zeta (DZ); those with three functions are known as triple-zeta (TZ) and so on.

Split-valence basis sets are those which treat core electrons with single-zeta basis sets while expanding the basis set used for valence electrons. This saves computational cost by using larger expanded basis functions for the valence electrons while only using a minimal set of basis functions for the core electrons. This is a reasonable assumption as valence electrons contribute more to most physical and chemical properties of molecules than core electrons. However, core electrons are important for magnetic properties such as nuclear magnetic shielding and spin-rotation constants, and so core basis functions are required for accurate calculations of magnetic properties. In such cases, using split-valance basis sets with only a minimal core is not ideal for accurate results.

Basis sets can also be extended with the inclusion of polarisation and diffuse functions. Polarisation functions are AO functions of higher angular momentum that allow for greater flexibility in the shape of the AOs and MOs. Diffuse functions are basis functions with a greater radial extent (smaller ζ exponent) and are essential when considering anions or very electronegative atoms such as fluorine.

Several notable families of basis sets have been developed, with the aim of improving the accuracy of results, computational cost, and smooth convergence to an exact result. The Pople family of basis sets have been widely used in computational chemistry. A double-zeta Pople basis set is denoted by X-YZG, where X represents the number of GTOs used for inner shells, and Y and Z are the number of functions for the valance shell.[31] Triple-zeta basis sets can be defined by using a third value after the hyphen, such as 6-311G. Inclusion of d-type polarisation functions for heavy (non-hydrogen) atoms and p-type polarisation functions for hydrogen atoms is denoted using parentheses, such as (d,p). The addition of diffuse functions is represented by "+" for non-hydrogen atoms only and "++" for all atoms. An example of a Pople basis set is 6-311++G(d,p), which is a triple-zeta basis set that uses 6-primitives for the inner shell, includes diffuse functions for all atoms, as well as d- and p-type polarisation functions.

Dunning's correlation consistent basis sets are designed to systematically recover the electron-correlation energy and converge smoothly to a value that would be calculated from an infinitely large basis set known as the complete basis set (CBS) limit. These basis sets have been optimised for the use of wave-function methods such as coupled-cluster to obtain accurate results from a small number of primitive basis functions. Correlation consistent basis sets are represented by the notation cc-pVXZ, which indicates a "correlation consistent polarised split-valence X zeta basis set", where X is the zeta magnitude. The basis set can be modified with diffuse functions or addition of core functions by using aug-cc-pVXZ and cc-pCVXZ, respectively. The notation for correlation consistent basis sets can be abbreviated to ACVXZ, which would represent a correlation consistent basis set with diffuse and core functions with a zeta magnitude of X. ACVXZ basis sets are ideal for the accurate calculation of magnetic properties due to their inclusion of extra core basis functions. The correlation consistent basis sets also include further sets for third period elements with tighter d polarisation in the form cc-pV(X+d)Z.

Jensen produced a set of polarisation consistent basis sets in the form pc-N (N = 0-4), where N denotes the number of polarisation functions, as a way to converge the HF and DFT energies quicker than the correlation consistent basis sets.[32] Diffuse functions can be added using the

form aug-pc-N. Jensen subsequently developed polarisation consistent basis sets of the form pcSseg-N (here S indicates inclusion of additional core basis functions), which have been optimised for DFT calculations of shielding and spin-spin coupling properties that require greater flexibility in the basis set description of core electrons.[32] The pcSseg-N basis sets can also be augmented with diffuse functions in the form aug-pcSeg-N.

Ahlrichs' series of "def2" basis sets are a modification of the "def" basis sets. The "def2" prefix is followed by a description of the valence zeta magnitude and level of polarisation basis functions such as def2-SVP or def2-TZVP.[33] Unlike the Dunning's correlation consistent or Jensen's polarisation consistent, Ahlrichs' basis sets are not designed to systematically converge to the CBS limit.

Whilst the above families of basis sets utilise GTOs, there are also available STO basis sets. The tz2p basis set is a triple-zeta basis set with two polarisation functions, along with a minimal number of core basis functions.

2.7 Combination of Method and Basis Set

The accuracy of a calculated result increases with the use of more extensive methods and larger basis sets, so ideally, it is best to utilise the most extensive methods in combination with the largest basis sets, as shown in Figure 2.1. However, increasing either method, basis set, or system size will rapidly increase the computational cost, and this is often not possible.

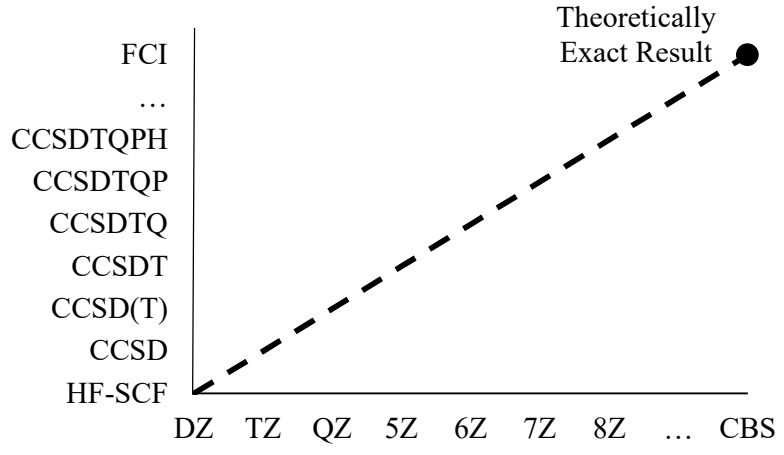

Figure 2.1: Expansion of method and basis set to approach the theoretically exact result.

It is possible to estimate HF-SCF and coupled-cluster basis set-limits from results with smaller correlation consistent basis sets. Due to the known convergence rate of the correlation consistent basis sets, calculated results can be used to extrapolate to the CBS limit for a given method. Feller has proposed an extrapolation of a property calculated with HF-SCF theory via:[35]

$$P_{\infty}^{\mathrm{HF}} = P_X - Ae^{-BX} \tag{2.9}$$

where X is the zeta value (cardinal number) of the correlation consistent basis set, P_X is the value calculated with that basis set, and P_{∞}^{HF} is the CBS value of the property. Using three consecutive basis set property values P_X, P_{X+1}, and P_{X+2}, yields the 3-point extrapolation property value:

$$P_{\infty}^{\mathrm{HF}} = \frac{P_{X+2}P_X - {P_{X+1}}^2}{P_X - 2P_{X+1} + P_{X+2}} \tag{2.10}$$

The contribution to a property associated with electron-correlation requires a different extrapolation equation due to the rate of convergence being different. Note that this is only the electron correlation contribution that is considered. That is, the single-double (SD) excitation contribution from CCSD is actually CCSD – HF-SCF, (T) is CCSD(T) – CCSD, T is CCSDT – CCSD(T) and so on. This can be extended to a FCI calculation, as seen in Figure 2.1. Extrapolation is performed by the equation:[36]

$$P_{\infty}^{\mathrm{corr}} = P_X^{\mathrm{corr}} - A^{\mathrm{corr}}X^{-3} \tag{2.11}$$

Combining two consecutive values provides the 2-point correlation extrapolation formula of:

$$P_{\infty}^{\mathrm{corr}} = \frac{P_{X+1}^{\mathrm{corr}}(X+1)^3 - P_X^{\mathrm{corr}}X^3}{(X+1)^3 - X^3} \tag{2.12}$$

For example, if basis sets aug-cc-pCVTZ (zeta = 3) and aug-cc-pCVQZ (zeta = 4) were used to extrapolate values calculated at the CCSD method, the extrapolation formula would become:

$$P_{\infty}^{\mathrm{corr}} = \frac{P_Q^{\mathrm{corr}}4^3 - P_T^{\mathrm{corr}}3^3}{4^3 - 3^3} \tag{2.13}$$

where $P_T^{\mathrm{corr}}$and P_Q^{corr} are the SD contributions to the calculated property from using the aug-cc-pCVTZ and aug-cc-pCVQZ basis sets, respectively, which can be represented as aug-cc-pCV[T,Q]Z. An assumption of this approach is that each component is independent and additive, which has been routinely used.[25]

2.8 Relativity

The effect of relativity is considered to be negligible for lighter elements, while it increases in significance with heavier elements. However, properties that depend on core electrons, such as magnetic properties, will be significantly impacted by relativistic effects. Therefore, it is important to consider the effect of relativity on nuclear shielding constants. Most quantum chemistry calculations tend to use the one-component non-relativistic Hamiltonian to solve the electronic Schrödinger equation. In order to expand results to a fully relativistic framework, the four-component Dirac-Coulomb Hamiltonian may be used instead of the non-relativistic Hamiltonian, although this tends to increase computational cost. To date, there are no available coupled-cluster implementations of four-component magnetic shielding or spin-rotation constant calculations, which requires the use of HF-SCF and DFT methods for the calculation of relativistic effects within a four-component approach.

2.9 Calculation Types

2.9.1 Geometry Optimisation and Vibrational Frequencies

Calculated properties of molecular systems are dependent on the geometry of the system. As such, it is important to perform geometry optimisation calculations beforehand to obtain an equilibrium geometry. Geometry optimisations perform searches on the potential energy surface (PES), which relates the energy of a molecule to the location of the nuclei. Stationary points on the PES represent equilibrium geometries (minima) and transition states (saddle points), with the global minimum of the PES corresponding to the equilibrium geometry, where the overall molecular energy is at its lowest. The search for the global minimum is achieved by calculating the gradient at an initial geometry, followed by a geometry change and recalculating the gradient. This procedure continues until a stationary point is found, at which point a vibrational frequency calculation is performed to determine if the given stationary point corresponds to a minimum instead of a saddle point. The distinction between a transition state and an equilibrium geometry has to do with the number of imaginary frequencies, for which there should be none for any minima. Vibrational frequency calculations are also used for thermochemical calculations such as zero-point energies as well as vibrational, rotational, and translational contributions to thermochemical effects which directly relate to property value differences between 0 K and 300 K.

2.9.2 Absolute Shielding and Spin Rotation Calculations

Absolute shielding and spin-rotation tensors have been calculated using gauge-including-atomic-orbitals (GIAOs) due to the dependence on the external magnetic field **B**. Additionally, all electron-correlation calculations have been performed to correlate all electrons (without using the frozen-core approximation) unless otherwise specified. Coupled-cluster absolute shieldings have been calculated in CFOUR,[37] which additionally calculates the spin-rotation tensor via eq. 1.6 after calculating the nuclear contribution to the spin-rotation tensor. Absolute shieldings calculated via DFT have been carried out using DALTON.[38]

2.9.3 Vibrationally Averaged Properties

Vibrational effects have been calculated using second-order perturbation theory, which is one of the most common ways to account for vibrational contributions to absolute shielding and spin rotation properties. Second-order perturbation theory expands the potential energy and property surfaces in terms of normal coordinates. Vibrational corrections have been accounted for using both CFOUR and DALTON programs for coupled-cluster and DFT calculations, respectively. The primary difference between how these separate programs calculate vibrational effects is the reference geometry employed for the surface expansion. In CFOUR, an equilibrium geometry is employed, whereas in DALTON, an effective geometry is used, which is first found by calculating gradients along the normal coordinates. The difference between these two approaches is expected to be small due to similar expansion techniques. Throughout this work, the default step size of both programs was used when calculating vibrational corrections to absolute shielding and spin-rotation tensors.

2.9.4 Relativistic Property Calculations

Relativistic corrections to shielding and spin-rotation tensors have been carried out with ReSpect 5.1.0.[39] For consistency, the relativistic and non-relativistic calculation were both carried out within the four-component relativistic framework, with the non-relativistic result achieved by increasing the speed of light which leads to the non-relativistic limit (within the four-component Hamiltonian). The difference of the two calculations then represents the overall effect of relativity (relativistic correction) on the molecular property. The four-component Dirac-Kohn-Sham Hamiltonian was selected for all four-component calculations.

Chapter 3:
NMR Shielding of H_2, HF, F_2, and FCl

3.1 Introduction

The calculation of the isotropic nuclear magnetic shielding in the H_2, HF, F_2, and FCl diatomics was first investigated as the smaller size of these molecules allows extensive calculations to be performed. While the main focus of this chapter is the calculation of ^{19}F nuclear shielding constants, an initial investigation of the ^{1}H shielding in H_2 allows for a benchmark study to investigate the accuracy of NMR shielding calculations. With only two electrons, a coupled-cluster single and double excitations (CCSD) calculation represents an FCI (exact) calculation.

3.2 Absolute ^{1}H Shielding in H_2

Calculation of the absolute ^{1}H shielding constant in H_2 with the FCI approach (CCSD) together with large basis sets, with a subsequent comparison against the recent experimentally determined gas-phase nuclear magnetic shielding of 26.293(5) ppm,[40] enables the methodology of calculating shielding constants used in this investigation to be validated. The experimental gas-phase shielding constant was determined at 300 K.

Calculation of the equilibrium shielding for H_2 has been performed at the CCSD/AVQZ optimised geometry (R_e = 0.74199 Å). The experimental geometry is 0.74151 Å.[12] In this work, an optimised geometry was employed to ensure a purely theoretical investigation, as well as benchmark the potential use of optimised geometries for the application of magnetic shielding since in practical theoretical investigations, an accurate experimental geometry is not always available. The nuclear shielding was calculated with AVXZ (X = D, T, Q, 5, 6, 7) basis sets at both the HF-SCF and CCSD levels of theory. Results from basis sets AVTZ to AV7Z are presented in Table 3.1. Since H_2 has no core electrons, the omission of core-functions in the AVXZ series of basis sets is appropriate for shielding calculations. The difference between the HF-SCF and the CCSD calculated shielding is the contribution from correlating single and double excitations (SD). Note that the CCSD shielding value is simply the sum of the separate HF-SCF and SD contributions for a particular basis set. The two contributions (HF-SCF and SD) were separately extrapolated to the CBS limit using eq. 2.10 and 2.12, respectively, with extrapolation from the largest basis set results (AV5Z to AV7Z for HF-SCF and AV6Z to

AV7Z for SD). The extrapolated contributions are summed to obtain an overall equilibrium shielding (Table 3.1).

Table 3.1: Equilibrium ^{1}H shielding in H_2 (ppm).

Contribution	AVTZ	AVQZ	AV5Z	AV6Z	AV7Z	CBS
HF-SCF	26.5032	26.5011	26.4806	26.4727	26.4702	26.4690
SD	0.1794	0.1778	0.1803	0.1811	0.1813	0.1818
Equilibrium Shielding						26.6507

Both the HF-SCF and SD results converge very smoothly with increasing the size of the basis set. It is unsurprising that the extrapolated CBS limit for both contributions is very similar to the AV7Z calculated values, as the 7Z basis set is already close to saturation. Note that the AV7Z basis set for hydrogen has up to *i* basis functions (16*s*7*p*6*d*5*f*4*g*3*h*2*i* primitives).

Sundholm and Gauss have previously reported a CCSD/8*s*4*p*3*d*2*f* (uncontracted) shielding of 26.6668 ppm (R_e = 0.74150 Å).[41] While the small difference in geometry would explain some of the deviation to the result presented in Table 3.1, the difference can largely be ascribed to basis set effects. The CCSD/ACV[6,7]Z result employs much larger basis sets than those used by Sundholm and Gauss, which is similar in magnitude to the AV5Z basis set (CCSD/AV5Z yields 26.6609 ppm). Analysis of basis set convergence highlights the basis set effect and provides support for the conclusion that the current CCSD/CBS (summation of HF-SCF/ACV[5,6,7]Z and CCSD/ACV[6,7]Z) value is more accurate. From results in Table 3.1, it is noted that the HF-SCF contribution converges from above (to a smaller value) while the SD contribution converges towards a larger value. However, the SD contribution is smaller in magnitude, and so the net CCSD values converge from above towards an asymptotic limit of a smaller value, which indicates that the CCSD/AV5Z or CCSD/8*s*4*p*3*d*2*f* result (with a finite basis set) will be larger in magnitude than the true equilibrium value. The analysis is consistent with the CCSD/CBS value of 26.6507 ppm being smaller than the CCSD/AV5Z or CCSD/8*s*4*p*3*d*2*f* results. The CCSD/CBS results for the magnetic shielding in H_2 are considered to the most accurate to date.

The calculated equilibrium value represents a non-relativistic, 0 K stationary molecule system that does not accurately represent an experimental value determined at a finite (non-zero) temperature. To account for this, vibrational and temperature effects were calculated. These were calculated with the CCSD method, at geometries optimised at the same CCSD/AVXZ

level of theory, where X is the zeta magnitude used for the corresponding anharmonic vibrational calculation. Results are presented in Table 3.2. Temperature effects correspond to the effect on the geometry and molecular properties between 0 K and a finite temperature. In the work presented here, a finite temperature of 300 K was employed, which is consistent with conditions in many experimental studies.

Table 3.2: CCSD Vibrational averaging and temperature effects on the ^{1}H shielding in H_2 (ppm).

Contribution	AVQZ	AV5Z	AV6Z	AV7Z	CBS
Vibrational averaging	-0.3335	-0.3326	-0.3324	-0.3322	-0.3319
Temperature (300 K)	-0.0393	-0.0392	-0.0391	-0.0390	-0.0387

Once again, the basis set convergence throughout these results is very smooth. Although the difference between each basis set is constant (2×10^{-4} ppm and 1×10^{-4} ppm for vibrational averaging and temperature effects, respectively), due to the small size of the variance between results, this is not a concern. In other words, these contributions have almost completely converged to the asymptotic limit. This is supported by the CBS extrapolated values being very close to the calculated results.

It is worth noting that the temperature effect on the absolute nuclear shielding (i.e. the change in nuclear shielding between a 0 K and a 300 K calculation) is very small and almost an order of magnitude less than that of the vibrational averaging effects. The combined effect is -0.3706 ppm. Sundholm and Gauss have carried out a detailed study of rovibrational effects of shielding constants in H_2, reporting a value of -0.3686 ppm (296 K),[41] which may be corrected to -0.3691 ppm at 300 K.[12] Sundholm and Gauss' rigours approach is expected to be more accurate than the method used here due to the calculation of rovibrational averaging as opposed to the vibrational averaging results in Table 3.2. Despite this, the deviation between the the CFOUR calculated vibrational effect and Sundholm and Gauss' reported rovibrational effect on shielding is only 0.0015 ppm.

Finally, relativistic effects have been calculated using the PBE0 density functional with both dyall-aug-vtz and dyall-aug-vqz basis sets (Table 3.3). The effect that relativity has on the absolute shielding has been calculated by taking the difference of a fully relativistic four-component absolute shielding and a non-relativistic absolute shielding calculated at the same level of theory (rel-nrel).

Table 3.3: PBE0 Relativistic effects on the ^{1}H shielding in H_2 (ppm).

Basis Set	Relativistic (rel)	Non-relativistic (nrel)	rel-nrel
dyall-aug-vtz	26.7345	26.7323	0.0022
dyall-aug-vqz	26.6830	26.6808	0.0022

It is unsurprising that the relativistic effects for the ^{1}H nuclei are very small, as the smaller the nuclear charge, the less the nuclear shielding is affected by relativity. However, consideration of relativity is of importance, being half of the experimental error bar alone in this instance. There is a basis set dependence in the calculated relativistic (rel) and non-relativistic (nrel) shielding constants; however, the difference between the two (rel-nrel) appears to be independent of the basis set. This could be considered a fortuitous cancellation of errors. Alternatively, it may be possible that the relativistic effects on the absolute shielding have a sizeable dependence on the basis set used; however, as the relativistic effects on the ^{1}H shielding are small, the level of basis set dependence is negligible. Therefore, dependence on the basis set used will also be investigated further for ^{19}F shielding constants.

After obtaining the equilibrium shielding, vibrational averaging, temperature, and relativistic effects, these values are added together to provide a relativistic, vibrationally averaged, absolute nuclear shielding constant that can be compared with experiment (Table 3.4).

Table 3.4: Calculated ^{1}H absolute shielding in H_2 (ppm).

Contribution	AV5Z	AV6Z	AV7Z	CBS/Best Value
HF-SCF	26.4806	26.4727	26.4702	26.4690
SD	0.1803	0.1811	0.1813	0.1818
Vibrational Effects		CCSD/AV[6+7]Z		-0.3319
Temperature Effects (300 K)		CCSD/AV[6+7]Z		-0.0387
Relativistic Effects		PBE0/dyall-aug-vqz		0.0022
Total Absolute Shielding				26.2824
Experimental Shielding				26.293(5)[40]

Summation of all contributions leads to an absolute shielding of 26.2824 ppm the proton in H_2, with an uncertainty of ±0.0002 ppm as a result from the convergence of the equilibrium, vibrational and relativistic effects. This is in close agreement with the experimental value of 26.293(5) ppm.[40] Sundholm and Gauss determined a non-relativistic CCSD/8*s*4*p*3*d*2*f* result of 26.2983 ppm (296 K),[41] which may be corrected to 26.2977 ppm at 300 K.[12] That result is

within the error bars of the experimental value. However, the addition of relativistic effects (0.0022 ppm) leads to a value of 26.2999 ppm that is outside the upper range of the experimental uncertainty. As discussed above, the equilibrium CCSD/8*s*4*p*3*d*2*f* value is too large (compared to the basis set limit), and hence the excellent agreement of the CCSD/8*s*4*p*3*d*2*f* value with the experimental value arises from some fortuitous cancellation of errors.

The rovibrational averaging treatment from Sundholm and Gauss may be considered more rigorous than the vibrational averaging approach employed in the current work. If their rovibrational averaging (-0.3691 ppm) is used in place of the CFOUR calculated contribution (-0.3706 ppm), then an overall nuclear magnetic shielding value of 26.2839 ppm is obtained, which is marginally closer to the experimental value.

The fully calculated CCSD/CBS value determined in the current work differs by 0.011 ppm from the experimental value of 26.293(5) ppm,[40] and lies only 0.006 ppm outside the lower limit of the experimental uncertainty. The deviation of only 0.04% to the current experimental shielding is considered excellent, especially considering that an optimised geometry rather than experimental geometry has been employed. Therefore, the methodology employed in the computational approach in completely deriving an absolute shielding constant for a nucleus may be considered valid. While the majority of calculated components that make up the total magnetic shielding are of a large enough magnitude to be considered important, the relativistic effects in the case of H_2 shielding is less than the deviation between theory and experiment. As discussed above, this may be due to the overall relativistic effects of H_2 being small. Therefore, the importance of relativistic effects will be further investigated in additional molecules to understand the true importance of considering relativity.

3.3 Absolute ^{1}H Shielding in HF

The approach employed for calculating isotropic nuclear magnetic shielding constants of H_2 was then extended to the HF molecule. For fluorine, specific core basis functions were included in all calculations, while methods could be extended beyond CCSD as a result of the greater electron count in HF compared to H_2. Geometries were optimised at the all-electron CCSD(T)/ACVQZ level of theory (R_e = 0.91724 Å). The experimental bond distance is 0.9150 Å. Consideration of electron-correlation method contribution was used again, investigating the

contribution of higher excitations to the equilibrium shielding constants with coupled-cluster calculations up to CCSDTQP being carried out. Results are collated in Table 3.5

Table 3.5: Equilibrium ^{1}H shielding in HF (ppm).

Contribution	ACVDZ	ACVTZ	ACVQZ	ACV5Z	ACV6Z	ACV7Z	CBS
HF-SCF	29.291	28.362	28.204	28.112	28.084	28.073	28.067
SD	0.806	0.773	0.646	0.616	0.602	0.598	0.591
(T)	0.073	0.069	0.070	0.070	0.070		0.070
T	0.005	0.007	0.007				0.008
Q	0.011	0.011					0.012
P							0.001[(a)]
Equilibrium Shielding							28.749

(a) tz2p basis set result.

Once again, smooth and rapid convergence has been obtained for all equilibrium excitation contributions. This is seen especially in the larger methods of CCSD(T) to CCSDTQ, where contributions are barely changing upon increasing the size of the basis set (i.e. the contribution is already converged).

A clear trend can also be noted, where each successive increase in the coupled-cluster expansion (method) generally yields a decreased contribution to the absolute shielding by approximately an order of magnitude. Although this seems to not be the case due to the triple excitation contribution being less than the quadruple excitation contribution, this is purely due to the perturbative triples already accounting for a large portion of the triple excitation contribution. The trend is evident if the combined (T) and T contributions are considered. Therefore, although pentuple (P) excitations are calculated with a smaller tz2p basis set, the level of contribution can be considered to be valid since high precision is not critical due to the small magnitude of the contribution. It can be expected that contributions from higher excitations will be negligible, leading to an uncertainty in the equilibrium shielding of much less than ±1 ppm. It can be concluded that for larger and more complex molecules, full treatment of extensive methods such as full triples or quadruples, although beneficial in terms of convergence and precision, may not be critical.

Sundholm *et al*. have reported CCSD(T)/8*s*4*p*3*d*2*f* results, with an equilibrium value of 29.01 ppm[12] which is larger than the CCSD(T)/ACV5Z value in Table 3.5 (28.749 ppm). The CCSD(T)/CBS value is 28.728 ppm (summing the HF-SCF, SD, and (T) contributions from

Table 3.5), which indicates that the Sundholm value is not converged within 0.25 ppm of the basis set limit.

Similar to that of H_2, vibrational and temperature effects were calculated at individually optimised geometries. However, unlike H_2, these contributions were calculated with the more extensive CCSD(T) method to give greater accuracy to the calculated effects (Table 3.6).

Table 3.6: CCSD(T) Vibrational averaging and temperature effects on the ^{1}H shielding in HF (ppm).

Contribution	ACVTZ	ACVQZ	ACV5Z	ACV6Z	CBS
Vibrational averaging	-0.313	-0.322	-0.321	-0.322	-0.324
Temperature (300 K)	-0.038	-0.037	-0.037	-0.037	-0.037

Unlike the results for H_2, the calculated vibrational averaging effects do not converge smoothly. A possible cause of this is the number of separate steps that go into calculating the vibrational corrections; geometry optimisation, then the anharmonic frequency calculation, followed by the final property calculation. These contributions could exhibit different rates of convergence. Therefore, it is not unreasonable to suspect that small variations in these calculations can lead to a lack of smooth convergence. In this case, the variation between the calculated results is very small (1×10^{-3} ppm), so this issue does not have a major effect on the extrapolated CBS limit result. Similar to the ^{1}H shielding in H_2, temperature effects on the absolute nuclear shielding are an order of magnitude smaller than the vibrational averaging effects. Sundholm *et al.* reported rovibrational and temperature (300 K) corrections of -0.323 and -0.035 ppm,[12] respectively, which are in very close agreement with the CCSD(T)/ACV[5,6]Z values reported in Table 3.6.

Although relativistic effects were shown to be very small for the ^{1}H nucleus in H_2, it is possible the magnitude of effect will increase when the H atom is a part of a larger molecule. The same procedure was conducted as with H_2, where the difference between a relativistic nuclear shielding and a non-relativistic nuclear shielding, calculated at the same level of theory, was used to determine the relativistic effect. These calculations have been performed with core basis functions added to the fluorine basis sets due to the presence of fluorine; however, this does not affect the results of ^{1}H (Table 3.7).

Table 3.7: PBE0 Relativistic effects on the ^{1}H shielding in HF (ppm).

Basis Set	Relativistic (rel)	Non-relativistic (nrel)	rel-nrel
dyall-aug-cvtz	29.772	29.627	0.145
dyall-aug-cvqz	29.443	29.296	0.147

Here the values for relativistic effects are much greater than in H_2. This is most likely due to the presence of a much heavier nucleus (^{19}F) not only being a part of the molecule but within close proximity to the ^{1}H nucleus. Where relativistic effects in H_2 were near negligible, they now make up 0.5% of the total shielding, which must be considered when high levels of precision are desired. There is a very small dependence on basis set. Unlike the relativistic effects calculated for the ^{1}H shielding in H_2, the relativistic effects on the ^{1}H shielding in HF are large enough that a dependence on basis set can be observed. However, the dependence on basis set is two orders of magnitude less than that of the total relativistic effects on shielding and thus may be considered negligible.

Nakatsuji *et al*. and Malkin *et al*. have previously investigated relativistic spin-orbit effects on the hydrogen shielding of HF, which yielded values of 0.18 ppm[42] and 0.16 ppm,[43,44] respectively, which are consistent with the PBE0 results calculated here. Sundholm *et al*. questioned the magnitude of the relativistic effect based on the close agreement (within 0.05 ppm) of their non-relativistic CCSD(T) results and the experimental value.[12] However, as discussed above, their CCSD(T) calculated value deviates by 0.26 ppm from the CBS value (28.749 ppm) given in Table 3.5. That serves to refute their suggestion that the calculated relativistic effect is too large but rather indicates that the discrepancy is due to their unconverged equilibrium shielding.

An absolute ^{1}H nuclear shielding in HF can be obtained by combining the extrapolated CBS equilibrium values for each coupled-cluster expansion, vibrational averaging, temperature, and relativistic effects. Results are presented in Table 3.8.

Table 3.8: Calculated ^{1}H absolute shielding in HF (ppm).

Contribution	Method/Basis	CBS/Best Value
HF-SCF	ACV[5,6,7]Z	28.067
SD	ACV[6,7]Z	0.591
(T)	ACV[5,6]Z	0.070
T	ACV[T,Q]Z	0.008
Q	ACV[D,T]Z	0.012
P	tz2p	0.001
Vibrational Effects	CCSD(T)/ACV[5,6]Z	-0.324
Temperature Effects (300 K)	CCSD(T)/ACV[5,6]Z	-0.037
Relativistic Effects	PBE0/dyall-aug-cvqz	0.147
Total Absolute Shielding		28.535
Experimental Shielding		28.53(20)

The fully calculated value of 28.535 ppm, with an expected uncertainty of ±0.005 ppm, is in excellent agreement with the experimentally derived value of 28.53 ± 0.2 ppm (δ(HF) = 2.10 ppm,[45] $\sigma(CH_4)$ = 30.633 ppm[40]), with a deviation from experiment of only 0.01 ppm. As discussed above, the vibrational averaging effect exhibits a non-monotonic convergence that suggests that the vibrational averaging contribution may lead to increased uncertainty in the calculated value. However, if in place of the CBS value (-0.324 ppm) the AV6Z (-0.322 ppm) or AV5Z (-0.321 ppm) values were employed, then the absolute nuclear shielding is 28.537 or 28.539 ppm, respectively, which remain well within the experimental uncertainty. It is suggested that a value of 28.53 ± 0.2 ppm represents the true value of the nuclear magnetic shielding of ^{1}H in HF.

Sundholm *et al*. reported a CCSD(T) value inclusive of rovibrational effects of 28.842 ppm,[12] although they neglected relativistic effects. Addition of relativistic effects (28.989 ppm) worsens agreement with experiment. Again, this is due to their unconverged equilibrium value.

The ^{1}H nuclear shielding results for H_2 and HF demonstrate that the additive procedure for contributions to the absolute nuclear shielding yields precise ^{1}H nuclear shielding constants when each component is treated with large basis sets and extensive methods. The same approach was subsequently used to obtain ^{19}F nuclear shielding constants.

3.4 Absolute ^{19}F Shielding in HF

All calculations that were carried out for the ^{1}H shielding in HF were also carried out for ^{19}F nuclear shielding. Therefore, the equilibrium nuclear shielding was investigated with extensive coupled-cluster methods and large basis sets (Table 3.9).

Table 3.9: Equilibrium ^{19}F shielding in HF (ppm).

Contribution	ACVDZ	ACVTZ	ACVQZ	ACV5Z	ACV6Z	ACV7Z	CBS
HF-SCF	419.136	414.615	414.237	413.989	413.915	413.897	413.891
SD	5.007	4.719	5.028	5.140	5.200	5.214	5.238
(T)	0.131	0.474	0.483	0.474	0.480		0.488
T	-0.048	-0.150	-0.172				-0.188
Q	-0.024	-0.036					-0.041
P							-0.003[(a)]
Equilibrium Shielding							419.384

(a) tz2p basis set result.

It is unsurprising that the overall equilibrium ^{19}F shielding is much larger in magnitude than the ^{1}H shielding. The increased number of electrons and electronegativity provides a much higher level of magnetic protection (shielding). Basis set convergence is very smooth for most of the coupled-cluster contributions. Additionally, the trend of decreasing contribution to the absolute shielding upon increasing excitation level is very prominent here. Once again, the P contributions to the equilibrium shielding constants are of almost negligible size. This allows the assumption that hextuple (H) and higher excitations are negligible, which is favourable due to the exceptionally large computational resources required to perform such calculations.

Sundholm *et al*. have reported a CCSD(T) calculated value of 419.075 ppm with basis sets of 8*s*4*p*3*d*2*f* (H) and 15*s*11*p*3*d*2*f* (F),[12] which can be compared to the CCSD(T)/CBS value of 419.617 ppm (Table 3.9). In the discussion of H_2 results above, it was indicated that the 8*s*4*p*3*d*2*f* basis set for H is similar to the AV5Z basis set. Here the CCSD(T)/ACV5Z value is 419.603 ppm, which still deviates significantly from the CCSD(T) result of Sundholm *et al*. It is concluded that the remaining deviation is a geometry effect, whereby Sundholm *et al*. used an experimental geometry while the present results used an all-electron CCSD(T)/ACVQZ calculated geometry.

Vibrational averaging and temperature effects on the ^{19}F magnetic shielding in HF were obtained alongside the investigation of ^{1}H magnetic shielding using the same geometries, methods, and basis sets (Table 3.10).

Table 3.10: CCSD(T) Vibrational averaging and temperature effects on the ^{19}F shielding in HF (ppm).

Contribution	ACVTZ	ACVQZ	ACV5Z	ACV6Z	CBS
Vibrational averaging	-9.233	-9.255	-9.268	-9.283	-9.304
Temperature (300 K)	-0.375	-0.373	-0.373	-0.373	-0.373

For CCSD(T) vibrational corrections, the largest basis set used was ACV6Z, which yielded an overall vibrational correction to the absolute shielding of -9.283 ppm. The vibrational correction contribution to the ^{19}F shielding is much larger than that for the ^{1}H shielding in HF, which was -0.324 ppm. This would be heavily influenced by the high sensitivity of ^{19}F shielding to environmental changes. That is, a slight bond stretch will cause a much greater change to the ^{19}F shielding than it would for ^{1}H shielding. The convergence of the vibrational corrections on the absolute ^{19}F shielding is once again not ideal. The lack of convergence appears to propagate between the ACV5Z and ACV6Z results for both the ^{19}F shielding and the ^{1}H shielding. As both shielding constants have errors originating from the same results, the hypothesis of errors within earlier calculations creating large deviations in final vibrational corrections is sound and has led to a possible overestimation within the extrapolated CBS value.

Sundholm *et al*. calculated a rovibrational contribution of -10.00 ppm with a temperature effect (to 300 K) of -0.42 ppm.[12] The combined contribution of -10.42 ppm is larger in magnitude than -9.74 ppm calculated in the present work (Table 3.10). Relativistic effects were calculated using the dyall-aug-cvqz basis set with the PBE0 functional (Table 3.11). Here, the addition of core basis functions to the basis set is necessary due to fluorine possessing core electrons.

Table 3.11: PBE0 Relativistic effects on the ^{19}F shielding in HF (ppm).

Basis Set	Relativistic (rel)	Non-relativistic (nrel)	rel-nrel
dyall-aug-cvtz	417.330	412.764	4.567
dyall-aug-cvqz	417.344	412.741	4.602

The effect of relativity on the ^{19}F magnetic shielding in HF is much greater than that for ^{1}H magnetic shielding in both H_2 and HF. This is due to the increased atomic number (and mass) of the fluorine atom, which directly influences relativistic effects. The relativistic (rel), non-relativistic (nrel), and the total relativistic effects (rel-nrel), have minimal dependence on the basis set. It is important to note that total relativistic effects are as much as 1% of the equilibrium shielding and are much larger than the temperature effects for the same nucleus. Therefore, it is not possible to neglect the effect of relativity on ^{19}F magnetic shielding if accurate nuclear magnetic shielding constants are to be obtained.

The calculated contributions and effects to the ^{19}F shielding are summed to obtain a fully calculated absolute ^{19}F magnetic shielding in HF (Table 3.12).

Table 3.12: Calculated ^{19}F absolute shielding in HF (ppm).

Contribution	Method/Basis	CBS/Best Value
HF-SCF	ACV[5,6,7]Z	413.891
SD	ACV[6,7]Z	5.283
(T)	ACV[5,6]Z	0.488
T	ACV[T,Q]Z	-0.188
Q	ACV[D,T]Z	-0.041
P	tz2p	-0.003
Vibrational Effects	CCSD(T)/ACV[5,6]Z	-9.304
Temperature Effects (300K)	CCSD(T)/ACV[5,6]Z	-0.373
Relativistic Effects	PBE0/dyall-aug-cvqz	4.602
Total Absolute Shielding		414.310
Experimental Shielding		409.6(10)[12]

Combining all the components of the absolute shielding results in a total absolute shielding of 414.310 ppm. Sundholm *et al.* have reported a semi-experimentally derived ^{19}F magnetic shielding in HF of 409.6 ± 1.0 ppm.[12] Our calculated value of 414.310 ppm deviates from this semi-experimental shielding by 4.7 ppm. The deviation is greater both in magnitude and relative percentage compared to the case of the ^{1}H magnetic shielding constant in HF. The difference could possibly be due to some uncertainty in the relativistic effects, propagating from their dependence on the chosen DFT functional, as well as incomplete methods and basis sets. However, the shielding reported by Sundholm *et al.* is a non-relativistic shielding, stating that relativistic effects to the diamagnetic shielding would be approximately 1 ppm, while the effect towards the paramagnetic shielding was more difficult to predict. Addition of the

relativistic effects calculated here to the Sundholm *et al.* semi-experimental shielding yields a value of 414.20 ± 1.0 ppm. The fully calculated shielding in Table 3.12 deviates from the experimental value by only 0.11 ppm, which is well within experimental error.

An alternative experimental ^{19}F magnetic shielding of HF may be derived from recently reported chemical shifts. Makulski has reported an updated SiF_4 chemical shift relative to $CFCl_3$ of 170.170(2) ppm extrapolated to the zero-density limit.[7] Combining this updated SiF_4 chemical shift along with the chemical shift of HF relative to SiF_4 of -46.85(35) ppm by Hindermann and Cornwell[14] yields an experimental HF chemical shift relative to $CFCl_3$ of -217.02(35) ppm. Combining the chemical shift relative to $CFCl_3$ with the absolute ^{19}F shielding in $CFCl_3$ of 197.07 ppm[25] with eq. 1.1 leads to an absolute ^{19}F shielding of 414.09(35) ppm in HF. The updated nuclear shielding constant is in excellent agreement with the fully calculated ^{19}F in HF reported here, with a deviation of only 0.22 ppm that is within the experimental uncertainty. The self-consistency of these two experimental values, derived from spin-rotation constants (414.20(10) ppm) and chemical shifts (414.09(35) ppm), provides confidence in the revised experimental value.

The high precision of the calculations used along with the large agreement with previously reported experimental chemical shifts and semi-experimental non-relativistic shielding constants enables the conclusion that the ^{19}F absolute shielding constant for HF reported here is the most accurate to date, with a conservative estimate of the uncertainty of ±0.5 ppm.

3.5 Absolute ^{19}F Shielding in F_2

The F_2 molecule represents a challenging case for computational methods due to the increased number of electronegative F atoms. The increase in mass and electron count from HF means that higher coupled-cluster excitation contributions cannot be calculated with such large basis sets. However, as shown with HF, these contributions are relatively small in magnitude. Calculations for F_2 have been carried out similar to that of HF calculations, utilising a CCSD(T)/ACVQZ optimised geometry (R_e = 1.41173 Å), with all shielding constants calculated with ACVXZ basis sets. Results are presented in Table 3.13.

Table 3.13: Equilibrium ^{19}F shielding in F_2 (ppm).

Contribution	ACVDZ	ACVTZ	ACVQZ	ACV5Z	ACV6Z	ACV7Z	CBS
HF-SCF	-148.618	-158.185	-165.679	-168.700	-169.615	-169.800	-169.847
SD	15.454	-1.539	-3.303	-3.650	-3.781		-3.960
(T)	-12.148	-14.476	-15.145	-15.387	-15.469		-15.582
T	-2.896	-3.831	-3.948				-4.033
Q	-1.547						-1.547
Equilibrium Shielding							-194.969

The resulting total equilibrium shielding is -194.969 ppm. As this shielding constant is negative in sign, it means that the presence of electrons enhances the effect that the magnetic field has on the nucleus. An exception to the decreasing method contribution is shown between the SD and (T) contributions. A reason behind this change of trend is not entirely known; however, it is likely due to the increased electron density within the molecule. Both T and Q contributions here are sizeable; however, due to the increased electron count and vast computational cost, P excitations were not able to be obtained. The magnitude of the Q contribution could be a result of the inaccuracy from the small DZ basis set used. As such, the uncertainty in the equilibrium shielding is conservatively estimated to be 2-3 ppm. Sundholm *et al*. reported a CCSD(T) value of -188.03 ppm[12] that is within 1.4 ppm of the CBS limit (CCSD(T)/CBS value is -189.389 ppm). However, it is the neglect of higher-level excitations that is more problematic, with T and Q contributions amounting to -5.580 ppm (Table 3.13).

Vibrational averaging and temperature effects on the nuclear shielding are expected to be large in F_2 due to the vibrational stretching frequency being larger than that in HF, which causes larger bond changes that cause greater shielding effects. Results are presented in Table 3.14.

Table 3.14: CCSD(T) Vibrational averaging and temperature effects on the ^{19}F shielding in F_2 (ppm).

Contribution	ACVTZ	ACVQZ	ACV5Z	ACV6Z	CBS
Vibrational averaging	-28.786	-28.246	-27.996	-27.952	-27.891
Temperature (300 K)	-4.126	-4.069	-3.996	-3.977	-3.950

The calculated CCSD(T)/ACV[5,6]Z vibrational corrections and temperature effects within Table 3.14 are sizable, at -27.891 ppm and -3.950 ppm, respectively. The vibrational corrections are actually larger in magnitude than that of the perturbative triple, (T), excitation

contribution to the equilibrium shielding, while temperature effects alone are of similar magnitude to the contribution of full triples, T. The importance of these contributions is clear and indicates the necessity to include these effects when trying to obtain accurate absolute isotropic shielding constants. Unlike the vibrational corrections within HF, the calculated vibrational corrections towards the ^{19}F nucleus in F_2 converge very well.

Sundholm *et al*. reported calculated rovibrational corrections at -30.87 ppm and temperature effects (at 300 K) to be -4.69 ppm for an overall effect of -35.56 ppm to the absolute shielding.[12] This deviates from the calculated effects here by 3.72 ppm. The deviation may be attributed to Sundholm *et al.* calculating rovibrational corrections as opposed to the purely vibrational corrects reported here. This deviation is somewhat accounted for by the consideration of higher excitations within the equilibrium shielding as discussed above.

The effect of relativity on ^{19}F shielding in F_2 is expected to increase compared to those in HF, just as the effects on the ^{1}H shielding in HF were larger than those in H_2. Results are presented in Table 3.15. Once again, the PBE0 functional has been used with dyall-aug-cvtz and dyall-aug-cvqz basis sets.

Table 3.15: PBE0 Relativistic effects on the ^{19}F shielding in F_2 (ppm).

Basis Set	Relativistic (rel)	Non-relativistic (nrel)	rel-nrel
dyall-aug-cvtz	-236.745	-242.512	5.768
dyall-aug-cvqz	-237.124	-242.865	5.740

The relativistic effects on the ^{19}F absolute shielding constants are slightly larger than the effects on ^{19}F shielding constants in HF. This trend does not follow what was seen in the ^{1}H shielding within H_2 and HF, which increased magnitudes in size upon fluorination. This is likely due to the relativistic effects to the ^{19}F shielding within HF already being substantial. Nonetheless, the presence of an additional fluorine atom seems to slightly increase the effect that relativity has on the absolute shielding. The basis set dependence of the calculated relativistic effects is of the same magnitude as that seen for the ^{19}F nucleus in HF.

As with the other studied nuclei, all these effects may be combined to obtain a total absolute shielding constant of F_2 at the CCSD(T)/ACVQZ optimised geometry (Table 3.16).

Table 3.16: Calculated ^{19}F absolute shielding in F_2 (ppm).

Contribution	Method/Basis	CBS/Best Value
HF-SCF	ACV[5,6,7]Z	-169.847
SD	ACV[5,6]Z	-3.960
(T)	ACV[5,6]Z	-15.582
T	ACV[T,Q]Z	-4.033
Q	ACVDZ	-1.547
Vibrational Effects	CCSD(T)/ACV[5,6]Z	-27.891
Temperature Effects (300 K)	CCSD(T)/ACV[5,6]Z	-3.950
Relativistic Effects	PBE0/dyall-aug-cvqz	5.740
Total Absolute Shielding		-221.070
Experimental Shielding		-221.93 ± 1[46]

The final fully calculated absolute shielding in F_2 is -221.070 ppm. This is in excellent agreement with the derived experimental value of -221.93 ± 1 ppm ($\delta(F_2)$ = -419 ± 1 ppm,[46] $\sigma(CFCl_3)$ = 197.07 ppm[25]) and within the 1 ppm experimental uncertainty. The good agreement can be attributed to consideration of higher excitations as well as the utilisation of large basis sets for smaller excitation contributions such as CCSD(T)/ACV6Z. Additionally, the consideration of all effects to the absolute shielding along with smooth convergence for all applicable contributions has led to the close agreement between theory and experiment. The level of uncertainty in the final absolute shielding is estimated to be ±2.0 ppm as a result of the unconverged and large Q contributions in the equilibrium shielding.

Jameson *et al.*[15] have reported an alternative ^{19}F chemical shift in F_2 of -595.96 ± 0.03 ppm relative to SiF_4, which results in an absolute magnetic shielding of -228.72 ± 0.032 ppm ($\sigma(SiF_4)$ = 170.170(2) + 197.07 = 362.870(2) ppm).[7,25] This nuclear shielding deviates by 7.65 ppm from the fully calculated shielding in Table 3.16. The deviation between the Jameson *et al.* and the fully calculated shielding constants likely arises due to the impact of higher excitations on the equilibrium shielding. Sundholm *et al*. have reported a non-relativistic CCSD(T) calculated value of -234.7 ppm.[12] Augmenting the Sundom *et al.* shielding with the relativistic corrections presented in Table 3.15 yields a shielding of -229.0 ppm, which is much closer to the shielding derived by experimental data from Jameson *et al.* It is suggested that the differences in theoretical shielding constants here and from Sundholm *et al.* are a result of geometry, where Sundholm *et al.* used an experimental geometry. Harding *et al.*[23] has investigated the relationship between the level of theory used in geometry optimisation and calculated shielding, with the difference in shielding between a CCSD(T)/VTZ and a

CCSD(T)/VQZ optimised geometry being almost 7 ppm. The shielding gradient in F_2 is approximately 3000 ppm/Å. That is, a deviation in the F–F bond distance of 0.001 Å will change the shielding constant by 3 ppm. Therefore, deviation in shielding constants between the use of an experimental and optimised geometry is unsurprising and a cause of great difficulty in the determination of accurate F_2 absolute shielding.

3.6 Absolute ^{19}F Shielding in FCl

The series of successive fluorination of diatomics was extended to include FCl. FCl has a much greater electron count than any molecule discussed thus far and, therefore, will be more challenging to calculate accurately. The FCl molecule was optimised at the CCSD(T)/ACVQZ level of theory (R_e = 1.62912 Å) for use in the equilibrium and relativistic calculations. Results are presented in Table 3.17.

Table 3.17: Calculated ^{19}F absolute shielding in FCl (ppm).

Contribution	Method/Basis	CBS/Best Value
HF-SCF	ACV[Q,5,6]Z	691.646
SD	ACV[5,6]Z	-41.252
(T)	ACV[Q,5]Z	-0.088
T	ACV[D,T]Z	-0.299
Vibrational Effects	CCSD(T)/ACV[Q,5]Z	-6.952
Temperature Effects (300 K)	CCSD(T)/ACV[Q,5]Z	-1.126
Relativistic Effects	PBE0/dyall-aug-cvqz	-1.003
Total Absolute Shielding		640.926
Experimental Shielding		640.97(10)

Calculation of Q contributions was not possible due to the large electron count of the FCl molecule and the corresponding requirement for very extensive computing resources; however, the small magnitude of the (T) and T excitation contributions shows that contributions of higher excitations to the overall shielding would be small (10^{-2} ppm), with a conservative estimate of a maximum of 0.05 ppm. Large ACV6Z basis set calculations were performed for the HF-SCF and SD contribution calculations and make up most of the overall shielding at 691.649 ppm and -41.252 ppm, respectively. The vibrational and temperature effects to the shielding are -6.952 ppm and -1.126 ppm, respectively, being much smaller than in F_2 and of similar magnitude to the ^{19}F shielding constant in HF. The relativistic correction of -1.003 ppm is much

smaller than for the ^{19}F shielding constants in HF and F_2. Interestingly, the relativistic effects here are of negative sign, whereas these effects are of positive sign in HF and F_2. This may be caused by the presence of the much heavier chlorine atom, whereas in HF and F_2, the ^{19}F atom was the heaviest atom in the molecule. A total calculated absolute ^{19}F shielding in FCl of 640.926 ppm was obtained with an expected uncertainty of ±0.2 ppm. The experimental value of 640.97 ± 0.1 ppm (δ(FCl) = -443.90 ppm ± 0.1,[7,47] $\sigma(CFCl_3)$ = 197.07 ppm[25]) once again agrees exceptionally well with the shielding calculated here with less than 0.05 ppm deviation and well within experimental error. This demonstrates that the methodology used throughout this chapter is effective even for heavier molecules where higher coupled-cluster excitations and large basis sets cannot readily be used.

3.7 Summary

The ^{1}H and ^{19}F absolute shielding constants have been evaluated in the H_2, HF, F_2, and FCl diatomic series. Most of the deviations between theory and experiment are extremely small, with theory being less than 1 ppm from experimental chemical shifts even in the case of the ^{19}F shielding in the heavier FCl diatomic. The only outlier is the ^{19}F absolute shielding in HF, which deviates from non-relativistic semi-experimental shielding constants by less than 5 ppm; however, is corrected to within experimental error when calculated relativistic effects are applied to the semi-experimental shielding.

The results reported throughout this chapter show that the technique of obtaining CBS values for separate contributions to the equilibrium shielding, then applying vibrational averaging, temperature, and relativistic effects is not only sound but also necessary to obtain experimentally accurate results. This methodology will be applied to larger fluorine-containing molecules in the following chapter.

Chapter 4:
Extending the ^{19}F Absolute Shielding Scale

4.1 Introduction

After analysis of the ^{19}F shielding constants for diatomic molecules, a set of larger molecules was chosen to be investigated. The molecules selected were the series H_2O, HOF, and F_2O, as well as CH_3F and FCN. These particular molecules were selected due to their lack of conformational flexibility, which decreases the complexity of calculations. Despite this, they are larger and more complex than the previously calculated diatomic molecules. Calculation run times for these molecules are presented in Table 4.1, which illustrates the effect that increased molecular complexity has on computational cost.

Table 4.1: Duration of calculation run time between molecules and methods (hours).

Molecule	CCSD[(a)]	CCSD(T)[(a)]	CCSDT[(b)]
HF	1.1	1.1	1.6
F_2	3.0	4.4	14.7
FCl	7.2	12.7	131.5
H_2O	3.6	4.4	5.2
HOF	104.2	205.4	171.8
F_2O	46.0	>167.0	>167.0
CH_3F	127.2	147.0	>261.7
FCN	23.7	99.9	251.0

(a) Calculated with an ACV5Z basis set.
(b) Calculated with an ACVTZ basis set.

Calculation run times for H_2O are similar to F_2 due to the balance of symmetry and number of electrons; however, the addition of fluorine in HOF (which has fewer electrons than F_2) and F_2O causes calculation run times to increase rapidly. Therefore, the extensive calculations performed for diatomics in Chapter 3 will not be as feasible for these additional molecules. As shown in Chapter 3, contributions from higher excitations tend to be small, so the inaccessibility of more extensive methods for this additional series should not be critical.

Calculations of the equilibrium nuclear magnetic shielding and the relativistic effects on the shielding were carried out at CCSD(T)/ACVQZ optimised geometries, which will be reported in the appropriate sections. Relativistic effects were calculated with the PBE0 functional using

the dyall-aug-cvqz basis set. As demonstrated in Chapter 3, the use of extensive basis sets for relativistic calculations is not critical; however, for consistency, the QZ basis set will continue to be used. Vibrational averaging and temperature effects on the absolute shielding are calculated with geometries optimised at the same level of theory. All experimental ^{19}F shielding constants used for comparison have been derived from referenced chemical shifts relative to $CFCl_3$ (either direct or indirect) and converting to a shielding via $\sigma(CFCl_3) = 197.07$ ppm.[25]

4.2 Absolute ^1H Shielding in H_2O and HOF

The all-electron CCSD(T)/ACVQZ calculated geometries of H_2O (r(OH) = 0.95810 Å, ∠(HOH) = 104.481°) and HOF (r(OH) = 0.96684 Å, r(OF) = 1.43382 Å, ∠(HOF) = 97.952°) were used for the calculation of ^1H absolute shielding constants. Equilibrium shielding calculations and CBS extrapolated values are presented in Tables 4.2 and 4.3 for H_2O and HOF, respectively, with the final calculated shielding constants with all contributions reported in Table 4.4.

Table 4.2: Equilibrium ^1H shielding in H_2O (ppm).

Contribution	ACVDZ	ACVTZ	ACVQZ	ACV5Z	ACV6Z	ACV7Z	CBS
HF-SCF	31.161	30.715	30.530	30.471	30.445	30.437	30.433
SD	0.319	0.258	0.159	0.134	0.125		0.112
(T)	0.029	0.016	0.014	0.013	0.013		0.013
T	0.003	0.005	0.006				0.006
Q	0.001						0.001
Equilibrium Shielding							30.565

Table 4.3: Equilibrium ^1H shielding in HOF (ppm).

Contribution	ACVDZ	ACVTZ	ACVQZ	ACV5Z	ACV6Z	CBS
HF-SCF	19.512	19.301	19.132	19.075	19.047	19.016
SD	1.206	0.954	0.809	0.771	0.758	0.739
(T)	-0.140	-0.184	-0.189	-0.190		-0.191
T	-0.040	-0.039				-0.039
Equilibrium Shielding						19.525

Table 4.4: Calculated CBS ^{1}H absolute shielding in H_2O and HOF (ppm).

Contribution	H_2O	HOF
HF-SCF	30.433	19.016
SD	0.112	0.739
(T)	0.013	-0.191
T	0.006	-0.039
Q	0.001	
Vibrational Effects	-0.509[(a)]	-0.688[(a)]
Temperature Effects (300 K)	-0.025[(a)]	-0.063[(a)]
Relativistic Effects	0.061[(b)]	0.013[(b)]
Total Absolute Shielding	30.092	18.787
Experimental Shielding	30.102(8)[40]	18.5[40,48]

(a) Calculated with CCSD(T)/ACV[T,Q]Z.
(b) Calculated with PBE0/dyall-aug-cvqz.

The calculated ^{1}H isotropic shielding constants of 30.092 ppm in H_2O and 18.787 ppm in HOF agree very well with the experimental values of 30.102(8) ppm[40] and 18.5 ppm (δ(HOF) = 12.1 ppm,[48] $\sigma(CH_4)$ = 30.633(6) ppm[40]), respectively. Due to the increased electron count and reduced symmetry, HOF is much more challenging to calculate than H_2O. As such, the quadruple excitation (Q) contributions to the ^{1}H shielding constant in HOF could not be determined. However, the size of T contributions towards the ^{1}H shielding constant in both H_2O and HOF are of similar magnitude, and thus it is reasonable to assume the Q contributions to the ^{1}H shielding constant in HOF are similarly negligible. Additionally, 7Z basis set values could not be obtained for HOF; however, the excitation contributions to the ^{1}H absolute shielding constant are converged without the need for 7Z basis sets, and thus it can be concluded that the equilibrium shielding constant is accurate.

Vibrational averaging and temperature effects on the ^{1}H absolute shielding constant in these molecules are significantly larger than that for the ^{1}H shielding constants in the diatomics considered in Chapter 3. This is likely due to the additional degrees of freedom within the larger molecules. It is worth noting that the ^{1}H absolute shielding constant within HOF is much smaller than in H_2O. This is likely due to extra deshielding that occurs due to the presence of the highly electronegative fluorine atom. The relativistic effects on the ^{1}H absolute shielding constant in H_2O and HOF are an order of magnitude greater than that in H_2 and an order of magnitude less than in HF. It is clear that relativistic effects can vary significantly depending on the environment of the individual nuclei. Consideration of the convergence of the

equilibrium, vibrational, and relativistic effects on shielding leads to an estimated uncertainty of ±0.01 ppm in H_2O and ±0.1 ppm in HOF.

4.3 Absolute ^{19}F Shielding in HOF and F_2O

The ^{19}F absolute shielding constant was also calculated in HOF (identical geometry as in Section 4.2) and F_2O (r(OF) = 1.40400 Å, ∠(FOF) = 103.032°). The equilibrium ^{19}F shielding constants are presented in Tables 4.5 and 4.6, then combined with vibrational averaging, temperature, and relativistic effects in Table 4.7.

Table 4.5: Equilibrium ^{19}F shielding in HOF (ppm).

Contribution	ACVDZ	ACVTZ	ACVQZ	ACV5Z	ACV6Z	CBS
HF-SCF	298.975	291.144	288.398	287.364	287.074	286.961
SD	-78.859	-83.723	-83.267	-83.241	-83.165	-83.060
(T)	-8.403	-11.297	-11.926	-12.168		-12.423
T	-0.392	-0.561				-0.633
Equilibrium Shielding						190.846

Table 4.6: Equilibrium ^{19}F shielding in F_2O (ppm).

Contribution	ACVDZ	ACVTZ	ACVQZ	ACV5Z	ACV6Z	CBS
HF-SCF	39.067	31.826	26.486	24.335	23.694	23.422
SD	-16.633	-29.431	-29.815	-29.867	-29.863	-29.858
(T)	-12.421	-13.739	-14.244			-14.613
T	-0.840					-0.840
Equilibrium Shielding						-21.889

Table 4.7: Calculated CBS ^{19}F absolute shielding in HOF and F_2O (ppm).

Contribution	HOF	F_2O
HF-SCF	286.961	23.422
SD	-83.060	-29.858
(T)	-12.423	-14.613
T	-0.633	-0.840
Vibrational Effects	-19.318[(a)]	-22.886[(b)]
Temperature Effects (300 K)	-2.108[(a)]	-2.851[(b)]
Relativistic Effects	5.879[(c)]	5.867[(c)]
Total Absolute Shielding	175.299	-41.759
Experimental Shielding	180.0[48]	

(a) Calculated with CCSD(T)/ACV[T,Q]Z.
(b) Calculated with CCSD(T)/ACV[D,T]Z.
(c) Calculated with PBE0/dyall-aug-cvqz.

Tables 4.5 and 4.6 show that the ^{19}F nucleus in HOF is much more shielded than the ^{19}F nuclei in F_2O. The trend is similar to that observed between HF and F_2. The ^{19}F nuclei in F_2O experience an increased effect of the magnetic field due to the presence of additional electrons, which is caused by interactions with the other fluorine atom within the molecule, much like the case with F_2. Quadruple excitation contributions with CCSDTQ could not be calculated for either molecule; however, given that the magnitude of T contributions is less than 1 ppm, Q contributions can be expected to be less than 0.1 ppm.

Table 4.7 reports the calculated ^{19}F absolute shielding in HOF and F_2O. The ^{19}F shielding obtained for HOF is in good agreement with the experimental ^{19}F absolute shielding of 180 ppm,[48] with a deviation of only 4.7 ppm. It is noted that the experimental chemical shift is reported as a liquid sample at 193 K. Nebgen *et al.* have shown that gas-liquid phase changes can cause chemical shifts to change from 1-4 ppm in fluorinated compounds.[46] Additionally, temperature effects in HOF contribute to over 2 ppm of the total absolute shielding (Table 4.7). Therefore, a deviation of 4.7 ppm when compared with a cooled liquid phase chemical shift is not unexpected. The HOF chemical shift is reported relative to F_2, which has multiple chemical shifts reported, as discussed in Section 3.5. It is possible to derive an updated experimental shielding for HOF of 173.24 ppm from the chemical shift of F_2 reported by Jameson *et al.* of -595.96(03) ppm.[15] This alternative absolute shielding deviates from the fully calculated shielding in Table 4.7 by only 2.06 ppm. Despite this, consideration of gas-liquid phase shifts and temperature effects is required to obtain a true experimental shielding for HOF.

In F_2O, there is a larger deviation between the experimental ^{19}F absolute shielding of -51 ppm[46] and the value of -41.759 ppm calculated here. The convergence of coupled-cluster excitation contributions in Table 4.6 is generally smooth, and T contributions are small, indicating the equilibrium shielding should be converged and accurate. However, the coupled-cluster contributions to the ^{19}F nuclear shielding in F_2O do not follow the trend of decreasing contribution with an increase in excitation consideration, with SD contributions being of larger size than HF-SCF contributions. It is feasible that Q excitations need to be considered for F_2O due to the large number of electrons within the molecule. Geometry effects may also contribute, as Harding *et al.* demonstrated the effect of geometry within F_2O, which was over 5 ppm between CCSD(T)/VTZ and CCSD(T)/VQZ optimised geometries.[23] However, the current CCSD(T)/ACVQZ geometries are expected to be converged to within 0.005 Å.

Harding *et al.* also reported non-relativistic shielding constants of ^{19}F in HOF and F_2O of 168.9 ppm and -46.3 ppm, respectively, using CCSD(T) with *13s9p4d3f* basis sets.[23] Non-relativistic shielding constants calculated here are 169.420 ppm and -47.626 ppm for HOF and F_2O, respectively (Table 4.7 CBS results, omitting relativistic contributions). These deviate from experiment less than those reported by Harding *et al.*, which may be attributed to the larger basis sets used, as well as consideration of higher excitations. Interestingly, the deviation between experiment and theory decreases with the addition of relativistic effects in the case of HOF, whilst in the case of F_2O, consideration of relativistic effects increases the deviation from experiment. The consistent deviation between theory and experiment for the ^{19}F shielding in F_2O indicates a re-investigation into the experimental chemical shift is warranted.

Vibrational and temperature effects on the ^{19}F shielding in these molecules are sizeable, being larger than the total equilibrium shielding in F_2O. This is attributed to the very flexible and anharmonic O–F bonds that cause large geometry changes, and as such, have a significant effect on the overall ^{19}F absolute shielding, much like that of F_2. Relativistic effects on the ^{19}F absolute shielding constants are yet again quite large and are very similar between HOF and F_2O. The relativistic contribution is also close to the relativistic effect calculated for F_2 and of similar magnitude to the effect calculated for ^{19}F in HF. It can be concluded that the values calculated for the relativistic effects are reliable. Convergence of the vibrational effects within F_2O via DZ and TZ basis sets cause the final CBS to become less reliable than previous extrapolated effects. Therefore, an uncertainty in the calculated shielding of F_2O of ±3 ppm is estimated after consideration of convergence in the equilibrium shielding and vibrational

effects. An uncertainty of ±1 ppm for HOF is estimated due to smoother convergence within the calculated components.

4.4 Absolute ^{19}F Shielding in CH_3F and FCN

The optimised geometries of CH_3F (r(CF) = 1.38312 Å, r(CH) = 1.08752 Å, ∠(FCH) = 108.767°) and FCN (r(CF) = 1.26511 Å, r(CN) = 1.15726 Å) were used in all equilibrium shielding and relativistic calculations during the investigation into their respective ^{19}F absolute shielding constants. The contributions to the ^{19}F equilibrium shielding constants for CH_3F and FCN are presented in Tables 4.8 and 4.9, respectively. These equilibrium ^{19}F absolute shielding constants are combined with vibrational averaging, temperature, and relativistic effects in Table 4.10.

Table 4.8: Equilibrium ^{19}F shielding in CH_3F (ppm).

Contribution	ACVDZ	ACVTZ	ACVQZ	ACV5Z	CBS
HF-SCF	483.054	485.791	485.605	485.598	485.598
SD	-1.216	-3.628	-3.260	-3.188	-3.112
(T)	-0.885	-1.034	-1.034	-1.040	-1.045
T	-0.252				-0.252
Equilibrium Shielding					481.189

Table 4.9: Equilibrium ^{19}F shielding in FCN (ppm).

Contribution	ACVDZ	ACVTZ	ACVQZ	ACV5Z	CBS
HF-SCF	384.353	380.429	379.378	378.857	378.345
SD	5.302	0.200	0.387	0.555	0.731
(T)	-3.787	-3.787	-3.911	-3.949	-3.989
T	-0.294	-0.488			-0.569
Equilibrium Shielding					374.518

Table 4.10: Calculated CBS ^{19}F absolute shielding in CH_3F and FCN (ppm).

Contribution	CH_3F	FCN
HF-SCF	485.598	378.345
SD	-3.112	0.731
(T)	-1.045	-3.989
T	-0.252	-0.569
Vibrational Effects	-9.550[(a)]	-6.478[(a)]
Temperature Effects (300 K)	-0.309[(a)]	-0.387[(a)]
Relativistic Effects	4.392[(b)]	3.830[(b)]
Total Absolute Shielding	475.721	371.483
Experimental Shielding	474.95(5)[15]	353.12

(a) Calculated with CCSD(T)/ACV[D,T]Z.
(b) Calculated with PBE0/dyall-aug-cvqz.

Basis set convergence is very smooth for the equilibrium ^{19}F shielding of CH_3F and FCN. Interestingly, the general trend of decreasing contribution to shielding with higher coupled-cluster excitation does not occur to its full extent within FCN. Nevertheless, full triple excitations are again small for both these molecules, and as such, it is not overly problematic that Q contributions could not be calculated as they may be expected to be less than 0.1 ppm. As such, it is believed that the equilibrium nuclear shielding constants are accurate.

The calculated ^{19}F shielding in CH_3F is in excellent agreement with the experimental value of 474.95 ± 0.05 ppm,[15] yielding a deviation of only 0.77 ppm. The excellent agreement may seem fortuitous considering the deviations in HOF and F_2O and smaller basis sets being used for CH_3F. However, Harding *et al.*[23] have reported an equilibrium ^{19}F shielding for CH_3F of 482.0 ppm from CCSD(T) calculations that agrees very well with the equilibrium shielding derived in Table 4.8. Additionally, the vibrational corrections in the present work agree well with MP2 calculations by Harding *et al.* Addition of relativistic effects to the Harding *et al.* calculated shielding would yield a total shielding of 477.3 ppm, which deviates further from experiment. The use of CCSD(T) rather than MP2 calculated vibrational averaging and temperature corrections, as well as the consideration of higher T excitations and closer agreement with experiment, enables the conclusion that the CH_3F ^{19}F nuclear shielding in Table 4.10 is the most accurate to date. Smooth convergence within the equilibrium shielding and considered effects results in an estimated uncertainty of ±0.1 ppm.

In contrast, the calculated ^{19}F shielding in FCN is quite far from the experimental value of 353 ppm,[49] with a difference between theory and experiment of 18 ppm. One possibility is that the

difference arises from a lack of extensive coupled-cluster excitations such as Q excitations, although it is difficult to be certain as the magnitude of such contributions is unknown. However, it is logical to assume such contributions would be relatively small in FCN, given that they have been small in all other molecules studied. As such, the deviation remains unresolved, and the cause for the significant discrepancy between experiment and theory remains unclear. Teale *et al.*[18] reported the equilibrium ^{19}F shielding in FCN at the CCSD(T)/ ACV[T,Q]Z level of theory as 374.10 ppm. This is within 0.42 ppm of the equilibrium shielding reported in Table 4.9. The deviation between the equilibrium shielding reported here and by Teale *et al.* is approximately the consideration of T excitations which contribute 0.57 ppm to the overall shielding. Additionally, Teale *et al.* utilised CCSD(T)/VTZ in the geometry optimisation of FCN, whereas CCSD(T)/ACVQZ has been used here. Consideration of higher T excitations along with a larger basis set used for geometry optimisations concludes that the ^{19}F absolute shielding of 353.12 ppm in Table 4.10 is the most accurate to date with an estimated uncertainty of ±1 ppm.

Vibrational averaging and temperature effects on the ^{19}F absolute shielding constants in CH_3F and FCN appear to be much smaller than that in HOF and F_2O but of similar magnitude to that of the diatomics in Chapter 3. This is believed to be caused by the fluorine atom in question not being within close proximity to other electronegative atoms such as oxygen or nitrogen. Relativistic effects on the ^{19}F shielding constants in CH_3F and FCN are also consistent with similar molecules considered above. These consistent results validate the total ^{19}F absolute shielding in FCN and thus warrants investigation into the experimental chemical shift.

4.5 Calculated ^{19}F Absolute Shielding Scale

For most of the investigated molecules, agreement with experimental ^{19}F absolute shielding is very good. All diatomic ^{19}F shielding constants in Chapter 3 are within 1 ppm of experimental shielding constants, or in the case of HF, agree with updated shieldings using updated chemical shift data. Throughout Chapters 3 and 4, the ^{19}F absolute shielding in $CFCl_3$ of 197.07 ppm[25] has been used to convert experimental chemical shifts to shielding constants. However, as it is possible to use any absolute shielding constant as the reference value, it is worth investigating the consistency between the calculated shielding constants thus far whilst using the calculated ^{19}F shielding within HF of 414.310 ppm (Table 3.12). This particular shielding constant has been selected over the other calculated shielding constants due to the excellent agreement with

previous experimental shielding constants, as well as the large calculations performed (up to CCSDTQP). Table 4.11 collects calculated nuclear shielding constants in comparison to experimental ^{19}F shielding constants derived from σ(HF) = 414.310 ppm together with a chemical shift of -217.02 ppm for HF relative to $CFCl_3$.[7,14]

Table 4.11: Comparison of calculated and corrected experimental absolute ^{19}F shielding constants (ppm).

Molecule	Calculated	Experimental[(a)]	Calc. – Expt.	Ref.	Ref. Notes
HF	414.310	414.31	0.00	This Work	Gas 300 K
F_2	-221.070	-221.71	0.64	46	Gas 300 K
FCl	640.926	641.19	0.26	7, 47	Gas 300 K
HOF	175.299	180.29	4.99	48	Liquid 77 K
F_2O	-41.759	-50.71	8.95	46	Gas 300 K
CH_3F	475.721	475.17	0.55	15	Gas 300 K
FCN	371.483	353.34	18.14	49	Liquid

(a) Chemical shifts converted to shielding constants using σ(^{19}F) in HF of 414.310 ppm

The corrected experimental ^{19}F shielding constants are in closer agreement with those calculated within this thesis, with most calculated shielding constants having a deviation of less than 1 ppm from the new experimental values. In all cases except FCl and HOF, correcting the experimental nuclear magnetic shielding with the calculated ^{19}F shielding in HF results in a decrease in deviation between the calculated and experimental values. The change in deviation is typically 0.22 ppm compared to previously discussed deviations, which is directly related to the deviation within the HF shielding constant discussed in Section 3.4.

The ^{19}F shielding constants in HOF, F_2O, and FCN are the only molecules with a deviation of greater than 1 ppm after correcting the experimental shielding constants. It is difficult to compare accurately with experiment for HOF and FCN due to the lack of experimental data for these molecules in the gas-phase at 300 K. As previously discussed, the reported HOF chemical shift is a liquid-phase value at 77 K.[48] Solvation is known to affect chemical shifts by approximately 1-4 ppm.[46] Additionally, the FCN experimental chemical shift is reported in the liquid-phase relative to CF_3COOH,[49] which unfortunately is too large a molecule to investigate via the high-level computational methods employed in this thesis. The absolute calculated ^{19}F shielding constant in F_2O deviates from experiment by approximately 9 ppm after correction.

While a direct cause of the deviation remains unknown, the results reported here are consistent with those in the literature, as discussed in Section 4.3.

The often-referenced semi-experimental ^{19}F absolute shielding in HF of 409.6 ppm from Sundholm *et al.*[12] deviates substantially from the corrected experimental values as well as the calculated ^{19}F shielding constant for HF. The deviation arises from an incorrect treatment of relativistic effects in the semi-experimental procedure. Sundholm *et al.* used relativistic experimental spin-rotation constant to determine a paramagnetic contribution to the absolute shielding, which, as discussed in Chapter 1, has since been found to not be valid.[11,12,16,17] Additionally, the ^{19}F shielding of HF here agrees well with Sundholm *et al.* 409.6 ppm[12] when relativistic effects are removed (see Section 3.4). As such, we believe the true ^{19}F absolute shielding of HF is closer to the calculated shielding constant presented in Chapter 3. Further support of this conclusion is provided by the strong agreement between our ^{19}F shielding constants in HF using the previously calculated shielding in $CFCl_3$ of 197.07 ppm[25] and the updated chemical shift of SiF_4 from Makulski.[7] Furthermore, deviations in shielding constants between theory and experiment decrease when the absolute shielding in HF of 414.310 ppm is used to convert experimental chemical shifts to absolute shieldings rather than the absolute shielding within $CFCl_3$ of 197.07 ppm.

4.6 Summary

The series of fluorine-containing molecules investigated for the accurate calculation of absolute shielding constants has been expanded with the addition of the H_2O, HOF, and F_2O series, as well as CH_3F and FCN. Absolute shielding constants have been calculated as accurately as possible using the same procedure that was employed for the diatomics series in Chapter 3. The calculated absolute shielding constants for both ^{1}H and ^{19}F nuclei agree very well with experimentally reported values with the exception of the ^{19}F shielding constants in F_2O and FCN, which have been discussed in detail. The combination of these calculated values with those reported in Chapter 3 produces a sizeable ^{19}F absolute shielding constant scale, with calculated shielding constants mostly within ±1 ppm of corrected experimental results.

Chapter 5:
Calculation of Spin-Rotation Constants

5.1 Introduction

Spin-rotation constants are valuable for the purpose of deriving accurate nuclear shielding constants; however, they are also of interest in their own right. The calculation of spin-rotation constants was carried out alongside the absolute shielding constant calculations. The determination of theoretical spin-rotation constants utilised the same computational methodology employed throughout Chapters 3 and 4. That is, coupled-cluster calculations of the spin-rotation constant were used to determine contributions from each term of the coupled-cluster expansion, extrapolated to the CBS limit. Summation of these contributions provided an equilibrium spin-rotation constant, which was further augmented with vibrational, temperature, and relativistic corrections before comparison with experiment. The conversion of experimental spin-rotation constants into semi-experimental absolute shielding constants via eq. 1.6 is explored in this chapter, including a direct comparison with those reported in Chapters 3 and 4.

5.2 H_2, HF, F_2, and FCl Spin-Rotation Constants

The calculation of spin-rotation constants for diatomic molecules was initially benchmarked for the case of H_2 due to the capacity to perform FCI calculations with the CCSD method. Additionally, the small size of the H_2 molecule permits the straightforward use of large basis sets up to AV7Z. All calculations were carried out at the CCSD/AVQZ optimised geometry (R_e = 0.74199 Å) that was also used for nuclear magnetic shielding calculations in Chapter 3. The experimental geometry is 0. 74151 Å.[12] An optimised geometry was employed to ensure a purely theoretical benchmark study since, in practical theoretical investigations, an accurate experimental geometry is not always available. The equilibrium spin-rotation constant was determined by calculating the contribution of HF-SCF and SD excitation levels. It is noted that the full CCSD spin-rotation constant is the summation of the HF-SCF and SD contributions. The separate contributions were then extrapolated to the CBS using eq. 2.10 and 2.12 and combined into an FCI/CBS equilibrium spin-rotation constant as presented in Table 5.1.

Table 5.1: Equilibrium ^{1}H spin-rotation constant in H_2 (kHz).

Contribution	AVTZ	AVQZ	AV5Z	AV6Z	AV7Z	CBS
HF-SCF	115.9737	115.5491	115.1187	114.9771	114.9755	114.9755
SD	0.5203	0.3360	0.3020	0.2903	0.2810	0.2653
Equilibrium Spin-Rotation						115.2407

The equilibrium spin-rotation constant is calculated to be 115.2407 kHz. The smooth convergence of both the HF-SCF and SD contributions provides confidence in the accuracy of the CBS value. The HF-SCF contribution is clearly converged with respect to the basis set limit, with the AV6Z and AV7Z basis set values differing by only 0.002 kHz, which results in the extrapolated CBS result being equal to the AV7Z spin-rotation constant to four decimal places. Additionally, the SD contribution is also converged, with the AV6Z and AV7Z basis set values differing by less than 0.01 kHz, which leads to a predicted CBS contribution within 0.016 kHz of the AV7Z calculated result.

Sundholm and Gauss have previously reported a corrected equilibrium spin-rotation constant of 115.468(30) kHz.[41] This value was derived by taking the experimental spin-rotation constant of 113.904(30) kHz from Harrick *et al.*[50] and removing calculated rovibrational effects and Thomas precession to convert the experimental constant into an equilibrium constant. The value reported by Sundholm *et al.* deviates by 0.227 kHz from the purely calculated equilibrium spin-rotation constant reported here. The small deviation may be attributed to a difference in geometry, for which Sundholm *et al.* used an experimental geometry as opposed to an all-electron CCSD(T)/AVQZ optimised geometry used here. Additionally, the differing computational methodologies of purely calculating a spin-rotation constant performed here as opposed to augmenting an experimental constant may cause differences in the compared values.

The fully calculated equilibrium spin-rotation constant presented in Table 5.1 is self-consistent with the Sundholm and Gauss[41] value that was obtained by removing vibrational and relativistic contributions from the experimental spin-rotation constant. Therefore, it is of interest to calculate vibrational, temperature, and relativistic effects to obtain a spin-rotation constant that can be directly compared with the experimental data. Vibrational and temperature effects were calculated with the CCSD method at geometries optimised at the same CCSD/AVXZ level of theory, where X is the zeta magnitude used for the corresponding anharmonic vibrational

calculation (Table 5.2). Relativistic corrections were calculated with PBE0 with the same CCSD/AVQZ geometry used to calculate the equilibrium spin-rotation constant (Table 5.3).

Table 5.2: CCSD Vibrational averaging and temperature effects on the ^{1}H spin-rotation constant in H_2 (kHz).

Contribution	AVQZ	AV5Z	AV6Z	AV7Z	CBS
Vibrational averaging	-0.6668	-0.6636	-0.6612	-0.6744	-0.6968
Temperature (300 K)	-1.1508	-1.1475	-1.1462	-1.1416	-1.1340

Table 5.3: PBE0 Relativistic effects on the ^{1}H spin-rotation constant in H_2 (kHz).

Basis Set	Relativistic (rel)	Non-relativistic (nrel)	rel-nrel
dyall-aug-vtz	115.5222	115.5240	-0.0018
dyall-aug-vqz	115.8681	115.8701	-0.0020

For the spin-rotation constant, the temperature effect is larger than the vibrational averaging effect, which is in contrast to the trend noted for shielding constants. There is evidence of non-monotonic convergence for the vibrational averaging and temperature effects in Table 5.2 that arises from the AV7Z results. Extrapolating to the CBS limit from the AV5Z and AV6Z results in place of the AV7Z results yields contributions of -0.6580 kHz and -1.1440 kHz for vibrational averaging and temperature effects, respectively. The sum of these vibrational and temperature effects deviate from those provided in Table 5.2 by 0.029 kHz; however, for the purpose of consistency with other molecular systems, the CBS results in Table 5.2 will continue to be used and discussed.

Relativistic effects are small at only -0.002 kHz. Although these are calculated using the DFT functional PBE0, they are considered to be accurate due to a cancellation of error within the overall relativistic effect on the spin-rotation constant. That is, although the individual relativistic and non-relativistic spin-rotation constants are prone to errors through the use of DFT, only the difference of the two values is considered as the effect of relativity which is expected to be minimally affected by choice of method. This is further demonstrated in the lack of basis set dependence on the effect of relativity. While the individual fully relativistic and non-relativistic 4-component values vary by 0.3 kHz between TZ and QZ basis sets, the difference (rel-nrel) is not affected by choice of basis set with a change of only 2×10^{-4} kHz.

The minimal dependence on basis set could simply result from relativistic effects being small in H_2 and so will be further explored for heavier molecules.

All contributions and the total spin-rotation constant are presented in Table 5.4. The combined effect on the spin-rotation constant from vibrational, temperature, and relativistic corrections is calculated to be -1.8329 kHz. Sundholm and Gauss reported corrections to the experimental spin-rotation tensor to be -1.564 kHz.[41] The difference of 0.27 kHz in part arises from the consideration of rotational states in Sundholm and Gauss' rovibrational and temperature corrections, that is expected to be more accurate than the vibrational and temperature corrections presented here. The vibrational and temperature corrections calculated here are also impacted by a lack of smooth basis set convergence. Despite this, it is considered that the error within the CBS results is within 0.05 kHz and much smaller than the 0.27 kHz deviation between effects calculated here and by Sundholm and Gauss.

Table 5.4: Calculated ^{1}H spin-rotation constant of H_2 (kHz).

Contribution	AV5Z	AV6Z	AV7Z	CBS/Best Value
HF-SCF	115.1187	114.9771	114.9755	114.9755
SD	0.3020	0.2903	0.2810	0.2653
Vibrational Effects		CCSD/ACV[6,7]Z		-0.6968
Temperature Effects (300 K)		CCSD/ACV[6,7]Z		-1.1340
Relativistic Effects		PBE0/dyall-aug-vqz		-0.0020
Total Spin-Rotation Constant				113.4079
Experimental Spin-Rotation				113.904(30)[50]

Combining the calculated equilibrium contribution with vibrational, temperature and relativistic effects provides a total spin-rotation constant of 113.4079 kHz with an uncertainty of ±0.03 kHz as a result of the rate of convergence in the SD and vibrational contributions. The reported experimental spin-rotation constant is 113.904(30) kHz,[50] which differs from the present calculated value by only 0.496 kHz. Employing the Sundholm and Gauss[50] rovibrational corrections in place of the vibrational and temperature corrections from Table 5.2 results in a spin-rotation constant of 113.9137 kHz, which is within the experimental uncertainty. It is concluded that the vibrational corrections calculated for the H_2 molecule are not as accurate as the rovibrational corrections previously reported by Sundholm and Gauss.

Calculation of the ^{19}F spin-rotation constant in HF was carried out using the same computational strategy as employed for H_2. All calculations employed the ACVXZ basis sets

that are augmented with core basis functions. Additionally, coupled-cluster methods beyond CCSD were utilised as the increased electron count of HF results in consideration of higher electron excitations being required. Once again, the extrapolation of contributions of each additional coupled-cluster expansion was utilised to determine a combined equilibrium spin-rotation constant. Results are collected in Table 5.5.

Table 5.5: Equilibrium ^{19}F spin-rotation constant in HF (kHz).

Contribution	ACVDZ	ACVTZ	ACVQZ	ACV5Z	ACV6Z	CBS
HF-SCF	-283.0948	-308.8521	-311.3177	-312.7905	-313.2015	-313.3607
SD	30.4819	25.6437	26.7220	27.1036	27.3364	27.6562
(T)	0.9062	2.8443	2.8959	2.8495	2.8814	2.9252
T	-0.2645	-0.8142	-0.9348			-1.0227
Q	-0.0842	-0.1756				-0.2141
P						-0.0153[(a)]
Equilibrium Spin-Rotation Constant						-284.0314
Experimental Equilibrium Spin-Rotation						-280.49(4)[51]

(a) tz2p basis set result

Combining the CBS contributions yields an equilibrium spin-rotation constant of -284.031 kHz. Throughout Table 5.5, the trend of decrease in contribution with an increase in excitation level is evident and is of similar structure to the trend discussed for shielding constants in Chapter 3. That is, each successive term of the coupled-cluster expansion decreases the magnitude of contribution towards the overall spin-rotation constant. It is therefore concluded that hextuple and higher excitation levels would contribute approximately 0.001 kHz and are thus deemed negligible. An experimental equilibrium spin-rotation constant of -280.49(4) kHz has been reported by Bass *et al.*[51] by determining the v=0 and v=1 vibrational state spin-rotation constants and extrapolating towards an equilibrium spin-rotation constant. Gauss *et al.*[52] calculated a HF-SCF equilibrium spin-rotation constant of -313.53 kHz using a 15*s*11*p*4*d*3*f* basis set, which is 0.17 kHz from the extrapolated HF-SCF spin-rotation constant calculated here. Teale *et al.*[18] calculated a CCSD(T)/ACVQZ spin-rotation constant of -280.08 kHz, for which the CCSD(T)/ACVQZ calculation in the present investigation yielded a spin-rotation constant of -281.70 kHz. The deviation between these results can be attributed to a change in geometry. Teale *et al.* utilised an all-electron CCSD(T)/VTZ optimised geometry, while an all-electron CCSD(T)/ACVQZ optimised geometry was utilised here. The deviation between the

overall equilibrium spin-rotation constant in Table 5.5 and the value reported by Teale *et al.* can also be attributed to the consideration of higher-level excitations in the present work, due to the good agreement in the HF-SCF to CCSD(T) methods with previous reports by Gauss *et al.* and Teale *et al*. The higher excitation contributions are considered to be accurate, due to the smooth convergence throughout each successive excitation. The only excitation level that does not follow exact monotonic convergence is the (T) contribution from the ACVQZ to ACV6Z basis sets. Nevertheless, the uncertainty in the equilibrium spin-rotation constant is expected to be at most ±0.5 kHz from that in Table 5.5 due to the large basis sets and methods utilised along with the good agreement with previous theoretical spin-rotation constants.

The contribution from vibrational and temperature effects is presented in Table 5.6, with relativistic effects presented in Table 5.7. All components are combined in Table 5.8 to provide a total spin-rotation constant for comparison with experiment.

Table 5.6: CCSD(T) Vibrational averaging and temperature effects on the ^{19}F spin-rotation constant in HF (kHz).

Contribution	ACVQZ	ACV5Z	ACV6Z	CBS
Vibrational averaging	-23.9768	-24.7178	-24.7721	-24.8466
Temperature (300 K)	-1.3973	-1.4383	-1.4388	-1.4396

Table 5.7: PBE0 Relativistic effects on the ^{19}F spin-rotation constant in HF (kHz).

Basis Set	Relativistic (rel)	Non-relativistic (nrel)	rel-nrel
dyall-aug-cvtz	-321.6279	-321.8482	0.2203
dyall-aug-cvqz	-320.9310	-321.1203	0.1893

Table 5.8: Calculated ^{19}F spin-rotation constant in HF (kHz).

Contribution	Method/Basis	CBS/Best Value
HF-SCF	ACV[Q,5,6]Z	-313.3607
SD	ACV[5,6]Z	27.6562
(T)	ACV[5,6]Z	2.9252
T	ACV[T,Q]Z	-1.0227
Q	ACV[D,T]Z	-0.2141
P	tz2p	-0.0153
Vibrational Effects	CCSD(T)/ACV[5,6]Z	-24.8466
Temperature Effects (300K)	CCSD(T)/ACV[5,6]Z	-1.4396
Relativistic Effects	PBE0/dyall-aug-cvqz	0.1893
Total Spin Rotation Constant		-310.1282
Experimental Spin-Rotation		-307.65(2)[51]

Combining all contributions yields a spin-rotation constant of -310.128 kHz, which deviates by 2.48 kHz from the experimental spin-rotation constant of -307.65(2) reported by Bass *et al.*[51] The agreement may be considered very good, given that the deviation in the equilibrium spin-rotation constant of HF presented in Table 5.5 is 3.54 kHz. Additionally, convergence within the vibrational and temperature contributions is smooth between ACVQZ and ACV6Z basis sets. Unlike the case of H_2, a decrease in magnitude for the temperature effects relative to the vibrational averaging corrections is evident, as was often the case when considering absolute shielding constants. Teale *et al.*[14] have calculated rovibrational and temperature corrections to be -28.26 kHz using B3LYP/ACVTZ, which deviates from the values presented in Table 5.6 by 1.97 kHz. However, if their rovibrational and temperature effects of -28.26 kHz are used in place of the -26.2862 kHz from Table 5.8, the total calculated spin-rotation constant deviates even further from the experimental constant from Bass *et al.* as the calculated spin-rotation constant overestimates the experimental constant. Consideration of the difference between the v=1 and v=0 experimental constants reported by Bass *et al.* results in a vibrational correction of -27.16 kHz, which differs by only 0.87 kHz from the combined vibrational and temperature corrections calculated here, which is considered good agreement.

Interestingly, relativistic effects change by 0.031 kHz between the dyall-cc-cvtz and dyall-cc-cvqz basis sets, which is of similar magnitude to the basis set differences in Table 3.15 (relativistic corrections to the ^{19}F absolute nuclear magnetic shielding). However, as the magnitude of the numerical relativistic contribution is much smaller for the spin-rotation constant, the difference between basis set results has a greater proportional impact on the final relativistic contribution for spin-rotation constants. Since the DFT functional PBE0 is used for relativistic effects together with Dyall's four-component relativistic basis sets, extrapolation formulae cannot be employed as readily as with the pairing of coupled-cluster methods and correlation-consistent basis sets. However, a two-point extrapolation yields a CBS relativistic contribution of 0.1667 kHz, which would alter the overall spin-rotation constant to -310.151 kHz. For consistency with other systems, the largest basis set result of 0.1893 kHz has been used in the determination of relativistic effects, although the lack of basis set convergence suggests a conservative estimate of the uncertainty of ±1.0 kHz.

The equilibrium ^{19}F spin-rotation constant of F_2 was calculated following the same strategy as for HF. Coupled-cluster methods up to CCSDTQ were used to calculate contributions from the coupled-cluster expansion by considering higher excitations. Due to the increased electron count of F_2 compared to HF, the same level of theory could not be used for each excitation

state. A CCSD(T)/ACVQZ optimised geometry was utilised throughout the equilibrium spin-rotation calculations. Results are presented in Table 5.9.

Table 5.9: Equilibrium ^{19}F spin-rotation constant in F_2 (kHz).

Contribution	ACVDZ	ACVTZ	ACVQZ	ACV5Z	ACV6Z	CBS
HF-SCF	-141.7368	-143.9965	-145.7355	-146.4344	-146.6446	-146.7351
SD	3.6140	-0.4067	-0.8307	-0.9178	-0.9508	-0.9962
(T)	-2.7849	-3.3192	-3.4728	-3.5284	-3.5473	-3.5732
T	-0.6645	-0.8789	-0.9059			-0.9256
Q	-0.3550					-0.3550
Equilibrium Spin-Rotation Constant						-152.5851

The equilibrium spin-rotation constant is determined to be -152.585 kHz. The basis set convergence with each excitation is smooth, with an increase in basis set resulting in a larger magnitude contribution. Interestingly, the contribution of the SD excitation level is of similar size to that of the T excitation contribution. This is different from what is regularly the case of decreasing contributions with each successive term of the coupled-cluster expansion. Gauss and Sundholm[53] have previously estimated the CCSD(T)/CBS equilibrium spin-rotation constant to be -151.27 kHz. While this deviates slightly from the fully calculated equilibrium spin-rotation including Q excitations, it is very close to the CCSD(T)/CBS value of -151.3045 kHz calculated here (sum of HF-SCF, SD and (T) contributions). Additionally, Hindermann and Williams[54] have reported an experimental equilibrium F_2 spin-rotation constant of -152.7 kHz after removing vibrational corrections. The calculated equilibrium value (Table 5.9) agrees very well with the vibrationally corrected experimental constant. Addition of vibrational and temperature effects from Table 5.10 as well as relativistic effects from Table 5.11 allows for comparison with the experimental spin-rotation constant (Table 5.12).

Table 5.10: CCSD(T) Vibrational averaging and temperature effects to the ^{19}F spin-rotation constant in F_2 (kHz).

Contribution	ACVQZ	ACV5Z	ACV6Z	CBS
Vibrational averaging	-3.7068	-3.6830	-3.6813	-3.6789
Temperature (300 K)	-0.6037	-0.5948	-0.5927	-0.5899

Table 5.11: PBE0 Relativistic effects on ^{19}F spin-rotation constant in F_2 (kHz).

Basis Set	Relativistic (rel)	Non-relativistic (nrel)	rel-nrel
dyall-aug-cvtz	-163.3232	-163.5226	0.1994
dyall-aug-cvqz	-163.3325	-163.5142	0.1817

Table 5.12: Calculated ^{19}F spin-rotation constant in F_2 (kHz).

Contribution	Method/Basis	CBS/Best Value
HF-SCF	ACV[Q,5,6]Z	-146.7351
SD	ACV[5,6]Z	-0.9962
(T)	ACV[5,6]Z	-3.5732
T	ACV[T,Q]Z	-0.9256
Q	ACVDZ	-0.3550
Vibrational Effects	CCSD(T)/ACV[5,6]Z	-3.6789
Temperature Effects (300K)	CCSD(T)/ACV[5,6]Z	-0.5899
Relativistic Effects	PBE0/dyall-aug-cvqz	0.1817
Total Spin-Rotation Constant		-156.672
Experimental Spin-Rotation		-156.85(10)[55]

Vibrational and temperature corrections combine to a total of -4.27 kHz, which is in close agreement with the corrections of -4.7 kHz reported by Hindermann and Williams[54] and -4.09 kHz calculated by Sundholm *et al.*[12] Basis set convergence of the vibrational and temperature effects is smooth, with the ACV5Z and ACV6Z basis set results being identical to the second decimal place. It is therefore concluded that the corrections are converged. Relativistic effects are of similar magnitude to those in the HF molecule. There is a small deviation between the two relativistic basis set results (0.018 kHz), although it is not as large in the case of HF, which suggests better basis set convergence with F_2. A two-point extrapolation yields a CBS relativistic contribution of 0.1667 kHz, which differs by only 0.0129 kHz from the dyall-aug-cvqz basis set result and is an estimate of the uncertainty due to lack of basis set convergence.

Combining all contributions yields a final calculated spin-rotation constant of -156.67 kHz that is in very close agreement with the experimental value of -156.85(10) kHz reported by Ozier and Ramsey.[55] Consideration of the smooth convergence of all considered components leads to a level of uncertainty of ±0.3 kHz

Extending spin-rotation constant calculations to FCl significantly increases the computational cost due to the larger number of electrons within the molecule. Due to the equilibrium spin-rotation calculations requiring consideration of core electron correlation (and unable to utilise

the frozen-core approximation), an increase in electron count cause very significant increases in computational effort. Nevertheless, coupled-cluster excitation contributions towards the equilibrium ^{19}F spin-rotation constant were carried out at the CCSD(T)/ACVQZ optimised geometry. Similarly, vibrational and temperature corrections, as well as relativistic effects to the spin-rotation constant were calculated with the CCSD(T) and PBE0 methods, respectively, to obtain an accurate spin-rotation constant for comparison with experiment. Results are presented in Table 5.13.

Table 5.13: Calculated ^{19}F spin-rotation constant in FCl (kHz).

Contribution	Method/Basis	CBS/Best Value
HF-SCF	ACV[Q,5,6]Z	29.314
SD	ACV[5,6]Z	-5.495
(T)	ACV[Q,5]Z	-0.002
T	ACVDZ	-0.051
Vibrational Effects	CCSD(T)/ACV[Q,5]Z	-0.825
Temperature Effects (300 K)	CCSD(T)/ACV[Q,5]Z	-0.180
Relativistic Effects	PBE0/dyall-aug-cvqz	-0.712
Total Spin-Rotation Constant		22.049
Experimental Spin-Rotation		22.41[56]

A fully calculated spin-rotation tensor is reported as 22.41 kHz. Consideration of the rate of convergence within the calculated components leads to an estimation of the uncertainty of ±0.04 kHz. CCSDT was the highest level of theory that was able to be run for FCl with the available resources. Therefore, an investigation into the contribution of Q excitations was not possible. While Q excitations make up between 0.2 kHz in HF and 0.4 kHz F_2, it is difficult to assume they would be of such magnitude in the case of FCl. The T excitation contributions for FCl are calculated to be a magnitude smaller than those calculated for HF and F_2 with similar basis sets. While the trends in HF and F_2 molecules is to increase the size of the contribution upon successive basis sets, it is not enough to justify the suggestion that T contributions, and thus Q contributions, would be of similar size to those of HF and F_2. The decrease in magnitude is likely due to the decrease in overall ^{19}F spin-rotation constant magnitude, with the spin-rotation constant in FCl being marginally smaller than the previous diatomics. Similar to that of the absolute shielding in Section 3.6, the relativistic effects to the ^{19}F spin-rotation constant are negative in sign, which contrasts those seen in the other diatomics discussed above. The

experimental spin-rotation constant is 22.41 kHz as reported by Fabricant and Muenter[56] and agrees well with the fully calculated spin-rotation constant of 22.049 kHz.

5.3 H_2, HF, F_2, and FCl Semi-Experimental Shielding Constants

Spin-rotation constants are often used in the calculation of the paramagnetic component of absolute nuclear magnetic shielding via eq. 1.6 in order to derive semi-experimental shielding constants. However, this approach can only be accurately achieved with an equilibrium spin-rotation constant, as the use of a vibrationally corrected spin-rotation constant would require calculating a vibrationally corrected diamagnetic absolute shielding. Additionally, Malkin *et al.*[16] has demonstrated that eq. 1.6 is not valid within the relativistic limit, and only non-relativistic spin-rotation constants may be converted to paramagnetic absolute shielding constants, as discussed in Section 1.2. As such, the vibrational, temperature, and relativistic effects calculated in Section 5.2 have been used to convert experimental spin-rotation constants into semi-experimental equilibrium nuclear magnetic shielding constants. Furthermore, it is worth noting that the equilibrium spin-rotation constants reported in Section 5.2 were not used to derive absolute shielding constants due to the inherent self-consistency between these calculated spin-rotation constants and the shielding constants reported in Chapter 3.

Deriving the semi-experimental ^{1}H and ^{19}F shielding constants in H_2, HF, F_2, and FCl requires the calculation of the diamagnetic contribution to the absolute shielding. In the case of H_2, an FCI investigation is performed through the use of the CCSD method, whereas for the larger diatomics, CCSD(T) and higher excitation levels were used to explore the effect of higher excitations within diamagnetic shielding. Extrapolation of each excitation level towards a CBS limit was performed, allowing each contribution to be combined to obtain an equilibrium diamagnetic shielding. Results for diatomic molecules are presented in Tables 5.14 to 5.17. The equilibrium value was then combined with a paramagnetic shielding constant contribution, which is derived by removing vibrational, temperature, and relativistic effects calculated in Section 5.2 from experimental spin-rotation constants and applying eq. 1.6 with the corrected experimental equilibrium spin-rotation constant. It is noted that for linear molecules, the value from applying eq. 1.6 must be multiplied by $\frac{2}{3}$ to provide a useable equilibrium paramagnetic absolute shielding. The paramagnetic and diamagnetic contributions are then combined with corrections reported in Chapter 3 to obtain a final semi-experimental shielding that can be compared with experiment. The contributions of the combined value are collected in Table 5.18.

Table 5.14: Diamagnetic ^{1}H shielding in H_2 (ppm).

Contribution	AVTZ	AVQZ	AV5Z	AV6Z	AV7Z	CBS
HF-SCF	32.1865	32.2099	32.2152	32.2159	32.2160	32.2161
SD	0.1481	0.1576	0.1621	0.1636	0.1643	0.1655
Diamagnetic Shielding						32.3816

Table 5.15: Diamagnetic ^{19}F shielding contribution in HF (ppm).

Contribution	ACVDZ	ACVTZ	ACVQZ	ACV5Z	ACV6Z	CBS
HF-SCF	481.882	482.138	482.218	482.242	482.245	482.245
SD	-0.647	-0.037	0.072	0.113	0.130	0.154
(T)	-0.037	-0.054	-0.054	-0.054	-0.055	-0.055
T	0.001	0.001	0.001			0.002
Q	-0.008	-0.004				-0.002
P						0.000[(a)]
Diamagnetic Shielding						482.344

(a) tz2p basis set result.

Table 5.16: Diamagnetic ^{19}F shielding contribution in F_2 (ppm).

Contribution	ACVDZ	ACVTZ	ACVQZ	ACV5Z	ACV6Z	ACV7Z	CBS
HF-SCF	529.346	529.633	529.723	529.749	529.751	529.752	529.752
SD	-0.306	0.234	0.319	0.352	0.366	0.371	0.381
(T)	-0.004	-0.002	-0.001	0.000	0.000		0.000
T	0.002	0.002	0.002				0.003
Q	0.002						0.002
Diamagnetic Shielding							530.138

Table 5.17: Diamagnetic ^{19}F shielding contribution in FCl (ppm).

Contribution	ACVDZ	ACVTZ	ACVQZ	ACV5Z	ACV6Z	CBS
HF-SCF	568.651	568.944	569.031	569.057	569.059	569.060
SD	-0.612	-0.044	0.039	0.072	0.085	0.103
(T)	-0.046	-0.070	-0.074	-0.075		-0.076
T	0.006					0.006
Diamagnetic Shielding						569.093

Table 5.18: Determination of semi-experimental ^{1}H and ^{19}F absolute shielding constants in H_2,[(a)] HF,[(b)] F_2,[(c)] and FCl.[(d)]

Constants	H_2 (^{1}H)	HF (^{19}F)	F_2 (^{19}F)	FCl (^{19}F)
$\boldsymbol{C}_0^{\mathrm{rel}}$ (kHz)	113.904(30)[50]	-307.65(2)[51]	-156.85(10)[55]	22.41(1)[56]
$\boldsymbol{C}_e^{\mathrm{nonrel}}$ (kHz)	115.737(30)	-281.55(2)	-152.76(10)	24.13(1)
σ_e^{p} (ppm)	-5.715(2)	-62.415(4)	-726.148(436)	83.24(11)
σ_e^{d} (ppm)	32.382(1)	482.344(15)	530.138(8)	569.093(15)
$\sigma_e^{\mathrm{nonrel}}$ (ppm)	26.667(3)	419.929(19)	-196.011(444)	652.33(13)
σ_0^{rel} (ppm)	26.298(3)	414.854(19)	-222.111(444)	643.25(13)

(a) R_e = 0.74150 Å for use of eq. 1.6
(b) R_e = 0.91680 Å for use of eq. 1.6
(c) R_e = 1.41184 Å for use of eq. 1.6
(d) R_e = 1.62800 Å for use of eq. 1.6

Tables 5.14 through 5.17 illustrate the determination of the equilibrium diamagnetic shielding in H_2, HF, F_2, and FCl. Basis set convergence is smooth throughout the extrapolation of each excitation contribution. Interestingly, the basis set convergence of each contribution occurs more rapidly within diamagnetic shielding constants than absolute shielding constants. Within HF, F_2, and FCl, contributions above SD converge as early as the ACVTZ basis set, whilst HF-SCF and SD excitation contributions appear to converge at the ACV5Z basis set. This is not the case for absolute shielding constants where basis set convergence was slower and required calculations with extensive basis sets. It is also evident that the decrease in the magnitude of each successive excitation exists even in the diamagnetic component of absolute shielding. Additionally, the amounts in which higher excitations contribute to the diamagnetic shielding is vastly smaller than in absolute shielding constants. Within HF, T excitations contribute approximately 0.2 ppm to the overall shielding (Table 3.9) while they contribute two orders of magnitude less towards diamagnetic shielding constants. These trends are due to method and basis set having an overall decreased effect on the diamagnetic contribution compared to the paramagnetic and absolute shielding. This is likely due to the diamagnetic shielding being more related to the nuclear contributions to shielding rather than electronic effects.[1,9,16]

Sundholm *et al.*[12] calculated diamagnetic shielding constants within H_2, HF, and F_2 for the purposes of semi-experimental shielding constants using CCSD(T) along with 8*s*5*p*3*d*2*f* and 15*s*11*p*3*d*2*f* basis sets for hydrogen and fluorine, respectively. Sundholm *et al.* produced diamagnetic shielding constants of 32.3885 ppm, 482.34 ppm, and 530.078 ppm for H_2, HF, and F_2, respectively. These agree with the diamagnetic shielding constants presented in Tables 5.14 to 5.16 extremely well, with the ^{1}H shielding in H_2 and ^{19}F shielding in HF deviating by

less than 0.01 ppm, and the ^{19}F shielding in F_2 deviating by 0.06 ppm. Any variation between numbers can be attributed to differences within the applied geometry, where Sundholm *et al.* utilised experimental geometries as opposed to the CCSD(T) optimised ones considered in this work. The consideration of higher coupled-cluster excitations is less likely to cause the deviation due to previously discussed minor impact these have on diamagnetic shielding constants.

Table 5.18 demonstrates the conversion of reported experimental spin-rotation constants into paramagnetic shielding constants for the purposes of creating semi-experimental absolute shielding constants yields shielding constants very similar to those presented in Chapter 3. F_2 is the only case of the molecules considered thus far where conversion of spin-rotation results in a larger paramagnetic shielding. This is due to the smaller rotational constant B, which is a magnitude less than that of HF. The reported uncertainties reported in Table 5.18 arise from the difference in the paramagnetic shielding that occurs if the spin-rotation constant was shifted to the error bar limit as well as the uncertainty estimated the diamagnetic shielding as a result of the rates of convergence. It is important to note that any difference between the semi-experimental shielding constants in Table 5.18 and those discussed in Chapter 3 arises purely from the paramagnetic contribution to the absolute shielding as the addition of vibrational corrections and relativistic effects occur in the same manner as in the investigation to absolute shielding constants.

The resulting shielding in H_2 is 26.298(3) ppm falls within experimental error compared to the experimental shielding of 26.293(5) ppm[40] and deviates from the fully calculated shielding by 0.016 ppm. It is believed that the semi-experimental value is therefore more accurate. It is also worth noting that if the largest basis set results for the vibrational corrections towards the H_2 spin-rotation constant are used to circumvent the non-monotonic convergence seen in Table 5.2, the overall semi-experimental shielding moves closer towards the measured shielding.

The semi-experimental ^{19}F shielding in HF comes to a total of 414.854(19) ppm. This is within close agreement with the fully calculated shielding of 414.310 ppm. Unlike the case of H_2, this semi-experimental shielding deviates from the corrected experimental shielding of 414.09 ppm.[7,14,25] Sundholm *et al.*[12] reported a semi-experimental shielding of 409.6 ± 1 ppm without the addition of relativistic corrections. The agreement between the updated semi-experimental shielding proposed here and the fully calculated shielding discussed in Section 3.4 further emphasises that the true absolute ^{19}F shielding in HF is closer to the fully calculated 414.310 ppm than the previously reported shielding by Sundholm *et al*. The fully calculated shielding

is believed to be more accurate in this case, due to the decreased deviation to both the corrected experimental shieling as well as the agreement with the semi-experimental shielding of 409.6 ppm from Sundholm *et al.*[12] when removing relativistic effects. Bass *et al.*[51] reported an experimental vibrationally corrected spin-rotation constant of -280.49 kHz. Using this spin-rotation constant in the generation of the paramagnetic shielding yields an absolute shielding of 415.051 ppm, which deviates further from the fully calculated shielding of 414.310 ppm than the shielding constant derived in Table 5.18.

Determination of the semi-experimental ^{19}F absolute shielding constant in F_2 results in a shielding constant of -222.111(444) ppm. Sundholm *et al.*[12] reported a semi-experimental ^{19}F shielding of -231.62 ppm. The deviation between these two results occurs mostly within calculated vibrational and temperature effects to the absolute shielding. This is evident as the equilibrium shielding of Sundholm *et al.* and that in Table 5.18 differs by less than 0.1 ppm as discussed previously. Therefore, any difference must occur outside the equilibrium shielding, for which differences have been discussed in detail within Chapter 3. Agreement between the semi-experimental shielding and fully calculated shielding presented in Table 3.16 is within 1.05 ppm. While this agreement is good, it is outside the error bars provided by the experimental spin-rotation data. This is attributed to the basis-set convergence within the fully calculated shielding not being as rapid as the diamagnetic shielding. Additionally, Q excitation contributions within the fully calculated shielding amount to greater than -1 ppm. Shielding contributions from higher (P and beyond) excitations could be sizeable and cause the overall shielding to be more negative, as is the case with Q excitations, causing the calculated shielding to shift closer to the semi-experimental shielding proposed here. There is a very close agreement with the experimental absolute shielding -221.93 ppm[25,46] as well as the corrected experimental shielding within Table 4.11, both of which occur within the experimental error from the spin-rotation constant. This agreement with experimental shielding constants, along with an accurate diamagnetic shielding, allows for the conclusion that the semi-experimental shielding is more precise than the fully calculated shielding presented in Chapter 3.

Use of experimental ^{19}F spin-rotation data for FCl provides a semi-experimental shielding of 643.25(13) ppm. This deviates from the experimental shielding of 640.94 ppm[7,25,47] by 2.3 ppm. The deviation occurs within the paramagnetic shielding component, as the fully calculated shielding in Table 3.17 appears very close to the experimental value. A possible cause of this error may be within the vibrational, temperature and relativistic effects to the spin-rotation constant. In the case of FCl, a change of 0.1 kHz to the spin-rotation constant results

in a shift in over 1 ppm to the paramagnetic shielding. As such, minor errors propagate rapidly in this conversion process.

5.4 H_2O, HOF, F_2O Spin-Rotation Constants

Extending calculations of spin-rotation constants to non-linear molecules requires extra consideration. Spin-rotation is a 3 x 3 tensor; for linear molecules, the spin-rotation constant is represented by a single unique value (xx and yy are degenerate components and zz component is 0). However, for non-linear molecules, the xx and yy components are not equivalent, and as such, the spin-rotation constant is referenced by separate $\boldsymbol{C}_{xx}$, $\boldsymbol{C}_{yy}$, and $\boldsymbol{C}_{zz}$ components. Additionally, eq. 1.6 utilises the individual components, so separation of the xx, yy, and zz components is important for the determination of semi-experimental shielding constants. For non-linear molecules H_2O, HOF, and F_2O, components of the spin-rotation tensor are reported.

Table 5.19: Calculated ^{1}H spin-rotation tensor elements in H_2O (kHz). Vibrational and Temperature effects calculated using CCSD(T). Relativistic effects calculated using PBE0/dyall-aug-cvqz.

C_{gg}	Contribution	ACVDZ	ACVTZ	ACVQZ	ACV5Z	ACV6Z	CBS
C_{xx}	HF-SCF	35.601	34.030	33.503	33.335	33.268	33.223
	SD	1.146	0.853	0.578	0.504	0.476	0.439
	(T)	0.148	0.140	0.136	0.135	0.135	0.134
	T	-1.295	-0.992	0.006			0.734
	Q	1.310					1.310
	Vibrational Effects	-1.667	-1.559	-1.547			-1.538
	Temperature (300K)	-0.128	-0.130	-0.127			-0.124
	Relativistic Effects						0.147
	Total						**34.325**
C_{yy}	HF-SCF	36.796	35.054	34.453	34.282	34.207	34.150
	SD	1.550	1.324	1.022	0.941	0.912	0.873
	(T)	0.239	0.240	0.243	0.244	0.244	0.244
	T	-1.789	-1.565	-0.001			1.141
	Q	1.809					1.809
	Vibrational Effects	-1.305	-1.184	-1.180			-1.177
	Temperature (300K)	-0.117	-0.120	-0.116			-0.113
	Relativistic Effects						0.274
	Total						**37.201**
C_{zz}	HF-SCF	33.724	32.069	31.485	31.309	31.236	31.184
	SD	0.979	0.726	0.466	0.393	0.369	0.335
	(T)	0.101	0.088	0.083	0.081	0.081	0.080
	T	-1.080	-0.813	0.006			0.603
	Q	1.089					1.089
	Vibrational Effects	-0.778	-0.620	-0.625			-0.628
	Temperature (300K)	-0.110	-0.113	-0.109			-0.106
	Relativistic Effects						0.208
	Total						**32.765**

Assessment of the ^{1}H spin-rotation constant in H_2O within Table 5.19 shows that a decrease in coupled-cluster excitation contribution is not prevalent for components of the spin-rotation tensor. In the case of H_2O, the contribution to the spin-rotation tensor component increases with higher excitation states from SD to Q excitations, if considering complete T contributions as a combination of (T) and T. However, the majority of the spin-rotation tensor element comes from the HF-SCF calculation as seen with all other properties thus far. It may be contended that the use of the ACVDZ basis set yields inaccurate results for the Q contributions; however,

it is difficult to conclude if an extrapolated CBS value would result in a larger or smaller contribution without further investigation into the effect of higher excitations on spin-rotation tensors. Vibrational averaging and temperature effects follow previously discussed trends, with vibrational corrections affecting the spin-rotation tensor elements by a magnitude more than temperature effects. These effects contribute approximately 1 kHz towards the tensor elements, which given the relatively small size of the components, is continued to be considered important.

Final calculated spin-rotation tensor elements of $\boldsymbol{C}_{xx}$, $\boldsymbol{C}_{yy}$, and $\boldsymbol{C}_{zz}$ amount to 34.325 kHz, 37.201 kHz, and 32.765 kHz, respectively. The uncertainties for each of the tensor elements is estimated to be ±1 kHz due to the unconverted (T) contributions to the equilibrium spin-rotation tensors. The reported tensor elements agree very well with experimental results of 32.91 kHz, 34.45 kHz, and 31.03 kHz from Puzzarini *et al.*[11] The largest deviation occurs within the $\boldsymbol{C}_{yy}$ component of 2.75 kHz. Due to the impact Q contributions have on the tensor elements, it may be expected that higher excitation contributions have a greater impact on spin-rotation tensors, and further excitations must be considered. Puzzarini *et al.* also reported CCSD(T)/ACV6Z equilibrium spin-rotation tensor elements augmented with vibrational corrects at the CCSD(T)/ACV5Z level of theory as 32.54 kHz, 34.27 kHz, and 31.16 kHz. These agree very well with the CCSD(T)/CBS equilibrium spin-rotation tensor elements augmented with vibrational, temperature and relativistic effects from Table 5.19 to within 0.3 kHz for each component. Therefore, it is believed an investigation into higher excitation contribution is required to understand the impact on spin-rotation tensor elements. Teale *et al.*[18] reported the ^{1}H equilibrium spin-rotation tensor elements of H_2O as 34.59 kHz, 35.91 kHz, and 32.35 kHz from extrapolating CCSD(T)/ACVTZ and CCSD(T)/ACVQZ results. These agree well with similar results presented here; however, the $\boldsymbol{C}_{xx}$ tensor component differs by over 2 kHz. This likely arises due to geometry differences, for which Teale *et al.* utilised a CCSD(T)/VTZ optimised geometry as opposed to the CCSD(T)/ACVQZ optimised geometry used here.

Table 5.20. Calculated ^{19}F spin-rotation tensor elements in HOF (kHz). Vibrational and Temperature effects calculated using CCSD(T). Relativistic effects calculated using PBE0/dyall-aug-cvqz.

C_{gg}	Contribution	ACVDZ	ACVTZ	ACVQZ	ACV5Z	ACV6Z	CBS
C_{xx}	HF-SCF	-7.303	-9.271	-9.077	-8.981	-9.013	-9.005
	SD	-0.854	-1.270	-1.453	-1.487	-1.479	-1.467
	(T)	-0.015	-0.247	-0.339	-0.372		-0.407
	T	-0.199	-0.274				-0.306
	Vibrational Effects	-6.769	-6.557				-6.469
	Temperature (300K)	-0.005	0.009				0.015
	Relativistic Effects						1.198
	Total						**-16.440**
C_{yy}	HF-SCF	-21.288	-23.303	-23.782	-23.966	-24.008	-24.021
	SD	-21.985	-22.561	-22.448	-22.456	-22.448	-22.437
	(T)	-1.927	-2.594	-2.730	-2.782		-2.837
	T	-0.011	-0.035				-0.045
	Vibrational Effects	-0.131	-0.023				0.023
	Temperature (300K)	-0.304	-0.263				-0.245
	Relativistic Effects						0.339
	Total						**-49.223**
C_{zz}	HF-SCF	-53.481	-54.973	-55.743	-56.028	-56.112	-56.147
	SD	-12.655	-14.429	-14.374	-14.370	-14.352	-14.327
	(T)	-1.770	-2.366	-2.502	-2.556		-2.612
	T	-0.152	-0.200				-0.220
	Vibrational Effects	-3.300	-3.048				-2.941
	Temperature (300K)	-0.463	-0.397				-0.368
	Relativistic Effects						0.150
	Total						**-76.465**

Table 5.20 demonstrates the ^{19}F spin-rotation tensor elements in HOF. Unlike the case of the ^{1}H spin-rotation tensor element in H_2O, Table 5.20 demonstrates the trend of decreasing contribution with consideration of additional excitation states. However, Q contributions to the equilibrium spin-rotation constant could not be determined, and as such, it is difficult to determine if the trend similar to H_2O would appear for HOF as well. The calculated components of the HOF ^{19}F spin-rotation tensor converge smoothly and rapidly, with the T contribution of the C_{xx} tensor element being the least converged amongst the equilibrium calculations. However, this is likely due to extrapolating from a DZ basis set. Regardless, the smooth and rapid convergence leads to estimated uncertainties of ±0.15 kHz within the final reported spin-rotation tensor elements. Interestingly, for the C_{yy} component, SD excitation contributions

make up almost the same amount as the HF-SCF calculations. SD contributions are of similar size within the $\boldsymbol{C}_{zz}$ component, however, are much smaller than the HF-SCF contribution, unlike what is seen for the $\boldsymbol{C}_{yy}$ component. (T) excitations contribute for more than 2 kHz for the $\boldsymbol{C}_{yy}$ and $\boldsymbol{C}_{zz}$ components and thus cannot be ignored when quantitative accuracy is desired. Interestingly, relativistic effects are of a similar magnitude within the HOF ^{19}F spin-rotation tensor as they are within the H_2O ^{1}H spin-rotation tensor. This contrasts trends within absolute shielding where relativistic effects were much larger in ^{19}F than that of ^{1}H. Teale *et al.*[18] calculated the ^{19}F equilibrium spin-rotation tensor within HOF as -17.48 kHz, -50.14 kHz, and -74.7 kHz from equilibrium CCSD(T) calculations. Whilst the $\boldsymbol{C}_{yy}$ and $\boldsymbol{C}_{zz}$ components are within very close agreement to the equilibrium spin-rotation tensor here, the $\boldsymbol{C}_{xx}$ component deviates by over 6 kHz. A possible cause of this deviation is a difference in the geometry, as discussed in the deviation within H_2O. However, an alternative possibility is a slight isotropic effect. Teale *et al.* reported the ^{19}F spin-rotation tensor along with the ^{16}O isotope, whereas the results presented here arise from the ^{17}O isotope. Sundholm and Gauss[41] have previously shown that the ^{1}H spin-rotation constant within H_2 can change by almost 30 kHz compared to HD. Whilst this effect is expected to be greater in H_2 due to the larger relative mass increase compared to that of the difference between ^{16}O and ^{17}O, the influence of isotope effects on the spin-rotation tensor cannot be underestimated and requires further investigation.

Table 5.21. Calculated ^{19}F spin-rotation tensor elements in F_2O (kHz). Vibrational and Temperature effects calculated using CCSD(T). Relativistic effects calculated using PBE0/dyall-aug-cvqz.

C_{gg}	Contribution	ACVDZ	ACVTZ	ACVQZ	ACV5Z	ACV6Z	CBS
C_{xx}	HF-SCF	-47.127	-47.775	-48.334	-48.561	-48.630	-48.660
	SD	1.949	0.522	0.456	0.451		0.446
	(T)	-0.864	-0.891	-0.926			-0.952
	T	-0.005					-0.005
	Vibrational Effects	-1.515	-1.443				-1.413
	Temperature (300K)	-0.210	-0.179				-0.166
	Relativistic Effects						0.611
	Total						**-50.139**
C_{yy}	HF-SCF	-34.426	-36.331	-36.946	-37.177	-37.235	-37.255
	SD	-12.144	-13.163	-13.113	-13.116		-13.121
	(T)	-2.232	-2.707	-2.806			-2.878
	T	-0.463					-0.463
	Vibrational Effects	-2.021	-1.897				-1.845
	Temperature (300K)	-0.108	-0.089				-0.081
	Relativistic Effects						0.058
	Total						**-55.584**
C_{zz}	HF-SCF	-18.453	-18.733	-18.972	-19.067	-19.095	-19.106
	SD	-3.019	-3.638	-3.659	-3.669		-3.679
	(T)	-0.878	-1.002	-1.036			-1.061
	T	-0.064					-0.064
	Vibrational Effects	-0.733	-0.682				-0.660
	Temperature (300K)	-0.144	-0.120				-0.110
	Relativistic Effects						0.028
	Total						**-24.652**

Trends within the F_2O ^{19}F spin-rotation tensor are not consistent between components. Whilst the C_{yy} and C_{zz} components follow the general trend of decreasing contributions from higher excitations, the C_{xx} tensor element follows a similar trend to that seen within H_2O, where the combination of (T) and T excitations is larger than the SD contribution. Additionally, the SD contribution accounts for a large amount of the C_{yy} and C_{zz} tensor components. Vibrational and temperature effects follow expected trends, with vibrational corrections contributing a magnitude more than the temperature effects to the final spin-rotation tensor. Relativistic effects are surprisingly small within F_2O, with the C_{yy} and C_{zz} relativistic effects being smaller than all relativistic effects within the ^1H spin-rotation tensor of H_2O. This is unexpected given the relativistic effects within HOF were of a similar size to those within H_2O, as well as all ^{19}F

shielding relativistic effects being much greater than relativistic effects to ^{1}H shielding constants. Once again, the convergence of the calculated components of the ^{19}F spin-rotation tensor elements is smooth and an uncertainty of ±1.0 kHz is estimated for each reported final spin-rotation element.

The equilibrium spin-rotation tensor was reported by Teale *et al.*[18] as 51.09 kHz, 52.81 kHz, and 24.07 kHz after extrapolating CCSD(T)/ACVTZ and CCSD(T)/ACVQZ results. These agree quite well with the equilibrium results presented in Table 5.21, with the largest deviation occurring within the $\boldsymbol{C}_{xx}$ component at 1.9 kHz. Consideration of vibrational effects from Teale *et al.* of 1.41 kHz, 1.48 kHz, and 0.54 kHz decreases the deviation between results here and those of Teale *et al*. Flygare[56] preformed microwave spectrometry to determine the spin-rotation tensor elements of F_2O of 49 kHz, 42 kHz, and 22 kHz. Whilst these are of similar size to the tensor elements reported here and by Teale *et al.*, there remains a large deviation of over 12 kHz within the $\boldsymbol{C}_{yy}$ tensor component from both calculated sources. This is most likely due to the process in which the experimental spin-rotation tensor was developed. Flygare converted a paramagnetic contribution to the F_2O absolute shielding and performed a least-squares fit against microwave spectrometry results to determine the most likely spin-rotation tensor elements given available data. However, a chemical shift of 205.2 for F_2O relative to F_2 was used in the calculation of the paramagnetic shielding, whereas the F_2O and F_2 chemical shifts have since been updated, resulting in a change to the chemical shift of approximately 35 ppm. Therefore, it is concluded that the calculated F_2O spin-rotation tensor elements reported here are the most accurate to date.

5.5 H_2O, HOF, F_2O Semi-Experimental Shielding Constants

The semi-experimental absolute shielding constants of the H_2O, HOF, and F_2O series have been determined via the process outlined in Section 1.2 and demonstrated in Section 5.3. First, diamagnetic shielding constants were determined by extrapolating the contributions of the coupled-cluster wave function expansion. Once an equilibrium diamagnetic shielding has been calculated, it can be combined with a paramagnetic shielding constant. The paramagnetic shielding was calculated through the use of eq. 1.6, utilising experimental spin-rotation tensors with calculated vibrational, temperature, and relativistic effects removed. It is noted that the result of using eq. 1.6 will not be multiplied by $\frac{2}{3}$ as the following molecules are not linear. The equilibrium non-relativistic paramagnetic and diamagnetic shielding constants will then be

combined along with vibrational, temperature, and relativistic corrections reported in Chapter 4 to generate a final semi-experimental absolute shielding constant.

Table 5.22: Diamagnetic ^{1}H shielding contribution in H_2O (ppm).

Contribution	ACVDZ	ACVTZ	ACVQZ	ACV5Z	ACV6Z	CBS
HF-SCF	102.233	102.415	102.445	102.452	102.453	102.453
SD	-0.128	-0.086	-0.080	-0.075	-0.074	-0.073
(T)	-0.028	-0.038	-0.039	-0.039	-0.039	-0.039
T	0.001	0.003	0.004			0.004
Q	-0.002					-0.002
Diamagnetic Shielding						102.343

Table 5.23: Diamagnetic ^{19}F shielding contribution in HOF (ppm).

Contribution	ACVDZ	ACVTZ	ACVQZ	ACV5Z	ACV6Z	CBS
HF-SCF	528.372	528.663	528.746	528.770	528.772	528.773
SD	-0.682	-0.117	-0.019	0.018	0.033	0.054
(T)	-0.024	-0.036	-0.037	-0.038		-0.038
T	0.007	0.007				0.007
Diamagnetic Shielding						528.796

Table 5.24: Diamagnetic ^{19}F shielding contribution in F_2O (ppm).

Contribution	ACVDZ	ACVTZ	ACVQZ	ACV5Z	ACV6Z	CBS
HF-SCF	561.901	562.201	562.288	562.313	562.315	562.316
SD	-0.446	0.095	0.184	0.219	0.232	0.251
(T)	-0.013	-0.017	-0.017			-0.018
T	0.010					0.010
Diamagnetic Shielding						562.559

Table: 5.25: Determination of semi-experimental ^{1}H and ^{19}F absolute shielding constants in H_2O,[(a)] HOF,[(b)] F_2O.[(c)]

Constants	H_2O (^{1}H)	HOF (^{19}F)	F_2O (^{19}F)
$\boldsymbol{C}_0^{\mathrm{rel}}$			
$\boldsymbol{C}_{xx}$ (kHz)	32.91(10)[11]		-49(2)[56]
$\boldsymbol{C}_{yy}$ (kHz)	34.45(19)[11]		-42(2)[56]
$\boldsymbol{C}_{zz}$ (kHz)	31.03(19)[11]		-22(2)[56]
$\boldsymbol{C}_e^{\mathrm{nonrel}}$			
$\boldsymbol{C}_{xx}$ (kHz)	34.43(10)	-11.185(150)[(d)]	-48(2)
$\boldsymbol{C}_{yy}$ (kHz)	35.47(19)	-49.339(150)[(d)]	-40(2)
$\boldsymbol{C}_{zz}$ (kHz)	31.56(19)	-73.306(150)[(d)]	-21(2)
σ_e^{p} (ppm)	-71.73(6)	-340.325(702)	-550(25)
σ_e^{d} (ppm)	102.343(0)	528.796(15)	562.559(15)
$\sigma_e^{\mathrm{nonrel}}$ (ppm)	30.62(6)	188.471(717)	13(25)
σ_0^{rel} (ppm)	30.14(6)	172.924(717)	-7(25)

(a) r(OH) = 0.9757 Å and ∠(HOH) = 104.51° for use of eq. 1.6
(b) r(OH) = 0.9600 Å, r(OF) = 1.4420 Å, and ∠(HOF) = 97.20° for use of eq. 1.6
(c) r(OF) = 1.4050 Å and ∠(FOF) = 103.10° for use of eq. 1.6
(d) Calculated spin-rotation tensor element

Basis set convergence is smooth for the determination of the diamagnetic shielding for H_2O, HOF, and F_2O. The largest difference between two extrapolated basis sets is 0.015 ppm within the SD contribution to the HOF diamagnetic shielding, which may be considered very good. Convergence towards a CBS value occurs much more rapidly than in the case of absolute shielding constants as shown in the estimated CBS contributions to the ^{1}H diamagnetic shielding in H_2O. The estimated CBS contributions to the diamagnetic shielding equal those calculated with the ACV6Z basis set outside of the SD contribution which differs by only 0.001 kHz. Additionally, consideration of higher excitations contributes much less to the diamagnetic shielding than seen for absolute shielding constants. Table 4.7 shows SD excitations contribute over 10 ppm to the overall shielding, whereas they make up less than 0.5 ppm within the diamagnetic shielding. These trends mirror those seen within the diatomics of Sections 5.3. Evidence of decreasing shielding contribution with an increase of excitation level is once again prevalent. Within all three molecules, deviation from fully calculated diamagnetic shielding constants and HF-SCF/ACVQZ calculated diamagnetic shielding constants is less than 1 ppm. Because of this, large molecules have the potential for high accuracy absolute shielding studies given accurate experimental spin-rotation data is available.

Table 5.25 shows the semi-experimental shielding constants for H_2O and F_2O based on experimental spin-rotation data along with fully calculated diamagnetic shielding constants. Error bars reported result from augmenting experimental spin-rotation tensor elements with provided error bars during the conversion to paramagnetic shielding constants. Calculation of the semi-experimental ^1H shielding within H_2O yields a final shielding constant that is within 0.04 ppm from the experimentally reported 30.102 ppm from Garbacz *et al.*[40] and is within 0.03 ppm of the fully calculated absolute shielding constant reported in Chapter 4. Both the experimental and fully calculated absolute shielding constants lie within the uncertainty of the semi-experimental shielding, which suggests that these values are reliable.

Due to experimental spin-rotation data not being available for the HOF molecule, the fully calculated equilibrium spin-rotation tensor is used instead. Use of an optimised geometry during application of eq. 1.6 results in an absolute shielding that deviates from the fully calculated shielding reported in Chapter 4 by less than 0.001 ppm. Therefore, Conversion of the spin-rotation tensor will use an experimental geometry so that the effects of the rotational constants and nuclear component of the spin-rotation tensor elements can be further understood. The ^{19}F absolute shielding via this method is 172.924(717) ppm, which deviates by 2.4 ppm to the fully calculated shielding of 175.299 ppm. It is thus concluded that the geometry effects have a large effect during the conversion process of eq. 1.6. A likely cause of this is the use of an experimental geometry along with calculated equilibrium spin-rotation constants when using eq. 1.6 as opposed to an equilibrium geometry. The absolute shielding derived via eq. 1.6 with use of experimental geometry deviates further from the experimental 180.07 ppm[48] than the fully calculated absolute shielding. This is likely due to the cross-use of a calculated spin-rotation tensor with an experimental geometry for constant conversion. While geometry effects on the conversion seem prevalent, they may be cancelled from experimental spin-rotation data. As such, further investigation into the effects of geometry is required.

The semi-experimental ^{19}F shielding within F_2O is calculated to be -7(25) ppm. This deviates from the experimental shielding by over 40 ppm[46] and the fully calculated shielding reported in Chapter 4 by almost 35 ppm. This is caused by the inaccuracies of the spin-rotation tensor, as discussed in Section 5.4. Large deviations within the paramagnetic shielding are not surprising due to the spin-rotation tensor elements being determined from outdated chemical shift data. The hypothesis that the error within the semi-experimental shielding arises from the provided spin-rotation can be examined using calculated spin-rotation tensor elements as opposed to the reported experimental constants. Exchanging the experimental spin-rotation

tensor elements with calculated equilibrium spin-rotation data presented here and by Teale *et al.*[18] results in shielding constants of -42.65 ppm and -56.56 ppm, respectively. Similarities between the fully calculated shielding in Chapter 4 and substituting fully calculated spin-rotation data from Table 5.24 results is unsurprising due to the relationship between the shielding constant and spin-rotation tensor elements, with the slight deviation arising due to the use of experimental geometry for the use of the rotational constants B_{gg} and the nuclear spin-rotation tensor elements. Deviations between the fully calculated shielding, the semi-experimental shielding, as well as the shielding constant using spin-rotation constants from Teale *et al.* demonstrate the effect of slight changes in the applied spin-rotation tensor elements as well as geometry as a whole on the overall absolute shielding constant.

5.6 CH_3F and FCN Spin-Rotation Constants

Spin-rotation tensors for ^{19}F nuclei have been further calculated for the CH_3F and FCN molecules. As FCN is a linear molecule, the spin-rotation constant will instead be reported, as was the case with the diatomics within Section 5.2. Due to the symmetry of CH_3F being C_{3v}, the $\boldsymbol{C}_{yy}$ and $\boldsymbol{C}_{zz}$ spin-rotation tensor elements are equal and will thus be reported together. The methodology of spin-rotation calculation is identical to that of the previous molecules, with equilibrium spin-rotation tensors and constants being derived via applying additional excitation levels of the coupled-cluster expansion. These are augmented with calculated vibrational, temperature, and relativistic effects to obtain spin-rotation tensor components that can be directly compared to experiment.

Table 5.26: Calculated ^{19}F spin-rotation tensor elements in CH_3F (kHz). Vibrational and Temperature effects calculated using CCSD(T). Relativistic effects calculated using PBE0/dyall-aug-cvqz.

C_{gg}	Contribution	ACVDZ	ACVTZ	ACVQZ	ACV5Z	CBS
C_{xx}	HF-SCF	-39.900	-43.241	-44.333	-44.480	-44.503
	SD	-4.258	-3.009	-2.593	-2.496	-2.395
	(T)	-1.125	-1.551	-1.569	-1.600	-1.632
	T	-0.174				-0.174
	Vibrational Effects	-2.339	-2.952			-3.211
	Temperature (300K)	-0.007	0.120			0.174
	Relativistic Effects					-0.165
	Total					-51.906
$C_{yy} = C_{zz}$	HF-SCF	6.525	6.521	6.552	6.557	6.558
	SD	-0.576	-0.526	-0.503	-0.504	-0.505
	(T)	-0.091	-0.086	-0.084	-0.083	-0.081
	T	-0.042				-0.042
	Vibrational Effects	-1.477	-1.424			-1.403
	Temperature (300K)	0.009	-0.082			-0.120
	Relativistic Effects					-0.001
	Total					4.407

Table 5.27: Calculated ^{19}F spin-rotation constant in FCN (kHz). Vibrational and Temperature effects calculated using CCSD(T). Relativistic effects calculated using PBE0/dyall-aug-cvqz.

Contribution	ACVDZ	ACVTZ	ACVQZ	ACV5Z	CBS
HF-SCF	-7.702	-8.081	-8.184	-8.234	-8.279
SD	0.520	0.005	0.014	0.026	0.038
(T)	-0.340	-0.339	-0.351		-0.359
T	-0.027	-0.043			-0.050
Vibrational Effects	-0.335	-0.305			-0.292
Temperature (300K)	-0.027	-0.018			-0.014
Relativistic Effects					-0.712
Total					-9.669

Calculation of the CH_3F ^{19}F spin-rotation tensor yields components C_{xx} = -51.906 kHz and $C_{yy} = C_{zz}$ = 4.407 kHz. The calculated equilibrium spin-rotation tensor elements are expected

to be accurate, as each extrapolated contribution to the $\boldsymbol{C}_{yy}$ and $\boldsymbol{C}_{zz}$ components converge to within 0.005 kHz while the contributions to the $\boldsymbol{C}_{xx}$ component converge within 0.1 kHz. These are considered very good, and therefore the calculated equilibrium spin-rotation tensor is accurate, with estimated uncertainties of ±0.3 kHz and ±0.05 kHz for the $\boldsymbol{C}_{xx}$and $\boldsymbol{C}_{yy}$ = $\boldsymbol{C}_{zz}$ components respectively. The spin-rotation tensor elements reported by Teale *et al.*[18] using CCSD(T) of -50.43 kHz and 6.54 kHz for the $\boldsymbol{C}_{xx}$ and $\boldsymbol{C}_{yy}$ = $\boldsymbol{C}_{zz}$ components, respectively. The equilibrium spin-rotation $\boldsymbol{C}_{xx}$ component calculated here is -48.703 kHz and deviates by over 1.7 kHz to Teale *et al.* results. Experimental spin-rotation tensor components of $\boldsymbol{C}_{xx}$ = -51.1(13) kHz and $\boldsymbol{C}_{yy}$ = $\boldsymbol{C}_{zz}$ = 4.0(19) kHz have been reported by Wofsy *et al*.[57] and are within 1.0 kHz and 0.4 kHz of the $\boldsymbol{C}_{xx}$ and the $\boldsymbol{C}_{yy}$ = $\boldsymbol{C}_{zz}$ tensor components calculated here, respectively. Comparatively, exchanging the equilibrium spin-rotation tensor elements with those by Teale *et al.* increases the deviation from experiment by almost 0.6 kHz for each component. Therefore, it is concluded that the calculated tensor in Table 5.26 is very accurate.

The ^{19}F spin-rotation constant of FCN is calculated to be -9.669 kHz, with the equilibrium spin-rotation constant of -8.65 kHz. The convergence throughout the equilibrium spin-rotation constant calculation is very smooth, with an estimated error of approximately 0.05 kHz. This agrees well with the equilibrium spin-rotation constant calculated by Teale *et al.*[18] of -8.66 kHz. Whilst there is no experimental data for the ^{19}F spin-rotation constant, the strong agreement between the calculated spin-rotation constant here and from Teale *et al.* demonstrates the accuracy of the calculated spin-rotation constant.

5.7 CH_3F and FCN Semi-Experimental Shielding Constants

Calculation of the semi-experimental ^{19}F shielding of CH_3F and FCN requires the calculation of the diamagnetic shielding following a similar procedure as the molecules investigated thus far. Combining an equilibrium diamagnetic shielding along with an equilibrium paramagnetic shielding as derived from eq. 1.6 produces an equilibrium semi-experimental shielding, which is further augmented with vibrational, temperature, and relativistic corrections. As CH_3F is a non-linear molecule, all components of the spin-rotation tensor will be used within the application of eq. 1.6, whereas the linear FCN will only apply the spin-rotation constant. Additionally, the result of applying eq. 1.6 for FCN will be multiplied by $\frac{2}{3}$ as was performed in Section 5.3.

Table 5.28: Diamagnetic ^{19}F shielding contribution in CH_3F (ppm).

Contribution	ACVDZ	ACVTZ	ACVQZ	ACV5Z	CBS
HF-SCF	526.716	527.008	527.085	527.108	527.118
SD	-0.738	-0.140	-0.030	0.011	0.053
(T)	-0.058	-0.074	-0.075	-0.075	-0.075
T	0.003				0.003
Diamagnetic Shielding					527.100

Table 5.29: Diamagnetic ^{19}F shielding contribution in FCN (ppm).

Contribution	ACVDZ	ACVTZ	ACVQZ	ACV5Z	CBS
HF-SCF	540.845	541.095	541.177	541.200	541.210
SD	-0.424	0.141	0.237	0.274	0.312
(T)	-0.044	-0.051	-0.050	-0.049	-0.049
T	0.005	0.003			0.003
Diamagnetic Shielding					541.476

Table: 5.30: Determination of semi-experimental ^{19}F absolute shielding constants in CH_3F[(a)] and FCN.[(b)]

Constants	CH_3F[(a)] (^{19}F)	FCN[(b)] (^{19}F)
$\boldsymbol{C}_0^{\mathrm{rel}}$		
$\boldsymbol{C}_{xx}$ (kHz)	-51.1(13)[57]	
$\boldsymbol{C}_{yy}$ (kHz)	4.0(19)[57]	
$\boldsymbol{C}_{zz}$ (kHz)	4.0(19)[57]	
$\boldsymbol{C}_e^{\mathrm{nonrel}}$		-8.650(50)[(c)]
$\boldsymbol{C}_{xx}$ (kHz)	-48.1(13)	
$\boldsymbol{C}_{yy}$ (kHz)	5.5(19)	
$\boldsymbol{C}_{zz}$ (kHz)	5.5(19)	
σ_e^{p} (ppm)	-47.6(91)	-166.925(550)
σ_e^{d} (ppm)	527.100(20)	541.476(35)
$\sigma_e^{\mathrm{nonrel}}$ (ppm)	479.5(91)	374.551(585)
σ_0^{rel} (ppm)	474.0(91)	371.516(585)

(a) r(CF) = 1.3830 Å, r(CH) = 1.0870 Å, and ∠(FCH) = 108.73° for use of eq. 1.6
(b) r(FC) = 1.2620 Å and r(CN) = 1.1590 Å for use of eq. 1.6
(c) Calculated spin-rotation constant

As with all diamagnetic shielding constants calculated thus far, basis set convergence is rapid throughout each excitation contribution, even in the case of the larger CH_3F molecule. It is noted that the difference between the HF-SCF/ACVTZ diamagnetic shielding and the fully calculated diamagnetic shielding of CH_3F differs by less than 0.1 ppm, which is an acceptable deviation within larger difficult to calculate molecules. The least converged contribution within Tables 5.28 and 5.29 is the SD contribution to the CH_3F diamagnetic shielding with a difference of 0.041 ppm between the ACVQZ and ACV5Z basis set results. However, this is deemed insignificant given the magnitude of the diamagnetic shielding of over 540 ppm, as well as the good estimate for the CBS result. The contribution of (T) excitations is minimal in both CH_3F and FCN, with the T excitation being of near negligible size.

The semi-experimental shielding of CH_3F is determined to be 474.0(91) ppm, which agrees well with the experimentally determined 474.95 ppm from chemical shift data reported by Jameson *et al.*,[15] as well as the fully calculated shielding of 475.721 ppm in Table 4.10. The experimental error of ±9.1 ppm is determined via inputting the extremes of the reported experimental error to the spin-rotation tensor elements. It should be noted, however, that while error bars of ±1.3 kHz and ±1.9 kHz were reported for the $\boldsymbol{C}_{xx}$ and $\boldsymbol{C}_{yy} = \boldsymbol{C}_{zz}$ tensor elements, respectively, the fully calculated spin-rotation tensor elements are within 0.6 kHz of experimental data, so the expected error of the paramagnetic shielding component is much less than 9.1 ppm. Using the calculated equilibrium spin-rotation tensor reported by Teale *et al.*[18] results in a much larger deviation to experiment of 2.89 ppm. Therefore, it is concluded that the accuracy of the spin-rotation tensor within Table 5.26 is the most accurate to date.

Due to the lack of experimental data, a true semi-experimental ^{19}F shielding of FCN could not be determined. However, much like the case of HOF, the use of calculated spin-rotation tensors along with experimental geometries allows the investigation into the effect of geometry on the paramagnetic shielding. Here, an absolute shielding of 371.516(585) ppm is derived, which agrees very well with the fully calculated shielding of 371.483 ppm within Table 4.10. This agreement contrasts the case of HOF, which had a larger deviation of 2.4 ppm between the calculated shielding derived from eq. 1.6 and the fully calculated shielding. This is likely caused by differences within the rotational constants B_{gg} between experimental geometries and CCSD(T)/ACVQZ optimised geometries. In the case of HOF, the rotational constants change by approximately 5500 MHz, 260 MHz, and 230 MHz for the B_{xx}, B_{yy}, and B_{zz} rotational constants, respectively, whereas the rotational constant of FCN only differs by approximately 15 MHz. As the HOF rotational constants change dramatically with a variation of geometry as

opposed to FCN, it is unsurprising why the effect geometry has on the paramagnetic shielding is much larger within HOF.

5.8 Summary

Throughout this Chapter, the spin-rotational constants and tensors of ^{1}H and ^{19}F containing molecules have been calculated. These have been thoroughly compared to experimentally reported spin-rotation constants as well has previously calculated spin-rotation constants from Teale *et al.*[18] The spin-rotation constants have been shown to be considerably accurate when compared to experimental data, and in the cases where larger deviations propagate, failures within the calculation or experimental data were discussed in detail. Diamagnetic shielding constants were calculated for the use of developing semi-experimental absolute shielding constants. In all cases, the diamagnetic shielding was shown to be extremely accurate due to fast convergence and minimal dependence on higher coupled-cluster excitations. It has been shown that accurate diamagnetic shielding constants can be produced from HF-SCF calculations alone, and the use of CCSD(T) provides extreme accuracy, with higher excitations being of negligible size. Experimental spin-rotation data was augmented with calculated vibrational, temperature and relativistic effects and applied to eq. 1.6 to produce equilibrium non-relativistic paramagnetic shielding constants. These were combined with the accurate diamagnetic shielding constants to produce semi-experimental shielding constants that were compared to experimental chemical shift data, as well as the fully calculated absolute shielding constants reported throughout Chapters 3 and 4. In the cases where accurate spin-rotation data was available, semi-experimental shielding constants agreed well with experimental and calculated absolute shielding constants. Therefore, it is concluded that as diamagnetic shielding constants can be calculated with high accuracy with small methods and basis sets, high accuracy semi-experimental shielding constants can be developed given spin-rotation data availability.

Chapter 6:
DFT Calculations of ^{15}N Chemical Shifts

6.1 Introduction

Although the use of coupled-cluster methods such as CCSD(T) are ideal when calculating nuclear shielding constants and chemical shifts, the routine application of such methods is not feasible for medium and large-sized molecules. Therefore, it is important to investigate popular and new DFT functionals and assess their accuracy and usefulness in calculating shielding constants. A focused study on the chemical shifts of ^{15}N containing molecules has been performed in collaboration with Dr Marcello de Oliveira of the São Carlos Institute of Chemistry. While the focus of the thesis thus far has had a large emphasis on ^{19}F shieldings, the work lead by Dr. de Oliveira has instead focused on ^{15}N. A series of 32 nitrogen-containing compounds has been considered in an investigation of the performance of DFT methods in the calculation of ^{15}N chemical shifts. The set of molecules were selected due to their lack of conformational flexibility, as any flexibility (bond rotation) would require consideration of conformational averaging effects that would occur naturally in an experiment but would cause difficulties in a computational study. Equilibrium gas-phase ^{15}N chemical shifts have been calculated, along with vibrational corrections and relativistic effects, to get an insight into the effect these have over DFT calculated magnetic shieldings.

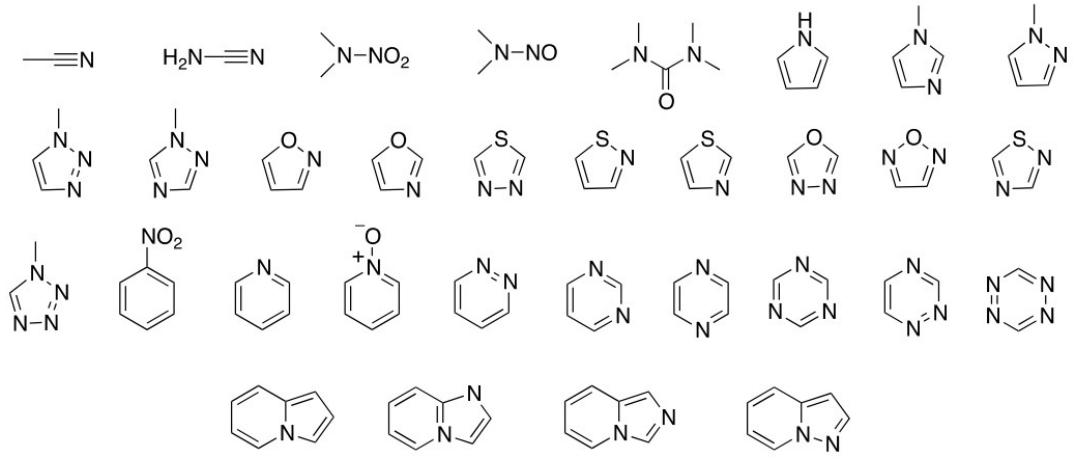

Figure 6.1: Series of 32 nitrogen-containing compounds considered throughout Chapter 6.

6.2 Gas-Phase Equilibrium Chemical Shifts

Throughout this thesis, only gas-phase nuclear shieldings have been calculated. This is due to considerations of solvation effects and intermolecular forces causing a shift in the absolute shielding compared to that of the single-molecule representation of most quantum chemistry calculations. Whilst it is possible to consider the effects of solvation on the shielding and chemical shift, here, only gas-phase shifts and shieldings will be explored. Gas-phase equilibrium chemical shifts have been calculated with the KTX (where X = 1, 2, or 3) GGA functionals in the DALTON program, whereas Dr. de Oliveira has kindly provided gas-phase chemical shifts calculated with the meta-GGA functional RevTPSS. The KTX functional were chosen as previous works have shown these to perform very well in regards to magnetic property calculations.[27] The decision to compare the KTX functionals with the RevTPSS meta-GGA provides insight to the relative accuracy of the GGA functionals. While Dr. de Oliverira utilised a number of meta-GGA functionals, the RevTPSS results were some of the most accurate amongst them and as such has been selected as the comparison functional of choice. M062X/6-311+G(2d,p) optimised geometries have been employed for all molecules. Jensen's pcSseg-2 basis set is used for all calculations to ensure the only deviation between calculated results is the functional in question. The DFT calculated shielding constants have been converted to chemical shifts using $\sigma(CH_3NO_2)$ = -135.8 ppm,[58] with the resulting chemical shifts reported in Table 6.1.

Table 6.1: ^{15}N chemical shifts from experiment and calculated DFT results (ppm).[(a)]

Molecule	Nuclei	Experimental	RevTPSS[(b)]	KT1	KT2	KT3
CH_3CN	N	-134.5	-117.0	-124.3	-122.0	-123.7
NH_2CN	N-1	-183.5	-168.5	-176.9	-174.1	-175.1
$NO_2N(CH3)_2$	N-1	-217.5	-227.0	-220.7	-214.1	-213.3
	N-2	-25.0	-37.8	-39.6	-34.1	-38.3
$NON(CH3)_2$	N-2	-149.2	-161.7	-164.1	-158.5	-157.7
$(CH_3)_2NCON(CH_3)_2$	N	-316.1	-312.6	-313.3	-310.0	-308.8
pyrrole	N	-234.7	-233.6	-234.8	-232.9	-234.3
1,3-diazole	N-1	-220.5	-217.8	-219.4	-216.9	-217.8
	N-3	-122.5	-106.8	-113.5	-109.9	-111.2
1,2-diazole	N-1	-179.4	-175.0	-177.7	-174.8	-176.6
	N-2	-73.7	-67.5	-72.4	-67.9	-69.9
1,2,3-triazole	N-2	-15.3	-11.5	-18.7	-12.9	-14.6
	N-3	-30.4	-23.9	-34.5	-28.7	-29.6
1,2,4-triazole	N-1	-173.6	-170.3	-173.2	-170.0	-171.2
	N-2	-83.6	-78.4	-83.8	-79.0	-80.3
	N-4	-129.8	-117.3	-124.1	-120.2	-121.1
isoxazole	N	2.5	6.7	-0.5	5.5	3.3
oxazole	N	-125.0	-114.5	-122.8	-118.5	-119.1
thiadiazole	N	-7.6	7.8	-2.5	2.7	1.3
isothiazole	N	-85.3	-72.2	-83.0	-77.9	-79.1
thiazole	N	-60.5	-47.9	-57.5	-53.4	-54.9
oxadiazole	N	-73.4	-57.2	-66.7	-61.6	-62.3
furazan	N	38.1	35.5	24.9	32.3	30.8
1,2,4-thiadiazole	N-4	-71.3	-94.7	-70.1	-65.4	-66.3
tetrazole	N-1	-154.6	-156.0	-160.5	-156.5	-157.2
	N-2	-9.9	-13.3	-22.4	-15.8	-16.3
	N-3	14.6	24.1	13.2	19.8	18.9
	N-4	-49.7	-41.1	-50.7	-45.1	-45.8
nitrobenzene	N	-10.0	-20.6	-30.3	-24.6	-27.5
pyridine	N	-68.7	-52.6	-60.3	-57.4	-58.9
pyroxide	N	-86.8	-69.6	-73.9	-71.0	-74.2
pyridazine	N	19.0	49.2	37.8	41.1	40.0
pyrimidine	N	-86.2	-76.9	-82.8	-79.8	-81.1
pyrazine	N	-47.8	-39.9	-48.7	-45.4	-46.6
1,3,5-triazine	N	-98.1	-90.1	-95.6	-92.8	-94.4
1,3,4-triazine	N-4	-80.2	-83.0	-90.9	-87.0	-88.1
tetrazine	N	12.7	23.8	11.1	15.2	14.9
indolizine	N	-190.0	-180.5	-181.7	-179.7	-181.9
imidpyr	N-1	-179.6	-170.2	-172.4	-169.8	-171.7
	N-2a	-143.9	-124.0	-131.8	-128.5	-129.4
imidpyr	N-1	-186.4	-178.1	-179.6	-177.2	-179.1
	N-5a	-112.2	-93.4	-102.2	-98.7	-100.1
pyrazolopyr	N-1	-144.5	-137.4	-139.9	-137.0	-139.5
	N-5a	-97.4	-87.2	-93.6	-89.2	-90.5
Mean Absolute Deviation (MAD)			**10.2**	**6.1**	**7.6**	**6.8**
Maximum Absolute Deviation (MAX)			**30.2**	**20.3**	**22.1**	**21.0**

(a) DFT shieldings converted to chemical shifts via $\sigma(CH_3NO_2)$ = -135.8 ppm.[58]

(b) Results provided by Dr. Marcelo de Oliveira.

Table 6.1 illustrates the chemical shifts calculated using the range of KTX and RevTPSS DFT functionals. The mean absolute deviation (MAD) of the KTX functionals range from 6 to 8 ppm, while the RevTPSS functional exhibits a MAD of 10.2 ppm. The results are consistent with those of Krivdin[26] and Teale *et al.*,[18] who concluded that KTX functionals, in particular KT2 and KT3, are the ideal DFT methods for chemical shift and nuclear shielding calculations. Despite this, and given that these investigations employ a finite set of molecules, it is always plausible that MAD results could change with a growing series of molecules. Krivdin performed calculations on 23 ^{15}N containing heterocycles for which KT3/pcS-3 yielded a MAD of 5 ppm. This is very close to the MAD determined in Table 6.1 of 6.8 ppm for KT3, although the use of a smaller pcSseg-2 basis set may be the cause of the small deviation. Teale *et al.* determined the MAD of KT2/ACVQZ to be 5.7 ppm for a series of 26 molecules. The series of molecules within the study from Teale *et al.* was not solely focused on ^{15}N; however, the agreement between the results presented here and by Krivdin show that the conclusions made by Teale *et al.* are still valid.

The calculated pyridazine chemical shift is responsible for the maximum absolute deviation (MAX) in all cases except KT1, where the MAX arises from the nitrobenzene. If pyridazine is omitted, the MAD for RevTPSS decreases to 9.7 ppm with a MAX of 23.4 ppm. Whilst the decrease in MAD is not surprising, the large difference between the MAX and the second-largest absolute error is almost 7 ppm, which is considered to be substantial. Comparison of MADs and MAXs within Table 6.1 shows KT1 to be the most accurate of the four functionals compared; however, with such a small deviation between the MADs and MAXs of the KTX functionals, the conclusion is difficult to support without extra investigation. Nonetheless, the GGA KTX functionals appear to be more accurate than the meta-GGA RevTPSS for the calculation of equilibrium chemical shifts. It is additionally noted that DFT is more inaccurate than coupled-cluster in the context of absolute shieldings and chemical shifts. Whilst the average MAD from experiment across the KTX functionals is approximately 6-7 ppm, this is much greater than the deviations from experiment for the absolute shieldings calculated throughout Chapters 3-4. This supports the current belief that coupled-cluster is required for quantitative absolute shieldings, whilst DFT is useful for molecules too large for coupled-cluster calculations.

6.3 Vibrational corrections calculated via DFT

Section 6.2 demonstrated the ability to calculate equilibrium chemical shifts via DFT. As seen in Chapters 3 and 4, it is important to consider vibrational corrections for calculated shieldings. Therefore, the requirement of vibrational corrections calculated via DFT will be investigated. Vibrational corrections to the nuclear shielding and chemical shift have been calculated via DFT functionals B3LYP and KT2, along with Jensen's pcS-2 basis set. Starting geometries provided by Dr Oliveira have been optimised using both functionals to obtain acceptable minimum energy optimised geometries for the given method and basis set combination. Vibrational effects are then calculated within DALTON via calculating an effective geometry for which the effects to the shielding are further calculated from. Comparison between the chosen functionals is performed by augmenting the KT2 results presented in Table 6.1 and further comparing with experiment.

Table 6.2: Vibrationally corrected DFT functional chemical shifts (ppm).

Molecule	Nuclei	Experimental	Equilibrium[(a)]	Vibrationally Corrected	
				KT2	B3LYP
CH_3CN	N	-134.5	-122.0	-115.9	-115.1
NH_2CN	N-1	-183.5	-174.1	-166.5	-165.0
$NO_2N(CH3)_2$	N-1	-217.5	-214.1	-201.0	-170.3
	N-2	-25.0	-34.1	-26.4	5.2
$NON(CH3)_2$	N-2	-149.2	-158.5	-155.8	-153.9
$(CH_3)_2NCON(CH_3)_2$	N	-316.1	-310.0	-303.3	-287.6
pyrrole	N	-234.7	-232.9	-224.9	-224.3
1,3-diazole	N-1	-220.5	-216.9	-210.8	-205.1
	N-3	-122.5	-109.9	-99.8	-91.6
1,2-diazole	N-1	-179.4	-174.8		-160.0
	N-2	-73.7	-67.9		-48.1
1,2,3-triazole	N-2	-15.3	-12.9	-2.0	24.0
	N-3	-30.4	-28.7	-19.5	-17.8
1,2,4-triazole	N-1	-173.6	-170.0	-163.4	-156.0
	N-2	-83.6	-79.0	-67.4	-59.4
	N-4	-129.8	-120.2	-110.7	-102.0
isoxazole	N	2.5	5.5	17.5	21.3
oxazole	N	-125.0	-118.5	-110.0	-107.8
thiadiazole	N	-7.6	2.7	10.8	15.0
isothiazole	N	-85.3	-77.9	-67.8	-69.1
thiazole	N	-60.5	-53.4	-45.6	-43.3
oxadiazole	N	-73.4	-61.6	-52.8	-48.3
furazan	N	38.1	32.3	42.5	43.9
1,2,4-thiadiazole	N-4	-71.3	-65.4	-57.1	-53.8
tetrazole	N-1	-154.6	-156.5	-153.2	-168.0
	N-2	-9.9	-15.8	-8.0	11.7
	N-3	14.6	19.8	23.1	65.3
	N-4	-49.7	-45.1	-36.0	-37.6
nitrobenzene	N	-10.0	-24.6	-11.5	8.8
pyridine	N	-68.7	-57.4	-49.4	-46.2
pyroxide	N	-86.8	-71.0	-65.1	-61.1
pyridazine	N	19.0	41.1	47.6	49.7
pyrimidine	N	-86.2	-79.8	-74.9	-74.5
pyrazine	N	-47.8	-45.4	-38.3	-37.6
1,3,5-triazine	N	-98.1	-92.8	-85.6	-84.8
1,3,4-triazine	N-4	-80.2	-87.0	-80.5	-80.9
tetrazine	N	12.7	15.2	15.5	23.8
indolizine	N	-190.0	-179.7	-177.1	-173.9
imidpyr	N-1	-179.6	-169.8	-163.4	-153.9
	N-2a	-143.9	-128.5	-119.8	-118.3
imidpyr	N-1	-186.4	-177.2	-170.4	-161.4
	N-5a	-112.2	-98.7	-90.0	-101.3
pyrazolopyr	N-1	-144.5	-137.0	-130.8	-130.1
	N-5a	-97.4	-89.2	-78.0	-72.2
Mean Absolute Deviation (MAD)			**7.6**	**13.4**	**20.4**
Maximum Absolute Deviation (MAX)			**22.1**	**28.6**	**50.7**

(a) KT2 equilibrium chemical shifts from Table 6.1.

Inclusion of KT2 vibrational corrections increases the MAD of calculated chemical shifts by 5.8 ppm, whilst vibrational corrections calculated via B3LYP increase the MAD by 12.8 ppm. Additionally, the MAX increases with the inclusion of vibrational effects. Table 6.2 demonstrates B3LYP to be less accurate than KT2 in terms of vibrational corrections; however, as the calculated vibrational corrections have been applied to equilibrium KT2 shieldings, it is possible the trend of B3LYP inaccuracy compared to that of KT2 is a result of the accuracy of the functional on calculated equilibrium chemical shifts. It is to be noted that if the RevTPSS results within Table 6.1 are used as the equilibrium chemical shifts, then the trends seen in Table 6.2 are still prominent, with KT2 producing smaller MAD and MAX values. Consideration of vibrational effects causing an increase in deviation from experiment contradicts discussions held throughout earlier Chapters of this thesis. This is likely due to the use of DFT functionals as opposed to the coupled-cluster methods that have been used for the majority of the work discussed prior to this Chapter. The parameterisation of DFT functionals with respect to experimentally reported data is likely a cause for this effect. Vibrational corrections are implicitly accounted for within experimental chemical shifts. As such, DFT functionals are optimised towards vibrationally corrected chemical shifts. Calculating and applying vibrational corrections to calculated chemical shifts therefore overcorrects the true theoretical chemical shift. Teale *et al.*[14] calculated vibrational corrections using B3LYP/aug-cc-pCVTZ, which was removed from experimental chemical shifts to determine empirical (equilibrium) experimental shifts. Fundamentally, comparison with these empirical experimental shifts is equivalent to vibrationally corrected chemical shifts compared with experimental data. Teale *et al.* showed that coupled-cluster calculated chemical shifts deviate less when vibrational effects calculated with DFT are considered; however, when equilibrium chemical shifts are calculated with DFT functionals, comparison with direct experimental data resulted in lower MADs and MAXs compared to those resulting from consideration of vibrational effects. The Teale *et al*. results agree with the conclusions developed here, where vibrational effects increase the deviation from experiment when applied to equilibrium chemical shifts calculated via DFT.

6.4 Relativistic corrections applied to DFT calculated chemical shifts

Relativistic effects towards the ^{15}N chemical shifts within the series of 32 molecules have been calculated to assess the requirement of considering relativity for the purposes of DFT calculated chemical shifts. Relativistic effects were shown to be important for the purposes of accurate absolute shieldings and spin-rotation constants calculated with coupled-cluster methods throughout Chapters 3 to 5. However, it is unknown if a trend similar to those seen in Section 6.3 for vibrational corrections may also be seen for relativistic effects. Geometries optimised by Dr Oliveira have been utilised in four-component relativistic calculations using the KT2 functional along with the upcJ-2 basis set within ReSpect. Identical calculations were run with an increased speed of light to approach the non-relativistic limits. The differences of these calculations have been determined as the effect of considering relativity towards the ^{15}N chemical shift. Application of relativistic effects to the KT2 equilibrium chemical shifts within Table 6.1 has been compiled and compared with experimental chemical shifts in Table 6.3.

Table 6.3: Relativistically corrected DFT functional chemical shifts (ppm).

Molecule	Nuclei	Experimental	Equilibrium[(a)]	Relativistic
CH_3CN	N	-134.5	-122.0	-123.7
NH_2CN	N-1	-183.5	-174.1	-175.9
$NO_2N(CH3)_2$	N-1	-217.5	-214.1	-215.7
	N-2	-25.0	-34.1	-37.6
$NON(CH3)_2$	N-2	-149.2	-158.5	-159.5
$(CH_3)_2NCON(CH_3)_2$	N	-316.1	-310.0	-311.8
pyrrole	N	-234.7	-232.9	-234.6
1,3-diazole	N-1	-220.5	-216.9	-218.4
	N-3	-122.5	-109.9	-111.7
1,2-diazole	N-1	-179.4	-174.8	-176.6
	N-2	-73.7	-67.9	-69.5
1,2,3-triazole	N-2	-15.3	-12.9	-14.6
	N-3	-30.4	-28.7	-30.4
1,2,4-triazole	N-1	-173.6	-170.0	-171.6
	N-2	-83.6	-79.0	-80.6
	N-4	-129.8	-120.2	-121.9
isoxazole	N	2.5	5.5	3.6
oxazole	N	-125.0	-118.5	-120.3
thiadiazole	N	-7.6	2.7	0.8
isothiazole	N	-85.3	-77.9	-80.7
thiazole	N	-60.5	-53.4	-55.3
oxadiazole	N	-73.4	-61.6	-63.4
furazan	N	38.1	32.3	30.3
1,2,4-thiadiazole	N-4	-71.3	-65.4	-67.2
tetrazole	N-1	-154.6	-156.5	-157.8
	N-2	-9.9	-15.8	-17.4
	N-3	14.6	19.8	18.0
	N-4	-49.7	-45.1	-46.8
nitrobenzene	N	-10.0	-24.6	-27.8
pyridine	N	-68.7	-57.4	-59.0
pyroxide	N	-86.8	-71.0	-73.7
pyridazine	N	19.0	41.1	39.3
pyrimidine	N	-86.2	-79.8	-81.4
pyrazine	N	-47.8	-45.4	-47.0
1,3,5-triazine	N	-98.1	-92.8	-94.4
1,3,4-triazine	N-4	-80.2	-87.0	-88.5
tetrazine	N	12.7	15.2	13.6
indolizine	N	-190.0	-179.7	-181.3
imidpyr	N-1	-179.6	-169.8	-171.3
	N-2a	-143.9	-128.5	-130.3
imidpyr	N-1	-186.4	-177.2	-178.7
	N-5a	-112.2	-98.7	-100.5
pyrazolopyr	N-1	-144.5	-137.0	-138.6
	N-5a	-97.4	-89.2	-90.8
Mean Absolute Error (MAD)			**7.6**	**6.5**
Maximum Absolute Deviation (MAX)			**22.1**	**20.3**

(a) KT2 equilibrium chemical shifts from Table 6.1.

Table 6.3 compares experimental ^{15}N chemical shifts with KT2 calculated equilibrium chemical shifts as well as equilibrium chemical shifts augmented with relativistic corrections. Relativistic effects make up between 1.5 and 2.0 ppm in almost 80% of the ^{15}N chemical shifts investigated here, and in all cases, the relativistically corrected chemical shift is more negative than the equilibrium chemical shift. As such, calculated equilibrium ^{15}N shifts that overestimated the chemical shift are more accurate after applying relativistic corrections. This occurs in almost 85% of the selected series of ^{15}N chemical shifts. As the consistent 1.5 to 2.0 ppm relativistic correction often causes a decrease in deviation from experiment, the decrease in the MAD and MAX between the KT2 equilibrium chemical shifts and chemical shifts with relativistic corrections of 1.1 and 1.8 ppm, respectively, is not surprising. This trend contrasts those discussed with respect to vibrational corrections, where consideration of relativistic corrections is important even when the equilibrium chemical shift is calculated via a DFT functional. The consistent magnitude of the relativistic corrections of 1.5 to 2.0 ppm is believed to be accurate, as equivalent effects calculated for ^{19}F were found to be approximately 4 to 5 ppm. The decrease in relativistic effect between ^{15}N and ^{19}F arises from the ^{19}F atoms increased mass and sensitivity with regards to NMR chemical shifts. These results mirror those reported previously by Samultsev *et al.*,[58] who showed relativistic effects in a series of gas-phase halogenated azines to be about 1 to 2 ppm when fluorine, chorine, or bromide is the bound halogen and decreased the MAD from experimentally reported chemical shifts. Samultsev *et al.* used KT3/pcS-3 for both the one-component and four-component calculations, which differs slightly from the method and basis set chosen here. Nonetheless, the agreement between the relativistic contributions of 1.5 to 2 ppm within Table 6.3 and the results reported by Samultsev *et al.* demonstrate that relativistic corrections should be considered for the purposes of DFT chemical shift investigations.

6.5 Summary

DFT functionals have been utilised for the purposes of calculating gas-phase ^{15}N chemical shifts for a series of 32 molecules in collaboration with Dr. de Oliveira. It has been shown that the KTX series of DFT functionals are accurate for the calculation of ^{15}N chemical shifts. Additionally, vibrational and relativistic corrections were further calculated with the KT2 functional and found that consideration of vibrational corrections decreases agreement with experimentally reported chemical shifts, whereas application of relativistic effects increases the agreement with experiment.

Chapter 7:
Conclusions and Further Work

The ^{19}F absolute shielding within a series of small molecules has been investigated via high-level quantum mechanical calculations. Results showed that coupled-cluster higher excitation contributions, although valuable, are not critical due to the decrease in the magnitude of the contribution to the shielding. It was concluded that at least triple excitations (CCSD(T) or CCSDT) are needed for accurate results. This allowed shielding constants of slightly larger molecules such as CH_3F and F_2O to be calculated with reasonable precision. Important effects on the absolute shielding tensor such as vibrational averaging, temperature, and relativistic effects have been calculated and were shown to be required for accurate absolute shielding constants. Vibrational averaging effects were found to be much larger when the fluorine atom interacted with other electronegative atoms, such as in the case of F_2 and F_2O. This trend extended to the temperature effects; however, the effect on the absolute shielding arising from temperature changes was an order of magnitude smaller than the effects from vibrational averaging. Relativistic effects on the ^{19}F shielding were shown to be sizeable, often much larger than the temperature effects.

All contributions to the absolute ^{19}F shielding were combined to obtain a fully theoretical shielding for each molecule. Calculated ^{19}F absolute shielding constants were compared with experimental shielding constants, which when updated with recent chemical shift and absolute shielding constants, are very close to the calculated values reported here. The excellent agreement between the calculated ^{19}F absolute shielding constants and corrected experimental shielding constants allows the conclusion that the shielding constants reported here are accurate. Additionally, consideration of spin-rotation tensors and development of semi-experimental shielding constants that agree with fully calculated shielding constants further increase the validity of our reported absolute shielding constants and the improvements made to the ^{19}F shielding scale.

An investigation into the absolute ^{19}F shielding of SiF_4 would benefit the work presented here by confirming that the experimental chemical shift produced by Makulski is accurate. Additionally, expanding the current equilibrium shielding calculations to more extensive methods and basis sets for the larger molecules will decrease the uncertainty in their respective ^{19}F shielding constants. Extrapolation via ACV[D,T]Z is not ideal and as such it is believed the

results for FCl, HOF, and FCN can be improved if larger basis sets were employed. Additionally, whilst the use of CCSDT as the largest method for multiple molecules is impressive, further results from CCSDTQ would confirm calculated absolute shieldings are approaching the theoretically exact value.

Further work may also be conducted in bridging the gap between the two projects within this thesis. Performing DFT absolute shielding calculations on the series of ^{19}F containing molecules, as well as benchmark coupled-cluster calculations on a small series of ^{15}N containing molecules would provide further insight to the difference between DFT and coupled-cluster benchmark calculations. Investigation into the effect of geometry on absolute shielding is also warranted. While CCSD(T)/ACVQZ geometries were used where possible for the coupled-cluster benchmark chapters of this thesis, there is reason to believe geometries optimised with larger methods or basis sets can provide more accurate absolute shieldings. The effects of using these higher optimised geometries should be compared with using experimental geometries as well as the results reported here to determine the level of importance with regard to the implicit computational cost associated with optimising geometries with larger levels of theory.

References

1. J. C. Facelli. Chemical Shift Tensors: Theory and Application to Molecular Structural Problems. *Prog. Nucl. Magn. Reson. Spectrosc.*, 2011, **58,** 176.

2. H. Fukui, T. Baba, J. Narumi, H. Inomata, K. Miura and H. Matsuda. Calculation of Nuclear Magnetic Shieldings. XI. Vibrational Motion Effects. *J. Chem. Phys.*, 1996, **105,** 4692.

3. M. Jaszuński, T. B. Demissie and K. Ruud. Spin-Rotation and NMR Shielding Constants in XF Molecules (X = B, Al, Ga, In, and Tl). *J. Phys. Chem. A,* 2014, **118,** 9588.

4. M. Jaszuński, M. Repisky, T. B. Demissie, S. Komorovsky, E. Malkin, K. Ruud, P. Garbacz, K. Jackowski and W. Makulski. Spin-rotation and NMR shielding constants in HCl. *J. Chem. Phys.,* 2013, **139,** 234302.

5. J. Gauss, K. Ruud and T. Helgaker. Perturbation-dependent atomic orbitals for the calculation of spin-rotation constants and rotational g tensors. *J. Chem. Phys.,* 1996, **105,** 2804.

6. T. B. Demissiea , M. Jaszuński, E. Malkina, S. Komorovsky and K. Ruud. NMR shielding and spin–rotation constants in XCO (X = Ni, Pd, Pt) molecules. *Mol. Phys.,* 2015, **113,** 1576.

7. W. Makulski. ^{19}F and ^{29}Si Nuclear Magnetic Shielding and Spin–Spin Coupling Constants in Silicon Tetrafluoride and Hexafluorodisiloxane in the Gaseous State. *J. Mol. Struct.*, 2013, **1036,** 168.

8. N. Ramsey. Magnetic Shielding of Nuclei in Molecules. *Phys. Rev.*, 1950, **78,** 699.

9. W. H. Flygare. Magnetic Interactions in Molecules and an Analysis of Molecular Electronic Charge Distribution from Magnetic Parameters. *Chem. Rev.*, 1974, **74,** 653.

10. W. H. Flygare, Spin—Rotation Interaction and Magnetic Shielding in Molecules. *J. Chem. Phys.*, 1964, **41,** 793.

11. C. Puzzarini, G. Cazzoli, M. E. Harding, J. Vázquez and J. Gauss. A New Experimental Absolute Nuclear Magnetic Shielding Scale for Oxygen Based on the Rotational Hyperfine Structure of $H_2{}^{17}O$. *J. Chem. Phys.*, 2009, **131,** 234304.

12. D. Sundholm, J. Gauss and A. Schäfer. Rovibrationally Averaged Nuclear Magnetic Shielding Tensors Calculated at the Coupled-Cluster Level. *J. Chem. Phys.*, 1996, **105,** 11051.

13. S. Komorovsky, M. Repisky, E. Malkin, K. Ruud and J. Gauss. The Absolute Shielding Scales of Oxygen and Sulfur Revisited. *J. Chem. Phys.*, 2015, **142,** 091102.

14. D. K. Hindermann and C. D. Cornwell. Vibrational Corrections to the Nuclear Magnetic Shielding and Spin–Rotation Constants for Hydrogen Fluoride. Shielding Scale for ^{19}F. *J. Chem. Phys.*, 1968, **48,** 4148.

15. C. J. Jameson, A. K. Jameson and P. M. Burrell. ^{19}F Nuclear Magnetic Shielding Scale from Gas Phase Studies. *J. Chem. Phys.*, 1980, **73,** 6013.

16. E. Malkin, S. Komorovsky, M. Repisky, T. B. Demissie and K. Ruud, The Absolute Shielding Constants of Heavy Nuclei: Resolving the Enigma of ^{119}Sn Shielding. *J. Phys. Chem. Lett.*, 2013, **4,** 459.

17. I. A. Aucar, S. S. Gómez, M. C. Ruiz de Azúa and C. G. Giribet. Theoretical Study of the Nuclear Spin-Molecular Rotation Coupling for Relativistic Electrons and Non-Relativistic Nuclei. *J. Chem. Phys.*, 2012, **136,** 204119.

18. A. M. Teale, O. B. Lutnæs, T. Helgaker, D. J. Tozer and J. Gauss. Benchmarking Density-Functional Theory Calculations of NMR Shielding Constants and Spin–Rotation

Constants Using Accurate Coupled-Cluster Calculations. *J. Chem. Phys.*, 2013, **138,** 024111.

19. K. Wolinsk, J. F. Hinton and P. Pulay. Efficient Implementation of the GIAO Method for Magnetic Properties: Theory and Application. *J. Am. Chem. Soc.*, 1990, **112,** 8251.

20. J. Gauss. Effects of Electron Correlation in the Calculation of Nuclear Magnetic Resonance Chemical Shifts. *J. Chem. Phys.*, 1993, **99,** 3629.

21. J. Gauss and J. F. Stanton. Electron-Correlation Methods of the Calculation of NMR Chemical Shifts. in *Calculation of NMR and EPR Parameters,* ed. M. Kaupp, M. Bühl and V. G. Malkin. Wiley-VCH Verlag GmbH & Co. KGaA, Weinheim, 2004, ch. 8, pp. 123-139.

22. G. Schreckenbach and T. Ziegler. The Calculation of NMR Shielding Tensors Based on Density Functional Theory and the Frozen-Core Approximation. *Int. J. Quantum Chem.*, 1995, **60,** 753.

23. M. E. Harding, M. Lenhart, A. A. Auer and J. Gauss. Quantitative Prediction of Gas-Phase ^{19}F Nuclear Magnetic Shielding Constants. *J. Chem. Phys.*, 2008, **128,** 244111.

24. C. P. Rosenau, B. J. Jelier and A. D. Gossert. Exposing the Origins of Irreproducibility in Fluorine NMR Spectroscopy. *Angew. Chem. Int. Ed.*, 2018, **57,** 9528.

25. T. E. Field-Theodore, M. Olejniczak, M. Jaszuński and D. J. D. Wilson. NMR Shielding Constants in Group 15 Trifluorides. *Phys. Chem. Chem. Phys.*, 2018, **20,** 23025.

26. L. B. Krivdin. Calculation of ^{15}N NMR chemical shifts: Recent advances and perspectives. *Prog. Nucl. Magn. Reson. Spectrosc.,* 2017, **102-103,** 98.

27. D. O. Samultsev, V. A. Semenov and L. B. Krivdin. On the accuracy of the GIAO-DFT calculation of ^{15}N NMR chemical shifts of the nitrogen-containing heterocycles – a gateway to better agreement with experiment at lower computational cost. *Magn. Reson. Chem.,* 2014, **52,** 222.

28. J. P. Perdew, A. Ruzsinszky, J. Tao, V. N. Staroverov, G. E. Scuseria and G. I. Csonka. Prescription for the design and selection of density functional approximations: More constraint satisfaction with fewer fits. *J. Chem. Phys.,* 2005, **123,** 062201.

29. N. Mardirossiana and M. Head-Gordon. Thirty years of density functional theory in computational chemistry: an overview and extensive assessment of 200 density functionals. *Mol. Phys.,* 2017, **115,** 2315.

30. J. P. Perdew, M. Ernzerhof and K. Burke. Rationale for mixing exact exchange with density functional approximations. *J. Chem. Phys.,* 1996, **105,** 9982.

31. R. Ditchfield, W. J. Hehre and J. A. People. Self-Consistent Molecular-Orbital Methods. IX. An Extended Gaussian-Type Basis for Molecular-Orbital Studies of Organic Molecules. *J. Chem. Phys.,* 1971, **54,** 724.

32. F. Jensen. Polarization consistent basis sets: Principles. *J. Chem. Phys.,* 2001, **115,** 9113.

33. F. Jensen. Segmented Contracted Basis Sets Optimized for Nuclear Magnetic Shielding. *J. Chem. Theory Comput.,* 2015, **11,** 132.

34. F. Weigend and R. Ahrichs. Balanced basis sets of split valence, triple zeta valence and quadruple zeta valence quality for H to Rn: Design and assessment of accuracy. *Phys. Chem. Chem. Phys.,* 2005, **7,** 3297.

35. M. W. Feyereisen, D. Feller and D. A. Dixon. Hydrogen Bond Energy of the Water Dimer. *J. Phys. Chem.,* 1996, **100,** 1993.

36. A. Halkier, W. Klopper, T. Helgaker and P. Jørgensen. Basis-set convergence of the molecular electric dipole moment. *J. Chem. Phys.,* 1999, **111,** 4424.

37. CFOUR, *a quantum chemical program package*, written by J. F. Stanton, J. Gauss, L. Cheng, M. E. Harding, D. A. Matthews, P. G. Szalay with contributions from A. A. Auer, R. J. Bartlett, U. Benedikt, C. Berger, D. E. Bernholdt, Y. J. Bomble, O. Christiansen, F. Engel, R. Faber, M. Heckert, O. Heun, M. Hilgenberg, C. Huber, T.-C. Jagau, D. Jonsson, J. Jusélius, T. Kirsch, K. Klein, W. J. Lauderdale, F. Lipparini, T. Metzroth, L. A. Mück, D. P. O'Neill, D. R. Price, E. Prochnow, C. Puzzarini, K. Ruud, F. Schiffmann, W. Schwalbach, C. Simmons, S. Stopkowicz, A. Tajti, J. Vázquez, F. Wang, J. D. Watts and the integral packages *MOLECULE* (J. Almlöf and P. R. Taylor), *PROPS* (P.R. Taylor), *ABACUS* (T. Helgaker, H. J. Aa. Jensen, P. Jørgensen, and J. Olsen), and ECP routines by A. V. Mitin and C. van Wüllen. For the current version, see http://www.cfour.de.

38. Dalton, *a molecular electronic structure program,* Release Dalton2018.2 (2019), written by K. Aidas, C. Angeli, K. L. Bak, V. Bakken, R. Bast, L. Boman, O. Christiansen, R. Cimiraglia, S. Coriani, P. Dahle, E. K. Dalskov, U. Ekström, T. Enevoldsen, J. J. Eriksen, P. Ettenhuber, B. Fernández, L. Ferrighi, H. Fliegl, L. Frediani, K. Hald, A. Halkier, C. Hättig, H. Heiberg, T. Helgaker, A. C. Hennum, H. Hettema, E. Hjertenæs, S. Høst, I.-M. Høyvik, M. F. Iozzi, B. Jansik, H. J. Aa. Jensen, D. Jonsson, P. Jørgensen, J. Kauczor, S. Kirpekar, T. Kjærgaard, W. Klopper, S. Knecht, R. Kobayashi, H. Koch, J. Kongsted, A. Krapp, K. Kristensen, A. Ligabue, O. B. Lutnæs, J. I. Melo, K. V. Mikkelsen, R. H. Myhre, C. Neiss, C. B. Nielsen, P. Norman, J. Olsen, J. M. H. Olsen, A. Osted, M. J. Packer, F. Pawlowski, T. B. Pedersen, P. F. Provasi, S. Reine, Z. Rinkevicius, T. A. Ruden, K. Ruud, V. Rybkin, P. Salek, C. C. M. Samson, A. Sánchez de Merás, T. Saue, S. P. A. Sauer, B. Schimmelpfennig, K. Sneskov, A. H. Steindal, K. O. Sylvester-Hvid, P. R. Taylor, A. M. Teale, E. I. Tellgren, D. P. Tew, A. J. Thorvaldsen, L. Thøgersen, O. Vahtras, M. A. Watson, D. J. D. Wilson, M. Ziolkowski, and H. Ågren, "The Dalton quantum chemistry program system", WIREs *Comput. Mol. Sci.,* 2014, 4:269–284 (doi: 10.1002/wcms.1172). For the current version, see http://daltonprogram.org.

39. ReSpect 5.1.0 (2019), *Relativistic Spectroscopy DFT Program*, written by M. Repisky, S. Komorovsky, V. G. Malkin, O. L. Malkina, M. Kaupp, K. Ruud, with contributions

from R. Bast, R. Di Remigio, U. Ekstrom, M. Kadek, S. Knecht, L. Konecny, E. Malkin and I. Malkin-Ondik. For the current version, see http://www.respectprogram.org/.

40. P. Garbacz, K. Jackowski, W. Makulski and R. E. Wasylishen. Nuclear Magnetic Shielding for Hydrogen in Selected Isolated Molecules. *J. Phys. Chem. A*, 2012 **116,** 11896.

41. D. Sundholm and J. Gauss. Isotope and temperature effects on nuclear magnetic shieldings and spin-rotation constants calculated at the coupled-cluster level. *Mol. Phys.,* 1997, **92,** 1007.

42. H. Nakatsuji, H. Takashima and M. Hada. Spin-orbit effect on the magnetic shielding constant using the ab initio UHF method. *Chem. Phys. Lett.,* 1995, **233,** 95.

43. V. G. Malkin, O. L. Malkina, L. A. Eriksson and D. R. Salahub, in Modern Density Functional Theory: A Tool for Chemistry, edited by J. M. Seminario and P. Politzer, Elsevier, Amsterdam, 1995.

44. V. G. Malkin, O. L. Malkina and D. R. Salahub. Spin-orbit correction to NMR shielding constants from density functional theory. *Chem. Phys. Lett.,* 1996, **261,** 335.

45. D. K. Hindermann and C. D. Cornwell. Fluorine and Proton NMR Study of Gaseous Hydrogen Fluoride. *J. Chem. Phys.*, 1968, **48,** 2017.

46. J. W. Nebgen, W. B. Rose and F. I. Metz. The ^{19}F Nuclear Magnetic Resonance Spectra of Liquid and Gaseous Fluorine, Oxygen Difluoride, and Nitrogen Trifluoride. *J. Mol. Spectrosc.*, 1966, **20,** 72.

47. L. G. Alexakos and C. D. Cornwell. NMR Spectra of ClF_3 and ClF: Gaseous Spectra and Gas-to-Liquid Shifts. *J. Chem. Phys.*, 1964, **41,** 2098.

48. J. C. Hindman, A. Svirmickas and E. H. Appelman. Proton and Fluorine Nuclear Magnetic Resonance Observations on Hypofluorous Acid, HOF. *J. Chem. Phys.*, 1972, **57,** 4542.

49. F. S. Fawcett and R. D. Lipscomb. Cyanogen Fluoride. *J. Am. Chem. Soc.*, 1960, **82,** 1509.

50. N. J. Harrick, R. G. Barnes, P. J. Bray and N. F. Ramsey. Nuclear Radiofrequency Spectra of D_2 and H_2 in Intermediate and Strong Magnetic Fields. *Phys. Rev.,* 1953, **90,** 260.

51. S. M. Bass, R. L. DeLeon and J. S. Muenter. Stark, Zeeman, and hyperfine properties of v=0, v=1, and the equilibrium configuration of hydrogen fluoride. *J. Chem. Phys.,* 1987, **86,** 4305.

52. J. Gauss, K. Ruud and T. Helgaker. Perturbation-dependent atomic orbitals for the calculation of spin-rotation constants and rotational g tensors. *J. Chem. Phys.,* 1996, **105,** 2804.

53. J. Gauss and D. Sundholm. Coupled-cluster calculations of spin-rotation constants. *Mol. Phys.,* 1997, **91,** 449.

54. D. K. Hindermann and L. L. Williams. Nuclear Magnetic Shielding in F_2. *J. Chem. Phys.,* 1969, **50,** 2839.

55. I. Ozier, and N. F. Ramsey. *Bull. Am. Phys. Soc.,* 1966, **11,** 23.

56. W. H. Flygare. Spin—Rotation Interaction and Magnetic Shielding in OF_2. *J. Chem. Phys.,* 1965, **42,** 1157.

57. S. C. Wofsy, J. S. Muenter and W. Kelmperer. Determination of Hyperfine Constants and Nuclear Shielding in Methyl Fluoride and Comparison with Other Molecules. *J. Chem. Phys.,* 1971, **55,** 2014.

58. D. O. Samultsev, Y. Y. Rusakov and Leonid B. Krivdin. On the long-range relativistic effects in the ^{15}N NMR chemical shifts of halogenated azines. *Magn. Reson. Chem.,* 2017, **55,** 990.